

1 T2K Neutrino and Anti-Neutrino 3-Flavour Joint Analysis of
2 Run 1-8 (1.4734×10^{21} -POT ν 7.558×10^{20} -POT $\bar{\nu}$) data sets

3 Costas Andreopoulos^{a,b}, Christopher Barry^b, Andrew Chappell^d, Thomas Dealtry^e, Steve Dennis
4 ^{a,b}, Davide Sgalaberna^f, Raj Shah^{a,c}

5 ^a*Science & Technology Facilities Council (STFC), Rutherford Appleton Laboratory,
6 Harwell Oxford Campus, OX11 0QX, UK*

7 ^b*University of Liverpool, Physics Department,
8 Liverpool, L69 7ZE, UK*

9 ^c*University of Oxford, Subdepartment of Particle Physics,
10 Oxford, OX1 3RH, UK*

11 ^d*University of Warwick, Physics Department,
12 Coventry, CV4 7AL, UK*

13 ^e*Lancaster University, Physics Department,
14 Lancaster, LA1 4YB, UK*

15 ^f*University of Geneva, Departement de physique nucleaire et corpusculaire,
16 1211 Geneve, Switzerland*

17 **Abstract**

18 We report the results of the 3-flavour, 5 sample $\nu/\bar{\nu}$ joint analysis, performed by the *VALOR*
19 group, on the Run 1-8 dataset, using data taken in both neutrino and antineutrino beam mode.
20 The goal of this analysis is to search for CP violation by setting limits on δ_{CP} and measure the os-
21 cillation parameters $\sin^2 \theta_{13}$, $\sin^2 \theta_{23}$, Δm_{32}^2 (Δm_{13}^2). Fits are performed under both mass hierarchy
22 hypotheses to show which is preferred by data.

23 The Run 1-8 dataset corresponds to an integrated J-PARC neutrino beam exposure of 1.4734×10^{21}
24 POT in neutrino mode and 7.558×10^{20} POT in antineutrino mode.

25 This analysis predicts 268.4 ± 11.8 (syst) for neutrino μ -like, 64.3 ± 2.4 (syst) for antineutrino
26 μ -like, 73.5 ± 5.3 (syst) for neutrino e -like, and 7.9 ± 0.6 (syst) for antineutrino e -like single-ring
27 0π events in Super-K and 6.9 ± 1.5 (syst) ν_e CC1 π^+ events, given the oscillation parameters of the
28 Asimov data set A in 2.1.1. We observe respectively 240 for neutrino μ -like, 68 for antineutrino
29 μ -like, 74 for neutrino e -like, 7 for antineutrino e -like and 15 for ν_e CC1 π^+ -like.

30 **Contents**

31	1 Introduction	4
32	1.1 Analysis procedure	4
33	1.1.1 Feldman-Cousins	6
34	2 Super-K samples used in the analysis	8
35	2.1 Predicted event rates	8
36	2.1.1 Definition of Asimov A and B	8
37	2.1.2 Event rates	9
38	2.1.3 Predicted and observed spectra	11
39	3 Systematic effects in the prediction of the single μ-like ring event energy spectrum	14
40	3.1 Flux and cross-section parameters (73 parameters)	14
41	3.1.1 Neutrino-nucleus interaction uncertainties	15
42	3.2 Super-K efficiencies & effects of intranuclear and secondary re-interactions (44 pa-	
43	rameters)	18
44	3.3 Super-K energy scale (1 parameter)	18
45	3.4 Oscillation parameters and mass hierarchy (7 parameters)	20
46	3.5 Systematic error on Super-K predictions	20
47		
48	4 Sensitivity studies	38
49	4.1 Asimov data sets	38
50	4.2 Results for Asimov sets A and B	39
51	4.2.1 Results for δ_{CP} vs $\sin^2 \theta_{13}$	39
52	4.2.2 Results for Δm_{32}^2 vs $\sin^2 \theta_{23}$	40
53	4.2.3 Results for δ_{CP}	41
54	4.2.4 Results for $\sin^2 \theta_{13}$	42
55	4.2.5 Results for $\sin^2 \theta_{23}$	43
56	4.2.6 Results for Δm_{32}^2	44
57	4.2.7 Comparison with previous analysis	44
58	5 Results of the $\nu\bar{\nu}$ joint analysis with the Run 1-8 dataset	45
59	5.1 Results for δ_{CP} vs $\sin^2 \theta_{13}$	49
60	5.2 Results for Δm_{32}^2 vs $\sin^2 \theta_{23}$	49
61	5.3 Results for δ_{CP}	50
62	5.4 Results for $\sin^2 \theta_{13}$	50
63	5.5 Results for $\sin^2 \theta_{23}$	51
64	5.6 Results for Δm_{32}^2	51
65	5.7 Feldman-Cousins simultaneous fit of δ_{CP} and mass hierarchy	51

66	5.7.1 Input oscillation parameters	52
67	5.7.2 Feldman-Cousins critical values and confidence intervals	53
68	5.8 Discussion of the Run 1-8 data fit results	53
69	5.9 Comparison of δ_{CP} versus mass hierarchy result with sensitivity	54
70	5.9.1 Expected sensitivity method	54
71	5.9.2 $\delta_{CP} = -\pi/2$ - normal hierarchy	55
72	5.10 Comparison of e -like event rates with expectation	55
73	6 Summary	60
74	Appendices	67
75	A Fitter details	67
76	A.1 Spectra prediction methodology	67
77	A.2 Construction of the nominal Super-K Monte Carlo templates	67
78	A.2.1 Normalisation of Monte Carlo samples	67
79	A.2.2 List of Monte Carlo templates	68
80	A.2.3 Binning of Monte Carlo templates	70
81	A.3 Applying neutrino oscillations	71
82	B Event rates	73
83	C Systematic variations	77
84	D Marginalisation studies	88
85	E Effect of systematic errors on Super-K predictions	91
86	F Effect of ν_e CC1π^+sample on constraint strength	93
87	G Matter effects and crust density	95
88	H Asimov B δ_{CP}/mass-hierarchy degeneracy	97

89 **1. Introduction**

90 In this technical note, we report the results of a 3-flavour $\nu/\bar{\nu}$ joint analysis performed by the
91 *VALOR* group, on the combined Run 1-8 dataset, using data taken in both neutrino-enhanced
92 forward horn current (FHC) mode (1.4734×10^{21} POT), and antineutrino-enhanced reverse horn
93 current (RHC) mode (7.558×10^{20} POT).

94 This analysis updates the previous analyses based on the additional data gathered at Super-K,
95 a new cross-section model and a change in the Super-K reconstruction method.

96 Section 2 describes the Super-K samples, section 3 describes the systematic errors considered
97 and their effects on the extrapolated single-ring event spectra, whilst the sensitivity of the various
98 fits is considered in section 4 before presenting the fit results in section 5.

99 In this analysis we move from the APFit reconstruction algorithm to the fiTQun algorithm [17].
100 Selection cuts are revisited and a significant improvement in statistics is achieved by modifying the
101 fiducial volume cuts to allow for a larger interaction mass [16]. This analysis includes new cross-
102 section model parameters. A 2p-2h shape parameter is added to the 2p2h normalisation parameters
103 already present in the previous analysis. Furthermore, the Random Phase Approximation (RPA)
104 is parameterised by a Bernstein polynomial (BeRPA) [15]. Each of these new parameters will be
105 described in section 3.

106 Confidence intervals for δ_{CP} are produced using the Feldman-Cousins method (see section 1.1.1),
107 while confidence intervals of the other oscillation parameters are set using the constant $\Delta\chi^2$ method.
108 Sensitivity studies are shown in section 4. The results of the measurement using the Run 1-8 dataset
109 are given in section 5 of this note.

110 Finally, a summary is given in section 6.

111 *1.1. Analysis procedure*

112 This analysis builds on our previous analysis in [12]. In this analysis we fit Super-K data using
113 a hybrid frequentist-Bayesian method [70], which consists of marginalising instead of profiling the
114 nuisance parameters. A description of the method can be found in section 4.2 of [10].

115 The analysis uses a binned likelihood-ratio method [66] where the estimation of the parameters of
116 interest, $\vec{\theta}$, is obtained by comparing the observed and predicted Super-K spectra for 1-ring events.
117 For the two one-ring μ -like samples the binning of data events is in one-dimensional reconstructed
118 neutrino energy space, whilst the three one-ring e -like samples bin data events in two-dimensional
119 reconstructed neutrino energy and lepton angle space.

120 The 2D binning scheme used for the e -like samples is to improve the separation of the different
121 reaction / flavour components, in particular $\bar{\nu}_\mu \rightarrow \bar{\nu}_e$ and $\nu_\mu \rightarrow \nu_e$, fundamental in measuring δ_{CP} .
122 The ν_e intrinsic beam and NC components can also be better separated from signal.

123 μ -like templates have 84 true energy bins and 73 reconstructed energy bins. e -like templates
124 have 84 true energy bins, 25 reconstructed energy bins and 15 reconstructed lepton angle bins.

125 For all templates the 84 true energy bins of constant width are the following:

- 126 • 6 50-MeV bins from 0-0.3 GeV,

₁₂₇ • 28 25-MeV bins from 0.3-1 GeV,

₁₂₈ • 40 50-MeV bins from 1-3 GeV,

₁₂₉ • 5 100-MeV bin from 3-3.5 GeV,

₁₃₀ • 1 bin from 3.5-4 GeV,

₁₃₁ • 1 bin from 4-5 GeV,

₁₃₂ • 1 bin from 5-7 GeV,

₁₃₃ • 1 bin from 7-10 GeV and

₁₃₄ • 1 bin from 10-30 GeV

₁₃₅ For μ -like samples the 73 reconstructed energy bins are the following:

₁₃₆ • 60 50-MeV bins from 0-3 GeV,

₁₃₇ • 4 250-MeV bins from 3-4 GeV,

₁₃₈ • 4 500-MeV bins from 4-6 GeV,

₁₃₉ • 4 1000-MeV bins from 6-10 GeV and

₁₄₀ • 1 bin from 10-30 GeV.

₁₄₁ For e -like samples the 25 reconstructed energy bins with constant width are the following:

₁₄₂ • 25 50-MeV bins from 0-1.25 GeV.

₁₄₃ The θ binning used for e -like samples is

₁₄₄ • 14 10° bins from 0° to 140° ,

₁₄₅ • 1 bin for the range $140^\circ - 180^\circ$.

₁₄₆ The method of calculation of these predicted spectra is presented in Appendix A. This analysis
₁₄₇ uses flux tuning based on NA61/SHINE 2009 data [23][60]. It also uses a model-based extrapolation
₁₄₈ from ND280 to Super-K, which is implemented via a fit of flux model and cross-section model pa-
₁₄₉ rameters to ND280 measurements of the muon momentum-angle distributions of $\bar{\nu}_\mu$ and ν_μ charged
₁₅₀ current interaction candidates for different event topologies with the neutrino interaction vertex
₁₅₁ either in FGD1 or FGD2 (BANFF fit) [36].

₁₅₂ The log-likelihood function used in the analysis is

$$-2 \ln \lambda(\vec{\theta}, \mathbf{a}) = 2 \cdot \sum_{i=0}^{N-1} \left(n_i^{obs} \cdot \ln(n_i^{obs}/n_i^{exp}) + (n_i^{exp} - n_i^{obs}) \right) \quad (1)$$

153 where n_i^{obs} is the observed number of events in the i^{th} bin and $n_i^{exp} = n_i^{exp}(\vec{\theta}; \mathbf{a})$ is the corresponding
 154 expected number of events, N is the number of reconstructed energy and lepton angle bins and \mathbf{a}
 155 is a vector of systematic parameters.

156 The total likelihood is then given by the sum of $-2 \ln \lambda(\vec{\theta}, \mathbf{a})$ from all of the Super-K samples

$$-2 \ln \lambda(\vec{\theta}, \mathbf{a}) = \sum_{s=1}^{N_{samples}} -2 \ln \lambda_s(\vec{\theta}, \mathbf{a}) \quad (2)$$

157 The postfit errors of covariance matrices which result from the BANFF fit and Super-K fits
 158 are used as prior uncertainties. The parameters are thrown using the Cholesky method, which
 159 allows throws according the parameters' multivariate distribution and existing correlations. Where
 160 systematic parameters have physical boundaries, any toy experiment where such a parameter is
 161 generated beyond its physical limits is rejected. Furthermore, values of systematic parameters that
 162 give a negative predicted number of events in any reconstructed energy bin in any interaction mode
 163 are not allowed. If a systematic throw gives a negative number of events, that toy experiment is
 164 rejected. All rejected toys are regenerated.

165 A single set of oscillation parameters in the 3-flavour framework is used to describe both neu-
 166 trino and antineutrino data. All 6 oscillation parameters float in the fit, with nuisance oscillation
 167 parameters marginalised while the parameters of interest are minimized with respect to the likeli-
 168 hood distribution. Flat priors are used for $\sin^2 \theta_{23}$, Δm_{32}^2 and δ_{CP} in all fits, whereas $\sin^2 \theta_{13}$ uses a
 169 flat prior when not applying constraints from reactor experiments and a gaussian prior when using
 170 the measurement found in reactor experiments. $\sin^2 \theta_{12}$ and Δm_{21}^2 uses gaussian priors in all fits
 171 due to the limited sensitivity of T2K to the solar parameters. Fits are performed for each mass
 172 hierarchy and both with and without the reactor constraint applied.

173 Oscillation probabilities include constant-density matter effects, with details of our oscillation
 174 probability calculations, estimates of their numerical accuracy and comparisons with calculations
 175 used by the alternative T2K oscillation analyses are given in Appendices A and B of Ref. [4].

176 1.1.1. Feldman-Cousins

177 In the gaussian approximation the constant $\Delta\chi^2$ method can be used. However, the oscillation
 178 probability is not linear in oscillation parameters and so in some cases the gaussian approximation is
 179 not reliable and the Feldman-Cousins method [69] must be used. In this method a different critical
 180 value for each point of the $\vec{\theta}$ grid, $\Delta\chi^2(\vec{\theta})_{crit}$, is calculated. Since the most important result of this
 181 analysis is the search for CP violation, this method is performed only for the simultaneous fit of
 182 δ_{CP} and mass hierarchy. In particular, critical values are calculated for 9 evenly spaced true values
 183 of δ_{CP} in the range $[-\pi, +\pi]$ for both normal and inverted mass hierarchy, and linearly interpolated
 184 between these points.

185 In the previous analysis the Feldman-Cousins implementation used the disappearance likelihood
 186 surface from the best-fit of the data to generate fake data sets during the procedure. However, this
 187 approach causes the critical values to become smaller in the vicinity of the best-fit for δ_{CP} because
 188 the generated fake data sets are closer to the real data. The new method [89] instead uses the data

best-fit for disappearance parameters, along with the PDG 2016 best-fit values for the remaining oscillation parameters (table 1), to perform additional Asimov fits in normal and inverted hierarchy. It is then the likelihood surfaces from these fits that are used to generate the fake data sets during the procedure. The procedure consists of the following steps:

1. At least 1×10^4 fake data sets are produced assuming the oscillation hypothesis of the grid point $\vec{\theta}$ and taking into account both the statistical and systematic uncertainties (i.e. nuisance parameters, including non-fit oscillation parameters, are marginalised);
2. For each fake data set:
 - (a) $\chi^2(\vec{\theta}_{fix})$ is obtained by computing $\chi^2(\vec{\theta})$ with respect to the marginalisation toys produced for the data fit, with the oscillation parameters $\vec{\theta}$ fixed to the values corresponding to the grid point.
 - (b) $\chi^2(\vec{\theta}_{bf})$ is obtained by minimizing $\chi^2(\vec{\theta})$ with respect to the marginalisation toys produced for the data fit, leaving the oscillation parameters $\vec{\theta}$ free.
 - (c) The test statistic is calculated as

$$\Delta\chi^2 = \chi^2(\vec{\theta}_{fix}) - \chi^2(\vec{\theta}_{bf}) \quad (3)$$

3. This results in a distribution of $\Delta\chi^2(\vec{\theta})$, $f(\Delta\chi^2)$.
4. Several critical values for $X\%$ CL (e.g. 68%, 90%...), $\Delta\chi^2(\vec{\theta})_{crit}$, can be defined as:

$$\Delta\chi^2_{crit} : \int_0^{\Delta\chi^2_{crit}} f(\Delta\chi^2) d(\Delta\chi^2) = X\% \quad (4)$$

where $f(\Delta\chi^2)$ is the p.d.f. of $\Delta\chi^2$ and $d(\Delta\chi^2)$ is the differential of the integral.

5. This procedure is repeated to produce critical values for all the points of the $\vec{\theta}$ grid.

Once a critical value, $\Delta\chi^2(\vec{\theta})_{crit}$, is computed for each oscillation hypothesis in the $\vec{\theta}$ grid, the confidence intervals are set by the condition

$$\Delta\chi^2(\vec{\theta}) > \Delta\chi^2_{crit} \quad (5)$$

with those values of $\Delta\chi^2(\vec{\theta})$ being excluded at the relevant confidence interval.

210 **2. Super-K samples used in the analysis**

211 This analysis is comprised of five samples based on the fitQun selection algorithm, which has
 212 improved reconstruction capabilities and can therefore reduce the background components of the
 213 selected samples. The five samples are:

- 214 • neutrino mode single μ -like ring sample
- 215 • antineutrino mode single μ -like ring sample
- 216 • neutrino mode single e -like ring sample
- 217 • antineutrino mode single e -like ring sample
- 218 • neutrino mode single e -like ring sample with one decay electron (referred to as ν_e CC1 π^+)

219 The Super-K MC templates contain events from the ν_μ , $\bar{\nu}_\mu$, ν_e , $\bar{\nu}_e$, oscillated ν_e and oscillated $\bar{\nu}_e$
 220 samples passing the Super-K selection cuts. Details of the selection cuts can be found in [42].

221 *2.1. Predicted event rates*

222 Predicted event rates for this analysis are determined for the case of two different sets of oscil-
 223 lation parameters based on previous best fit results from T2K and NOvA. These parameter sets
 224 are referred to as Asimov A and B, with their definitions and associated event rates given in the
 225 following sections.

226 *2.1.1. Definition of Asimov A and B*

227 Table 1 shows the definitions used for the Asimov data sets. Asimov A represents parameter
 228 values close to the T2K best fit for Run 1-7, whilst Asimov B modifies these parameters such that
 229 CP is conserved and changes the $\sin^2 \theta_{23}$ octant.

Parameter(s)	Asimov A	Asimov B
$\sin^2 \theta_{23}$	0.528	0.450
$\sin^2 \theta_{13}$ reactors	0.0219	0.0219
$\sin^2 \theta_{12}$	0.304	0.304
$ \Delta m_{32}^2 $ (NH) / $ \Delta m_{31}^2 $ (IH)	2.509×10^{-3} eV $^2/c^4$	2.509×10^{-3} eV $^2/c^4$
Δm_{21}^2	7.53×10^{-5} eV $^2/c^4$	7.53×10^{-5} eV $^2/c^4$
δ_{CP}	-1.601	0
Mass Hierarchy	Normal	Normal

Table 1: Values of oscillation parameters used to compute the event rates, systematic effects and sensitivity studies. Each set of oscillation parameters correspond to a different Asimov data set, which is the MC expected distribution in a certain oscillation hypothesis. In the Asimov data set A the nominal values of $\sin^2 2\theta_{13}$, $\sin^2 2\theta_{12}$ and Δm_{21}^2 are from [81], while all the other oscillation parameter values corresponds to the most probable values obtained by the Bayesian analysis on the T2K run 1-4 neutrino mode data [20]. The mass hierarchy is not marginalised but fixed to either NH or IH.

230 2.1.2. Event rates

231 Table 2 shows the expected event rates in Super-K for the Asimov A data set, but with δ_{CP}
 232 varied at $-\pi/2$, 0 , $\pi/2$ and π .

	$\delta_{CP} = -\pi/2$	$\delta_{CP} = 0$	$\delta_{CP} = \pi/2$	$\delta_{CP} = \pi$
FHC e -like sample	73.47354	61.43388	49.90582	61.94533
FHC μ -like sample	268.40351	268.05327	268.37281	268.81441
FHC ν_e CC1 π^+ -like sample	6.92243	6.00922	4.86656	5.77983
RHC e -like sample	7.91206	9.02311	10.02989	8.91886
RHC μ -like sample	64.27306	64.12292	64.27392	64.43654

Table 2: Predicted total number of events in each sample obtained after applying the BANFF weight for a total exposure of 1.4734×10^{21} POT. The Asimov data set A in 1 is used, but with varying δ_{CP} .

233 Tables 3 to 7 present the expected event rates in Super-K corresponding to the Asimov A data
 234 set. Event rates in other oscillation scenarios can be found in Appendix B. In each case the normal
 235 hierarchy is assumed and all rates are generated for an integrated exposure corresponding to Run
 236 1-8.

	ν_μ	ν_e	$\bar{\nu}_\mu$	$\bar{\nu}_e$	Osc. ν_e	Osc. $\bar{\nu}_e$	Total
CCQE	175.62883	0.00413	11.03473	0.00019	0.02245	0.00015	186.69049
CC1pi	27.69898	0.00199	2.61604	0.00009	0.02406	0.00007	30.34123
CCcoherent	0.28837	0.00000	0.09218	0.00000	0.00000	0.00000	0.38055
2p2h	35.57284	0.00151	1.41213	0.00008	0.02551	0.00004	37.01211
CCother	5.46647	0.00086	0.40615	0.00008	0.00011	0.00001	5.87368
NC1pi0	0.61495	0.01841	0.02120	0.00143	N/A	N/A	0.65599
NC1piPM	4.90783	0.09799	0.17531	0.00975	N/A	N/A	5.19089
NCcoherent	0.00000	0.00000	0.00043	0.00003	N/A	N/A	0.00047
NCother	2.05619	0.07378	0.13055	0.00912	N/A	N/A	2.26963
Total	252.23446	0.19867	15.88872	0.02078	0.07214	0.00027	268.41504

Table 3: Predicted number of events in the neutrino mode μ -like sample obtained after applying the BANFF weight for a total exposure of 1.4734×10^{21} POT. The Asimov data set A in 1 is used.

	ν_μ	ν_e	$\bar{\nu}_\mu$	$\bar{\nu}_e$	Osc. ν_e	Osc. $\bar{\nu}_e$	Total
CCQE	15.29349	0.00085	29.88622	0.00093	0.00094	0.00137	45.18379
CC1pi	3.95485	0.00033	4.53265	0.00025	0.00060	0.00061	8.48929
CCcoherent	0.04705	0.00000	0.17567	0.00005	0.00000	0.00006	0.22283
2p2h	4.47453	0.00026	2.84291	0.00027	0.00044	0.00021	7.31861
CCother	0.94199	0.00012	0.60584	0.00000	0.00000	0.00000	1.54795
NC1pi0	0.06000	0.00222	0.06147	0.00169	N/A	N/A	0.12538
NC1piPM	0.35950	0.01527	0.46009	0.01235	N/A	N/A	0.84721
NCcoherent	0.00000	0.00000	0.00201	0.00000	N/A	N/A	0.00201
NCother	0.31580	0.01640	0.20064	0.00789	N/A	N/A	0.54073
Total	25.44720	0.03544	38.76749	0.02342	0.00198	0.00226	64.27780

Table 4: Predicted number of events in the antineutrino mode μ -like sample obtained after applying the BANFF weight for a total exposure of 7.558×10^{20} POT. The Asimov data set A in 1 is used.

	ν_μ	ν_e	$\bar{\nu}_\mu$	$\bar{\nu}_e$	Osc. ν_e	Osc. $\bar{\nu}_e$	Total
CCQE	0.16115	6.30178	0.00634	0.25566	46.25561	0.27811	53.25866
CC1pi	0.04703	0.93168	0.00280	0.06750	4.49505	0.04745	5.59150
CCcoherent	0.00011	0.00830	0.00018	0.00397	0.03445	0.00327	0.05028
2p2h	0.03033	1.59694	0.00117	0.04275	8.68112	0.03893	10.39125
CCother	0.01329	0.12803	0.00034	0.00942	0.08850	0.00326	0.24284
NC1pi0	1.70203	0.03706	0.06012	0.00356	N/A	N/A	1.80278
NC1piPM	0.16854	0.00472	0.01020	0.00057	N/A	N/A	0.18404
NCcoherent	0.52817	0.00715	0.04794	0.00294	N/A	N/A	0.58619
NCother	0.31767	0.01695	0.02120	0.00128	N/A	N/A	0.35711
NC1gamma	0.94222	0.01687	0.04983	0.00233	N/A	N/A	1.01125
Total	3.91054	9.04948	0.20014	0.38998	59.55473	0.37103	73.47589

Table 5: Predicted number of events in the neutrino mode e -like sample obtained after applying the BANFF weight for a total exposure of 1.4734×10^{21} POT. The Asimov data set A in 1 is used.

	ν_μ	ν_e	$\bar{\nu}_\mu$	$\bar{\nu}_e$	Osc. ν_e	Osc. $\bar{\nu}_e$	Total
CCQE	0.01288	0.50911	0.02388	0.84721	1.02586	2.85198	5.27090
CC1pi	0.00763	0.10111	0.00733	0.14431	0.14337	0.33485	0.73858
CCcoherent	0.00002	0.00099	0.00042	0.01066	0.00114	0.03130	0.04455
2p2h	0.00295	0.14379	0.00219	0.11301	0.23285	0.33042	0.82521
CCother	0.00390	0.02116	0.00120	0.01154	0.01042	0.00668	0.05491
NC1pi0	0.13849	0.00541	0.17659	0.00468	N/A	N/A	0.32516
NC1piPM	0.02475	0.00127	0.02001	0.00080	N/A	N/A	0.04683
NCcoherent	0.04776	0.00221	0.20260	0.00317	N/A	N/A	0.25574
NCother	0.05664	0.00221	0.02672	0.00097	N/A	N/A	0.08654
NC1gamma	0.07943	0.00439	0.17490	0.00383	N/A	N/A	0.26255
Total	0.37445	0.79164	0.63583	1.14019	1.41363	3.55523	7.91097

Table 6: Predicted number of events in the antineutrino mode e -like sample obtained after applying the BANFF weight for a total exposure of 1.4734×10^{21} POT. The Asimov data set A in 1 is used.

	ν_μ	ν_e	$\bar{\nu}_\mu$	$\bar{\nu}_e$	Osc. ν_e	Osc. $\bar{\nu}_e$	Total
CCQE	0.02857	0.02442	0.00117	0.00174	0.21123	0.00265	0.26979
CC1pi	0.07582	0.76065	0.00257	0.00383	4.85325	0.00227	5.69839
CCcoherent	0.00027	0.01765	0.00008	0.00007	0.11121	0.00011	0.12939
2p2h	0.01012	0.02195	0.00049	0.00095	0.16017	0.00105	0.19473
CCother	0.03770	0.11225	0.00116	0.00279	0.12085	0.00150	0.27625
NC1pi0	0.02049	0.00076	0.00083	0.00008	N/A	N/A	0.02216
NC1piPM	0.06474	0.00165	0.00382	0.00033	N/A	N/A	0.07053
NCother	0.20584	0.00830	0.01304	0.00088	N/A	N/A	0.22807
NC1gamma	0.02844	0.00000	0.00067	0.00007	N/A	N/A	0.02918
Total	0.47199	0.94764	0.02382	0.01075	5.45671	0.00758	6.91850

Table 7: Predicted number of events in the neutrino mode ν_e CC1 π^+ -like sample obtained after applying the BANFF weight for a total exposure of 1.4734×10^{21} POT. The Asimov data set A in 1 is used.

237 *2.1.3. Predicted and observed spectra*

238 In this section, we present the expected spectra in Super-K for Asimov A and unoscillated sce-
 239 narios, assuming normal hierarchy. All plots are generated for an integrated exposure corresponding
 240 to Run 1-8.

241 Predicted single ring Super-K spectra are shown in figs. 1 and 2. By comparing neutrino and
 242 antineutrino mode e -like plots it is clear that θ vs E_{reco} distributions are differently populated by
 243 $\nu_\mu \rightarrow \nu_e$ and $\bar{\nu}_\mu \rightarrow \bar{\nu}_e$ events.

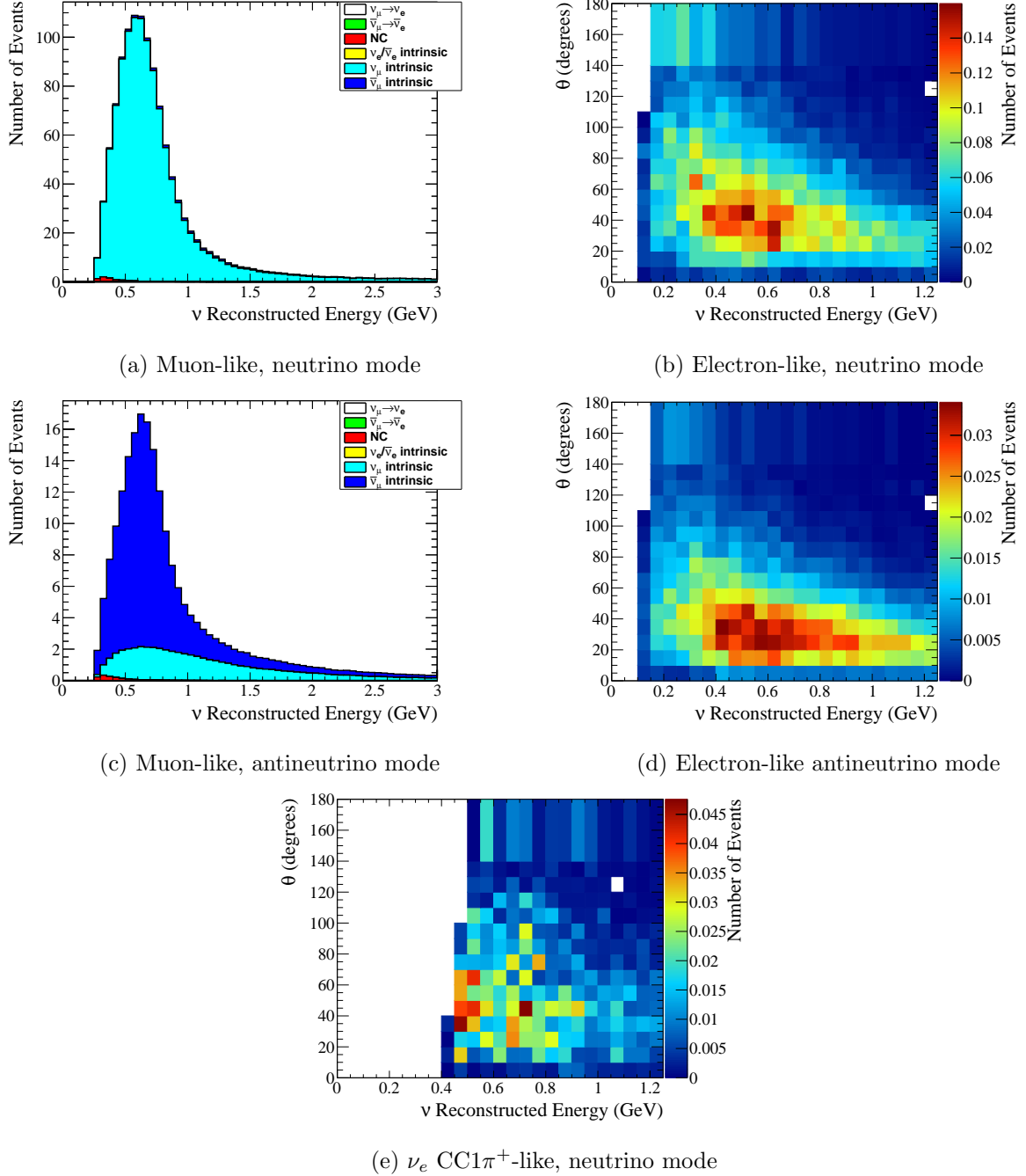


Figure 1: Predicted unsoscillated spectra. μ -like distributions are a function of the reconstructed neutrino energy, while the e -like, including ν_e CC1 π^+ , distributions are functions of both the reconstructed neutrino energy and the reconstructed angle between the outgoing lepton and the neutrino direction. The distributions correspond to the statistics collected in the full Run 1-8 data set. The spectra are generated with the systematic parameters described in section 3.

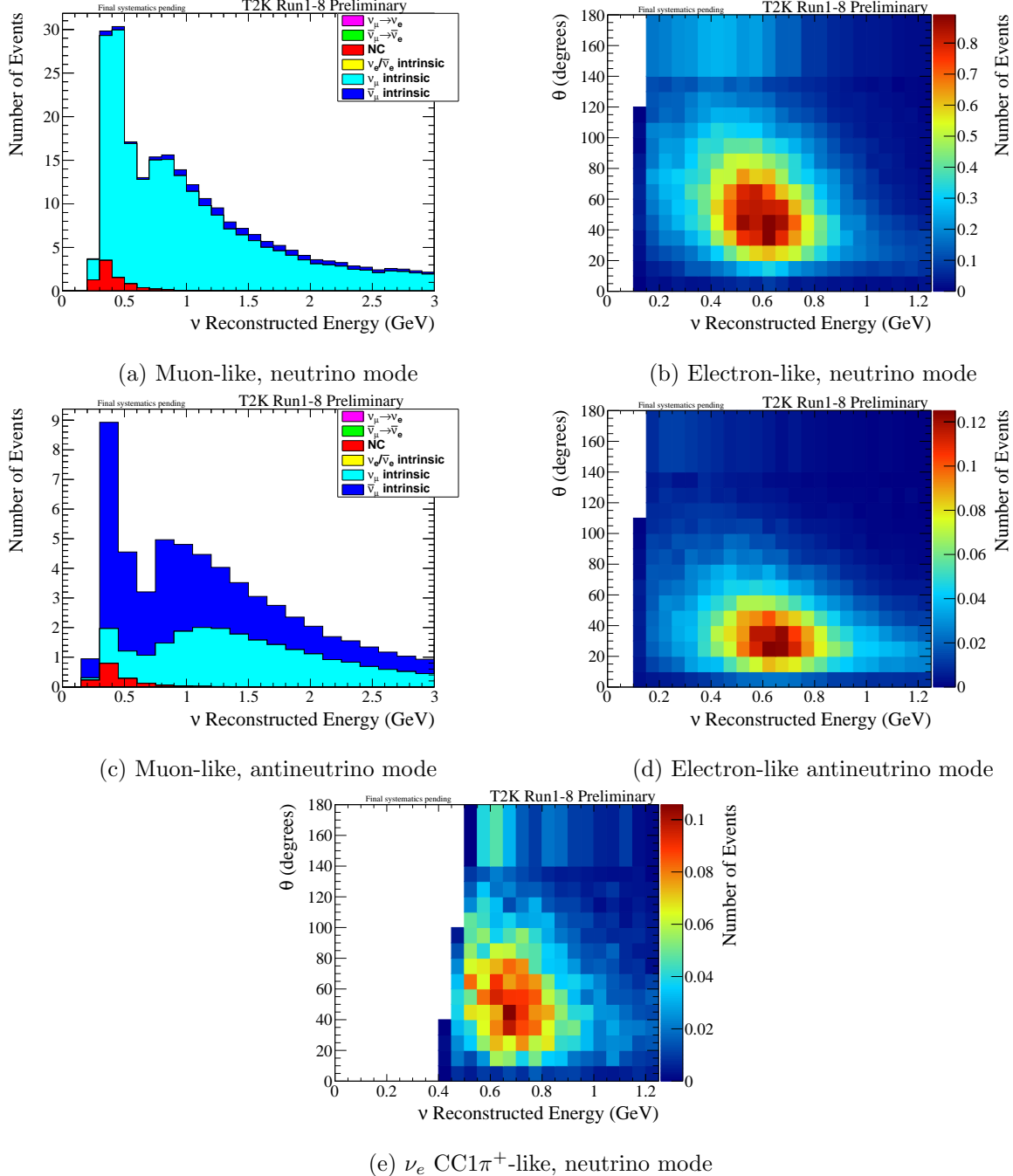


Figure 2: Predicted Asimov A spectra. μ -like distributions are a function of the reconstructed neutrino energy, while the e -like, including ν_e CC1 π^+ , distributions are functions of both the reconstructed neutrino energy and the reconstructed angle between the outgoing lepton and the neutrino direction. The distributions correspond to the statistics collected in the full Run 1-8 data set. The spectra are generated with the systematic parameters described in section 3 and the oscillation parameters corresponding to the Asimov data set A shown in table 1.

244 **3. Systematic effects in the prediction of the single μ -like ring event energy spectrum**

245 This analysis considers 110 flux, cross section and Super-K detector systematic parameters plus
 246 7 oscillation parameters, which can be treated as either nuisance ps or as parameters of interest,
 247 depending on the analysis that is performed.

248 *3.1. Flux and cross-section parameters (73 parameters)*

249 In this analysis, all the flux and cross-section systematic parameters are included in the ND280
 250 data (BANFF) fit. However, since ND280 is not sensitive to the electron neutrino cross section and
 251 the NC1 γ parameters they remain unconstrained. The parameters fit are 11 ν_μ , 5 $\bar{\nu}_\mu$, 7 ν_e and 2
 252 $\bar{\nu}_e$ neutrino mode (FHC) flux parameters, 5 ν_μ , 11 $\bar{\nu}_\mu$, 2 ν_e and 7 $\bar{\nu}_e$ antineutrino mode (RHC) flux
 253 parameters and 23 cross-section parameters. Best-fit values of these parameters and a covariance
 254 matrix giving their correlated uncertainties are obtained by the BANFF group from a fit of the $\bar{\nu}_\mu$
 255 and ν_μ ND280 samples as described in Ref [36]. A list of the BANFF parameters, their best-fit
 256 values and their prefit and postfit errors can be found in tables 8 to 10.

257 The best-fit values are used to reweight the templates as described in Appendix A, and the
 258 postfit errors in the covariance matrix are used as prior uncertainties in this analysis. All the cross
 259 section parameters set to 1 correspond to the NEUT nominal value, except “CC other shape” and
 260 “2p2h shape O”, for which the NEUT nominal value is 0. For all the normalisation parameters, 1
 261 is the nominal pre-BANFF fit value.

262 The effects of these correlated uncertainties (see fig. 3) are evaluated using the Cholesky method,
 263 that allows throws of the systematic parameters according to their multivariate distribution taking
 264 into account existing correlations.

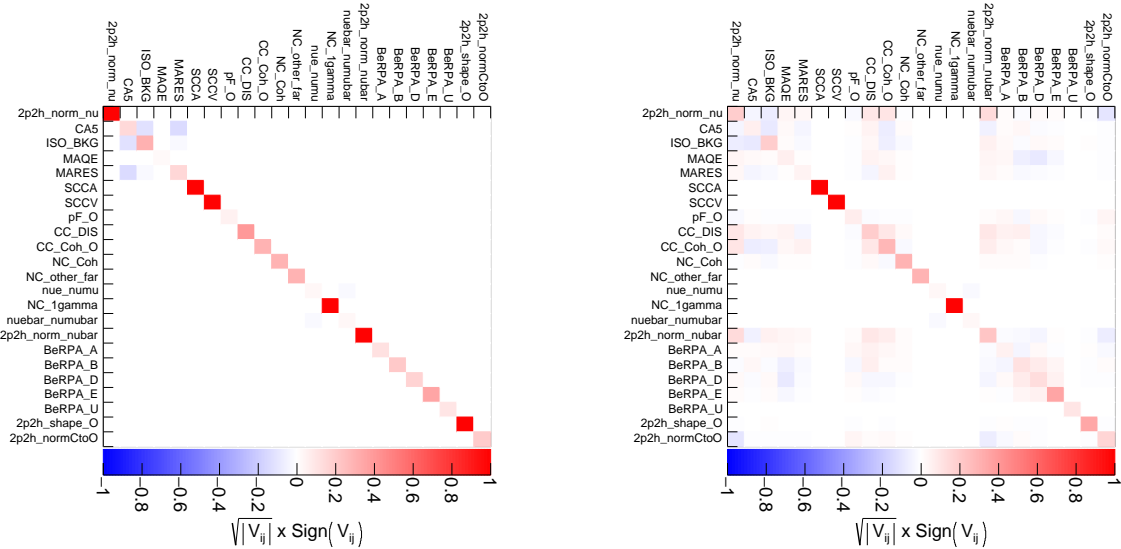


Figure 3: The pre-BANFF (left) and post-BANFF (right) cross-section covariance matrix, with the values shown as the sign of the element times the square root of the absolute value of the element.

Index	Parameter	Description	Best fit	1σ pre/postfit fractional error
0	$f_{0;t,r}^{banff}$	FHC ν_μ flux normalisation, E = 0.0 - 0.4 GeV	1.026	0.099 / 0.057
1	$f_{1;t,r}^{banff}$	FHC ν_μ flux normalisation, E = 0.4 - 0.5 GeV	1.050	0.103 / 0.052
2	$f_{2;t,r}^{banff}$	FHC ν_μ flux normalisation, E = 0.5 - 0.6 GeV	1.032	0.096 / 0.045
3	$f_{3;t,r}^{banff}$	FHC ν_μ flux normalisation, E = 0.6 - 0.7 GeV	0.991	0.087 / 0.042
4	$f_{4;t,r}^{banff}$	FHC ν_μ flux normalisation, E = 0.7 - 1.0 GeV	0.943	0.113 / 0.054
5	$f_{5;t,r}^{banff}$	FHC ν_μ flux normalisation, E = 1.0 - 1.5 GeV	0.963	0.092 / 0.049
6	$f_{6;t,r}^{banff}$	FHC ν_μ flux normalisation, E = 1.5 - 2.5 GeV	1.030	0.070 / 0.042
7	$f_{7;t,r}^{banff}$	FHC ν_μ flux normalisation, E = 2.5 - 3.5 GeV	1.047	0.074 / 0.044
8	$f_{8;t,r}^{banff}$	FHC ν_μ flux normalisation, E = 3.5 - 5.0 GeV	1.038	0.087 / 0.041
9	$f_{9;t,r}^{banff}$	FHC ν_μ flux normalisation, E = 5.0 - 7.0 GeV	1.003	0.098 / 0.040
10	$f_{10;t,r}^{banff}$	FHC ν_μ flux normalisation, E = 7.0 - 30.0 GeV	0.991	0.114 / 0.048
11	$f_{11;t,r}^{banff}$	FHC $\bar{\nu}_\mu$ flux normalisation, E = 0.0 - 0.7 GeV	0.989	0.103 / 0.074
12	$f_{12;t,r}^{banff}$	FHC $\bar{\nu}_\mu$ flux normalisation, E = 0.7 - 1.0 GeV	0.986	0.079 / 0.048
13	$f_{13;t,r}^{banff}$	FHC $\bar{\nu}_\mu$ flux normalisation, E = 1.0 - 1.5 GeV	0.996	0.084 / 0.057
14	$f_{14;t,r}^{banff}$	FHC $\bar{\nu}_\mu$ flux normalisation, E = 1.5 - 2.5 GeV	1.042	0.086 / 0.062
15	$f_{15;t,r}^{banff}$	FHC $\bar{\nu}_\mu$ flux normalisation, E = 2.5 - 30.0 GeV	1.104	0.086 / 0.065
16	$f_{16;t,r}^{banff}$	FHC ν_e flux normalisation, E = 0.0 - 0.5 GeV	1.030	0.090 / 0.046
17	$f_{17;t,r}^{banff}$	FHC ν_e flux normalisation, E = 0.5 - 0.7 GeV	1.031	0.090 / 0.042
18	$f_{18;t,r}^{banff}$	FHC ν_e flux normalisation, E = 0.7 - 0.8 GeV	1.029	0.086 / 0.041
19	$f_{19;t,r}^{banff}$	FHC ν_e flux normalisation, E = 0.8 - 1.5 GeV	1.017	0.081 / 0.039
20	$f_{20;t,r}^{banff}$	FHC ν_e flux normalisation, E = 1.5 - 2.5 GeV	1.034	0.079 / 0.040
21	$f_{21;t,r}^{banff}$	FHC ν_e flux normalisation, E = 2.5 - 4.0 GeV	1.036	0.084 / 0.041
22	$f_{22;t,r}^{banff}$	FHC ν_e flux normalisation, E = 4.0 - 30.0 GeV	1.050	0.094 / 0.059
23	$f_{23;t,r}^{banff}$	FHC $\bar{\nu}_e$ flux normalisation, E = 0.0 - 2.5 GeV	1.050	0.074 / 0.054
24	$f_{24;t,r}^{banff}$	FHC $\bar{\nu}_e$ flux normalisation, E = 2.5 - 30.0 GeV	1.093	0.128 / 0.114

Table 8: Summary of neutrino mode flux systematics included in the VALOR joint fit analysis. A description of how the BANFF fit constrained these systematics can be found in [36].

Many of the cross-section parameters are the same as those used in the previous analysis [12]. However, the binding energy for ^{16}O is no longer included in this analysis and a number of new parameters have been included, see section 3.1.1. Five of these new parameters (2p2h, BeRPA A, B, D and E) are implemented using cubic splines, details for which can be found in [12], while one of the new parameters (BeRPA U) is fixed in the analysis.

3.1.1. Neutrino-nucleus interaction uncertainties

Overall normalisation uncertainties for 2p2h interactions were included in previous analyses, but this analysis includes a 2p2h shape uncertainty (using best-fit value and errors from the BANFF fit) to describe the uncertainty in the cross-section strength between Delta-like, non-Delta-like and interference terms of the 2p2h model, determined by redistributing the cross-section strength of

Index	Parameter	Description	Best fit	1σ pre/postfit fractional error
25	$f_{0;t,r}^{banff} RHC$	RHC ν_μ flux normalisation, E = 0.0 - 0.7 GeV	0.993	0.094 / 0.066
26	$f_{1;t,r}^{banff} RHC$	RHC ν_μ flux normalisation, E = 0.7 - 1.0 GeV	1.003	0.079 / 0.049
27	$f_{2;t,r}^{banff} RHC$	RHC ν_μ flux normalisation, E = 1.0 - 1.5 GeV	1.018	0.077 / 0.045
28	$f_{3;t,r}^{banff} RHC$	RHC ν_μ flux normalisation, E = 1.5 - 2.5 GeV	1.061	0.081 / 0.049
29	$f_{4;t,r}^{banff} RHC$	RHC ν_μ flux normalisation, E = 2.5 - 30.0 GeV	1.051	0.080 / 0.043
30	$f_{5;t,r}^{banff} RHC$	RHC $\bar{\nu}_\mu$ flux normalisation, E = 0.0 - 0.4 GeV	1.012	0.104 / 0.065
31	$f_{6;t,r}^{banff} RHC$	RHC $\bar{\nu}_\mu$ flux normalisation, E = 0.4 - 0.5 GeV	1.028	0.102 / 0.052
32	$f_{7;t,r}^{banff} RHC$	RHC $\bar{\nu}_\mu$ flux normalisation, E = 0.5 - 0.6 GeV	1.008	0.096 / 0.045
33	$f_{8;t,r}^{banff} RHC$	RHC $\bar{\nu}_\mu$ flux normalisation, E = 0.6 - 0.7 GeV	0.988	0.085 / 0.041
34	$f_{9;t,r}^{banff} RHC$	RHC $\bar{\nu}_\mu$ flux normalisation, E = 0.7 - 1.0 GeV	0.986	0.125 / 0.052
35	$f_{10;t,r}^{banff} RHC$	RHC $\bar{\nu}_\mu$ flux normalisation, E = 1.0 - 1.5 GeV	0.997	0.105 / 0.047
36	$f_{11;t,r}^{banff} RHC$	RHC $\bar{\nu}_\mu$ flux normalisation, E = 1.5 - 2.5 GeV	1.036	0.080 / 0.042
37	$f_{12;t,r}^{banff} RHC$	RHC $\bar{\nu}_\mu$ flux normalisation, E = 2.5 - 3.5 GeV	1.063	0.074 / 0.046
38	$f_{13;t,r}^{banff} RHC$	RHC $\bar{\nu}_\mu$ flux normalisation, E = 3.5 - 5.0 GeV	1.069	0.094 / 0.063
39	$f_{14;t,r}^{banff} RHC$	RHC $\bar{\nu}_\mu$ flux normalisation, E = 5.0 - 7.0 GeV	1.044	0.093 / 0.056
40	$f_{15;t,r}^{banff} RHC$	RHC $\bar{\nu}_\mu$ flux normalisation, E = 7.0 - 30.0 GeV	1.007	0.130 / 0.093
41	$f_{16;t,r}^{banff} RHC$	RHC ν_e flux normalisation, E = 0.0 - 2.5 GeV	1.050	0.069 / 0.047
42	$f_{17;t,r}^{banff} RHC$	RHC ν_e flux normalisation, E = 2.5 - 30.0 GeV	1.048	0.085 / 0.065
43	$f_{18;t,r}^{banff} RHC$	RHC $\bar{\nu}_e$ flux normalisation, E = 0.0 - 0.5 GeV	1.018	0.095 / 0.051
44	$f_{19;t,r}^{banff} RHC$	RHC $\bar{\nu}_e$ flux normalisation, E = 0.5 - 0.7 GeV	1.018	0.091 / 0.043
45	$f_{20;t,r}^{banff} RHC$	RHC $\bar{\nu}_e$ flux normalisation, E = 0.7 - 0.8 GeV	1.016	0.091 / 0.044
46	$f_{21;t,r}^{banff} RHC$	RHC $\bar{\nu}_e$ flux normalisation, E = 0.8 - 1.5 GeV	1.018	0.084 / 0.040
47	$f_{22;t,r}^{banff} RHC$	RHC $\bar{\nu}_e$ flux normalisation, E = 1.5 - 2.5 GeV	1.043	0.080 / 0.051
48	$f_{23;t,r}^{banff} RHC$	RHC $\bar{\nu}_e$ flux normalisation, E = 2.5 - 4.0 GeV	1.046	0.089 / 0.064
49	$f_{24;t,r}^{banff} RHC$	RHC $\bar{\nu}_e$ flux normalisation, E = 4.0 - 30.0 GeV	1.083	0.156 / 0.133

Table 9: Summary of antineutrino mode flux systematics included in the VALOR joint fit analysis. A description of how the BANFF fit constrained these systematics can be found in [36].

275 these terms subject to (approximately) maintaining the total 2p2h event rate (see Section 2 of [14]).
 276 In terms of energy transfer (q_0) and three-momentum transfer (q_3) kinematics, the distribution of
 277 events in this space for neutrino and antineutrino interactions on oxygen are shown in figs. 4 and 5
 278 respectively (see Section 2 of [14]).

279 This analysis also introduces 5 BeRPA parameters (A, B, D, E and U) to describe the collective
 280 effects of interactions between neutrinos and nucleons inside nuclei. These effects modify the Q^2
 281 dependence of the neutrino-nucleus cross-section and in BeRPA are described by a cubic polynomial
 282 transitioning to an exponential above a Q^2 threshold, as described in [15]. Neither the 2p2h shape
 283 parameter nor the BeRPA parameters apply to interactions on free protons.

Index	Parameter	Description	Best fit	1σ pre/postfit fractional error
50	$f_{Norm_{2p2h}}^{banff}$	Two particle two hole normalisation for ^{16}O	1.426	1.000 / 0.182
51	$f_{C_5^A}^{banff}$	C_5^A nucleon to Δ transition axial form factor	0.977	0.149 / 0.059
52	f_{BgRES}^{banff}	Scale of isospin 1/2 nonresonant background	0.979	0.308 / 0.190
53	$f_{M^{QE}}^{banff}$	CCQE axial-mass scaling factor	0.903	0.025 / 0.057
54	$f_{M^{RES}}^{banff}$	Resonance-production axial-mass scaling factor	0.822	0.158 / 0.045
55	f_{SCCA}^{banff}	BANFF; Second current class axial	1.000	- / -
56	f_{SCCV}^{banff}	BANFF; Second current class vector	1.000	- / -
57	$f_{p_f}^{banff}$	Fermi momentum for ^{16}O	0.916	0.058 / 0.072
58	$f_{Shape_{CCoth}}^{banff}$	CC other shape	0.519	0.400 / 0.187
59	$f_{Norm_{CCcoh}}^{banff}$	CC coherent for ^{16}O normalisation	0.906	0.300 / 0.275
60	$f_{Norm_{NCcoh}}^{banff}$	NC coherent normalisation	0.939	0.300 / 0.297
61	$f_{Norm_{NCother}}^{banff}$	NC other normalisation	1.000	- / 0.300
62	$f_{Norm_{\nu_e \rightarrow \nu_\mu}}^{banff}$	CC ν_e normalisation	1.000	- / 0.028
63	$f_{Norm_{NC1\gamma}}^{banff}$	NC 1γ normalisation	1.000	- / 1.000
64	$f_{Norm_{\bar{\nu}_e \rightarrow \bar{\nu}_\mu}}^{banff}$	CC $\bar{\nu}_e$ normalisation	1.000	- / 0.028
65	$f_{Norm_{2p2hBar}}^{banff}$	Antineutrino two particle two hole normalisation for ^{16}O	0.552	1.000 / 0.201
66	$f_{Shape_{BeRPA_A}}^{banff}$	Bernstein Polynomial coefficient A	0.663	0.118 / 0.056
67	$f_{Shape_{BeRPA_B}}^{banff}$	Bernstein Polynomial coefficient B	1.647	0.210 / 0.117
68	$f_{Shape_{BeRPA_D}}^{banff}$	Bernstein Polynomial coefficient D	0.988	0.170 / 0.128
69	$f_{Shape_{BeRPA_E}}^{banff}$	Bernstein Polynomial coefficient E	0.876	0.352 / 0.355
70	$f_{Shape_{BeRPA_U}}^{banff}$	Bernstein Polynomial coefficient U	1.200	0.100 / 0.100
71	$f_{Shape_{2p2h\nu}}^{banff}$	Neutrino two particle two hole ^{16}O shape	0.997	3.000 / 0.338
72	$f_{Norm_{2p2hCtoO}}^{banff}$	Two particle two hole ^{12}C to ^{16}O normalisation	0.940	0.200 / 0.161

Table 10: Summary of cross section systematics included in the VALOR joint fit analysis. Parameters with no prefit error were unconstrained. A description of how the BANFF fit constrained these systematics can be found in [36].

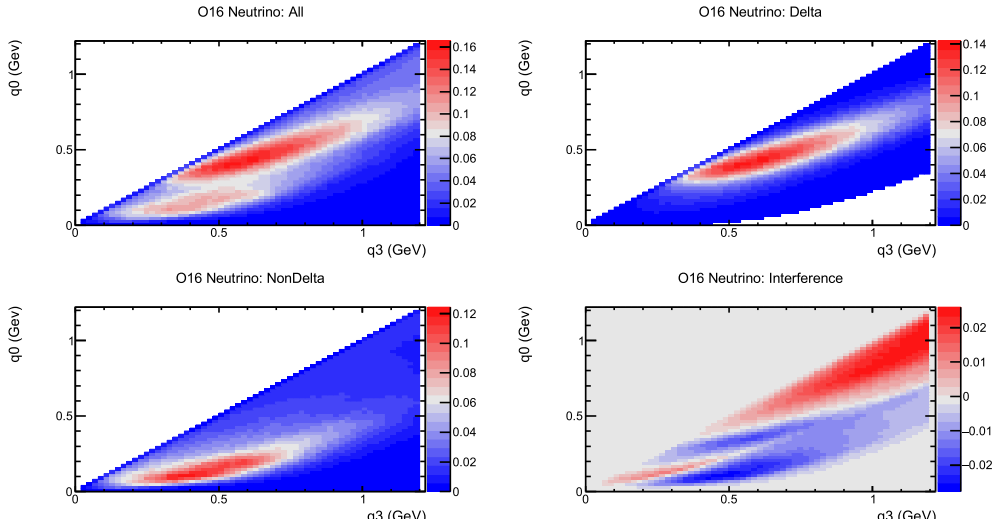


Figure 4: Distribution of neutrino events for 2p2h and each 2p2h term in q_0 - q_3 space [14].

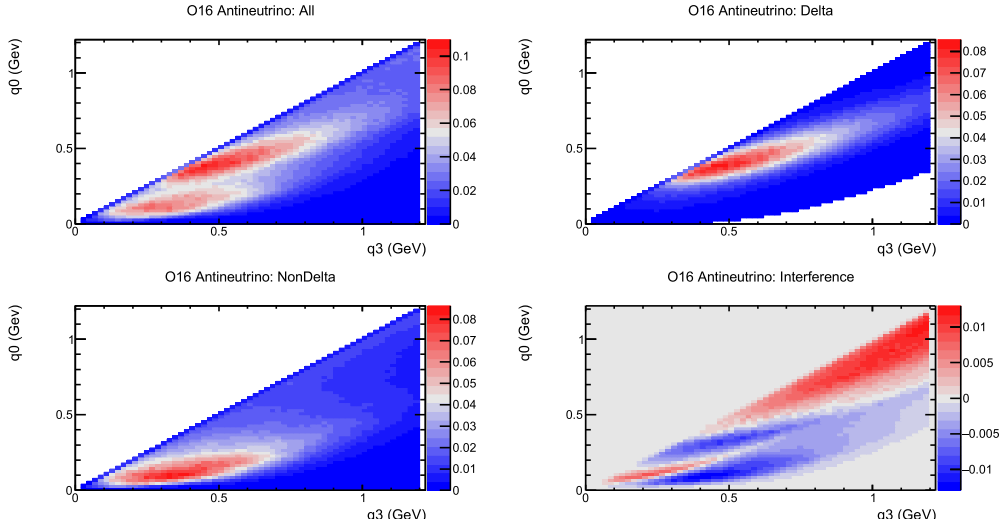


Figure 5: Distribution of antineutrino events for 2p2h and each 2p2h term in q_0 - q_3 space [14].

284 *3.2. Super-K efficiencies & effects of intranuclear and secondary re-interactions (44 parameters)*

285 The Super-K detector uncertainties include the efficiencies of the fiducial volume and reduction
 286 chain, and the OD, ring-counting, PID, momentum and decay-electron cuts. These uncertainties
 287 have been evaluated by comparisons between SK-IV atmospheric data and atmospheric neutrino
 288 Monte Carlo. Ring counting errors are evaluated using ν_μ CCQE, ν_μ CCnQE, NC, and ν_e CC-
 289 enriched control samples from atmospheric neutrinos. The NC PID error is evaluated using a
 290 NC-enriched control sample, obtained by not using the PID information during the selection. All
 291 the Monte Carlo control samples are fitted simultaneously to the data with a χ^2 function using the
 292 selection efficiencies as fit parameters [37] [38].

293 Intranuclear final-state interactions (FSI) have significant effects in the T2K energy range and
 294 result in event topologies, for scattering from nuclear targets, which are drastically different from
 295 those created in neutrino scattering from free nucleons. Uncertainties due to FSI were estimated
 296 by simultaneously varying NEUT parameters that scale interaction probabilities as described in
 297 section 2 of [26]. Uncertainties due to secondary pion interactions (SI) were also evaluated by
 298 allowing variations in the interaction probabilities. Details of this are given in [29]. Since the
 299 same model is used for FSI and SI, it is possible to evaluate the uncertainties in both FSI and SI
 300 simultaneously. Details of this procedure are described in section 8 of [25].

301 A list of the Super-K parameters and their errors can be found in table 11. We consider the
 302 Super-K detector efficiency and FSI+SI+PN systematics together, adding their covariance matrices
 303 linearly and evaluating the effects of these uncertainties using the Cholesky method. Details of all
 304 parameters can be found in [12].

305 *3.3. Super-K energy scale (1 parameter)*

306 The systematic parameter $f_{E;r}^{SK}$ is included to estimate the effects of uncertainty in the Super-K
 307 reconstructed energy scale. This uncertainty is estimated to be 2.4% [39]; its effects are calculated

Index	Parameter	Description	1σ fractional error
0	$f_{0,t,r}^{SK+FSI}$	SKDet + FSI/SI 0; Ereco range 0.00 - 0.40 GeV; numu/numubar CCQE (1Rmu)	0.009
1	$f_{1,t,r}^{SK+FSI}$	SKDet + FSI/SI 1; Ereco range 0.40 - 1.10 GeV; numu/numubar CCQE (1Rmu)	0.007
2	$f_{2,t,r}^{SK+FSI}$	SKDet + FSI/SI 2; Ereco range 1.10 - 30.00 GeV; numu/numubar CCQE (1Rmu)	0.007
3	$f_{3,t,r}^{SK+FSI}$	SKDet + FSI/SI 3; Ereco range 0.00 - 30.00 GeV; numu/numubar CCnQE (1Rmu)	0.169
4	$f_{4,t,r}^{SK+FSI}$	SKDet + FSI/SI 4; Ereco range 0.00 - 30.00 GeV; nue/nuebar/signue CC (1Rmu)	1.005
5	$f_{5,t,r}^{SK+FSI}$	SKDet + FSI/SI 5; Ereco range 0.00 - 30.00 GeV; all NC (1Rmu)	0.658
6	$f_{6,t,r}^{SK+FSI}$	SKDet + FSI/SI 6; Ereco range 0.00 - 0.35 GeV; oscillated nue CC (1Re)	0.181
7	$f_{7,t,r}^{SK+FSI}$	SKDet + FSI/SI 7; Ereco range 0.35 - 0.80 GeV; oscillated nue CC (1Re)	0.036
8	$f_{8,t,r}^{SK+FSI}$	SKDet + FSI/SI 8; Ereco range 0.80 - 1.25 GeV; oscillated nue CC (1Re)	0.042
9	$f_{9,t,r}^{SK+FSI}$	SKDet + FSI/SI 9; Ereco range 0.00 - 0.35 GeV; numu/numubar CC (1Re)	0.300
10	$f_{10,t,r}^{SK+FSI}$	SKDet + FSI/SI 10; Ereco range 0.35 - 0.80 GeV; numu/numubar CC (1Re)	0.321
11	$f_{11,t,r}^{SK+FSI}$	SKDet + FSI/SI 11; Ereco range 0.80 - 1.25 GeV; numu/numubar CC (1Re)	0.393
12	$f_{12,t,r}^{SK+FSI}$	SKDet + FSI/SI 12; Ereco range 0.00 - 0.35 GeV; nue/nuebar CC (1Re)	0.135
13	$f_{13,t,r}^{SK+FSI}$	SKDet + FSI/SI 13; Ereco range 0.35 - 0.80 GeV; nue/nuebar CC (1Re)	0.070
14	$f_{14,t,r}^{SK+FSI}$	SKDet + FSI/SI 14; Ereco range 0.80 - 1.25 GeV; nue/nuebar CC (1Re)	0.077
15	$f_{15,t,r}^{SK+FSI}$	SKDet + FSI/SI 15; Ereco range 0.00 - 0.35 GeV; all NC (1Re)	0.194
16	$f_{16,t,r}^{SK+FSI}$	SKDet + FSI/SI 16; Ereco range 0.35 - 0.80 GeV; all NC (1Re)	0.181
17	$f_{17,t,r}^{SK+FSI}$	SKDet + FSI/SI 17; Ereco range 0.80 - 1.25 GeV; all NC (1Re)	0.472
18	$f_{0,t,r}^{SK+FSI} RHC$	SKDet + FSI/SI 0; Ereco range 0.00 - 0.40 GeV; numu/numubar CCQE (1Rmu); RHC	0.009
19	$f_{1,t,r}^{SK+FSI} RHC$	SKDet + FSI/SI 1; Ereco range 0.40 - 1.10 GeV; numu/numubar CCQE (1Rmu); RHC	0.007
20	$f_{2,t,r}^{SK+FSI} RHC$	SKDet + FSI/SI 2; Ereco range 1.10 - 30.00 GeV; numu/numubar CCQE (1Rmu); RHC	0.007
21	$f_{3,t,r}^{SK+FSI} RHC$	SKDet + FSI/SI 3; Ereco range 0.00 - 30.00 GeV; numu/numubar CCnQE (1Rmu); RHC	0.130
22	$f_{4,t,r}^{SK+FSI} RHC$	SKDet + FSI/SI 4; Ereco range 0.00 - 30.00 GeV; nue/nuebar/signue CC (1Rmu); RHC	1.005
23	$f_{5,t,r}^{SK+FSI} RHC$	SKDet + FSI/SI 5; Ereco range 0.00 - 30.00 GeV; all NC (1Rmu); RHC	0.657
24	$f_{6,t,r}^{SK+FSI} RHC$	SKDet + FSI/SI 6; Ereco range 0.00 - 0.35 GeV; oscillated nue CC (1Re); RHC	0.108
25	$f_{7,t,r}^{SK+FSI} RHC$	SKDet + FSI/SI 7; Ereco range 0.35 - 0.80 GeV; oscillated nue CC (1Re); RHC	0.036
26	$f_{8,t,r}^{SK+FSI} RHC$	SKDet + FSI/SI 8; Ereco range 0.80 - 1.25 GeV; oscillated nue CC (1Re); RHC	0.057
27	$f_{9,t,r}^{SK+FSI} RHC$	SKDet + FSI/SI 9; Ereco range 0.00 - 0.35 GeV; numu/numubar CC (1Re); RHC	0.349
28	$f_{10,t,r}^{SK+FSI} RHC$	SKDet + FSI/SI 10; Ereco range 0.35 - 0.80 GeV; numu/numubar CC (1Re); RHC	0.342
29	$f_{11,t,r}^{SK+FSI} RHC$	SKDet + FSI/SI 11; Ereco range 0.80 - 1.25 GeV; numu/numubar CC (1Re); RHC	0.417
30	$f_{12,t,r}^{SK+FSI} RHC$	SKDet + FSI/SI 12; Ereco range 0.00 - 0.35 GeV; nue/nuebar CC (1Re); RHC	0.085
31	$f_{13,t,r}^{SK+FSI} RHC$	SKDet + FSI/SI 13; Ereco range 0.35 - 0.80 GeV; nue/nuebar CC (1Re); RHC	0.056
32	$f_{14,t,r}^{SK+FSI} RHC$	SKDet + FSI/SI 14; Ereco range 0.80 - 1.25 GeV; nue/nuebar CC (1Re); RHC	0.078
33	$f_{15,t,r}^{SK+FSI} RHC$	SKDet + FSI/SI 15; Ereco range 0.00 - 0.35 GeV; all NC (1Re); RHC	0.214
34	$f_{16,t,r}^{SK+FSI} RHC$	SKDet + FSI/SI 16; Ereco range 0.35 - 0.80 GeV; all NC (1Re); RHC	0.191
35	$f_{17,t,r}^{SK+FSI} RHC$	SKDet + FSI/SI 17; Ereco range 0.80 - 1.25 GeV; all NC (1Re); RHC	0.465
36	$f_{0,t,r}^{SK+FSI} MultiRing$	SKDet + FSI/SI 0; Ereco range 0.30 - 0.80 GeV; oscillated nue CC (MultiRe); MultiRing	0.249
37	$f_{1,t,r}^{SK+FSI} MultiRing$	SKDet + FSI/SI 1; Ereco range 0.80 - 1.25 GeV; oscillated nue CC (MultiRe); MultiRing	0.215
38	$f_{2,t,r}^{SK+FSI} MultiRing$	SKDet + FSI/SI 2; Ereco range 0.30 - 0.80 GeV; numu/numubar CC (MultiRe); MultiRing	0.507
39	$f_{3,t,r}^{SK+FSI} MultiRing$	SKDet + FSI/SI 3; Ereco range 0.80 - 1.25 GeV; numu/numubar CC (MultiRe); MultiRing	0.236
40	$f_{4,t,r}^{SK+FSI} MultiRing$	SKDet + FSI/SI 4; Ereco range 0.30 - 0.80 GeV; nue/nuebar CC (MultiRe); MultiRing	0.244
41	$f_{5,t,r}^{SK+FSI} MultiRing$	SKDet + FSI/SI 5; Ereco range 0.80 - 1.25 GeV; nue/nuebar CC (MultiRe); MultiRing	0.235
42	$f_{6,t,r}^{SK+FSI} MultiRing$	SKDet + FSI/SI 6; Ereco range 0.30 - 0.80 GeV; all NC (MultiRe); MultiRing	0.983
43	$f_{7,t,r}^{SK+FSI} MultiRing$	SKDet + FSI/SI 7; Ereco range 0.80 - 1.25 GeV; all NC (MultiRe); MultiRing	0.524
44	$f_{E,r}^{SK}$	SK energy scale	0.024

Table 11: Summary of SK detector + FSI + SI + PN systematics included in the VALOR joint fit analysis.

by scaling the bin edges of the MC templates and, assuming uniform distribution of events within the bins, calculating the number of events gained from/lost to other bins (including bins that are not immediately adjacent). This systematic is applied after all other systematics have been applied, because it affects reconstructed rather than true energy, does not commute with spline-based systematics, which are generated without consideration of energy scale variation and also does not commute with the other Super-K systematics, which are determined from data without any energy scale variation.

Parameter(s)	Prior	Range
$\sin^2 \theta_{23}$	uniform	$[0.3; 0.7]$
$\sin^2 2\theta_{13}$ ($\sin^2 \theta_{13}$) reactors	gaussian	0.0857 ± 0.0046
$\sin^2 2\theta_{13}$ ($\sin^2 \theta_{13}$) T2K only	uniform	$[0; 0.4]$
$\sin^2 2\theta_{12}$	gaussian	0.846 ± 0.021
$ \Delta m_{32}^2 $ (NH) / $ \Delta m_{13}^2 $ (IH)	uniform	$[2.3; 2.7] \times 10^{-3} \text{ eV}^2/\text{c}^4$
Δm_{21}^2	gaussian	$(7.53 \pm 0.18) \times 10^{-5} \text{ eV}^2/\text{c}^4$
δ_{CP}	uniform	$[-\pi; +\pi]$
Mass Hierarchy	fixed	NH or IH

Table 12: Treatment of the oscillation parameters in the $\nu/\bar{\nu}$ joint analysis. All the gaussian priors are from [81]. The parameter $\sin^2 2\theta_{13}$ can be constrained with the measurement of reactor experiments using the gaussian prior, otherwise a uniform prior is used and the measurement relies only on the T2K data. The nominal values of $\sin^2 2\theta_{13}$, $\sin^2 2\theta_{12}$ and Δm_{21}^2 are from [81], while all the other oscillation parameter values corresponds to the most probable values obtained by the Bayesian analysis on the T2K run 1-4 neutrino mode data [20]. The mass hierarchy is not marginalised but fixed to either NH or IH.

315 3.4. Oscillation parameters and mass hierarchy (7 parameters)

316 The 3-flavour oscillation probability is used. All the nuisance oscillation parameters, i.e. those
 317 parameters which are not shown in a given contour, are marginalised except the mass hierarchy
 318 which is fixed to either normal or inverted hierarchy.

319 For $\sin^2 \theta_{13}$ two different priors can be used, depending on whether the reactor constraint is
 320 applied, denoted as “reactors”, when applied and “T2K only” when not applied.

321 3.5. Systematic error on Super-K predictions

322 The effect of each category of systematic parameter on the expected event rate for Super-K
 323 sample is given in tables 39 to 43 (details of per-sample event rates for 1σ and 3σ variations of each
 324 independent systematic parameter can be found in Appendix C). The mean and RMS of 10000
 325 throws of the respective systematics (with correlations taken into account) is computed for each
 326 sample and in the case of pre-BANFF and post-BANFF errors. When not measuring the effect
 327 of oscillation parameters variations, the oscillation parameters are fixed at Asimov A values (see
 328 section 2.1.1).

329 For the measurement of δ_{CP} it is important to understand the effect of the systematic uncer-
 330 tainties on the ratio of the number of events between neutrino and antineutrino mode samples. If
 331 correlations do not reproduce the physics correctly, a fake asymmetry between neutrino and an-
 332 tineutrino oscillations can be seen. Furthermore, if correlations exist but are not taken into account,
 333 the measurement of δ_{CP} could be biased. The true value of δ_{CP} determines whether correlations
 334 or anti-correlations between systematic parameters have the greatest effect in hiding any oscillation
 335 asymmetry. In particular, if true $\delta_{CP} = \pm\pi/2$ then anti-correlation in the e -like samples could
 336 hide any oscillation asymmetry. Alternatively, in the case that true $\delta_{CP} \sim 0$ it is uncorrelated
 337 parameters that reduce the sensitivity to δ_{CP} . The uncertainties on the ratios between neutrino
 338 and antineutrino mode events due to the systematic parameters are shown in table 13. The most
 339 critical systematic parameters are σ_{ν_e} and $\sigma_{\bar{\nu}_e}$ which are applied respectively to ν_e and $\bar{\nu}_e$ events.

³⁴⁰ Their fractional error from the BANFF covariance matrix is 2.83% (see table 10) and they are
³⁴¹ partially anti-correlated with non-diagonal elements in the covariance matrix of -0.0004.

³⁴² It can be seen in tables 39 to 43 (Appendix E) that the reduction in the error on flux and
³⁴³ constrained cross-section systematics achieved through the BANFF fit reduces the fractional error
³⁴⁴ due to all systematics from $\sim 14\%$ to $\sim 4\%$ and $\sim 11\%$ to $\sim 3\%$ in the neutrino- and antineutrino-
³⁴⁵ mode μ -like samples respectively, from $\sim 16\%$ to $\sim 7\%$ and $\sim 13\%$ to $\sim 8\%$ in the neutrino- and
³⁴⁶ antineutrino-mode e -like samples respectively, and from $\sim 25\%$ to $\sim 22\%$ in the ν_e CC1 π^+ -like
³⁴⁷ sample. A summary of the effects of the systematic errors is given in table 13.

Error source	1-Ring μ		1-Ring e			
	FHC	RHC	FHC	RHC	FHC 1 d.e.	FHC/RHC
SK Detector	1.86	1.51	3.03	4.22	16.69	1.60
SK FSI+SI+PN	2.20	1.98	3.01	2.31	11.43	1.57
Flux + Xsec constrained	3.22	2.72	3.22	2.88	4.05	2.50
$\sigma(\nu_e)/\sigma(\bar{\nu}_e)$	0.00	0.00	2.63	1.46	2.62	3.03
NC1 γ	0.00	0.00	1.08	2.59	0.33	1.49
NC Other	0.25	0.25	0.14	0.33	0.98	0.18
Osc	0.04	0.03	3.86	3.60	3.78	0.79
All Systematics	4.40	3.76	6.10	6.51	20.94	4.77
All with osc	4.40	3.76	7.27	7.44	21.24	4.85

Table 13: Percentage error on event rate by error source and sample. Final column is the percentage error on the ratio of FHC/RHC events in the one-ring e sample.

³⁴⁸ The error envelopes corresponding to tables 39 to 43 are shown in figs. 6 to 21. These error
³⁴⁹ envelopes are determined by performing 1×10^4 correlated throws of the systematic parameter
³⁵⁰ group under consideration and plotting the mean and Gaussian 1σ error resulting.

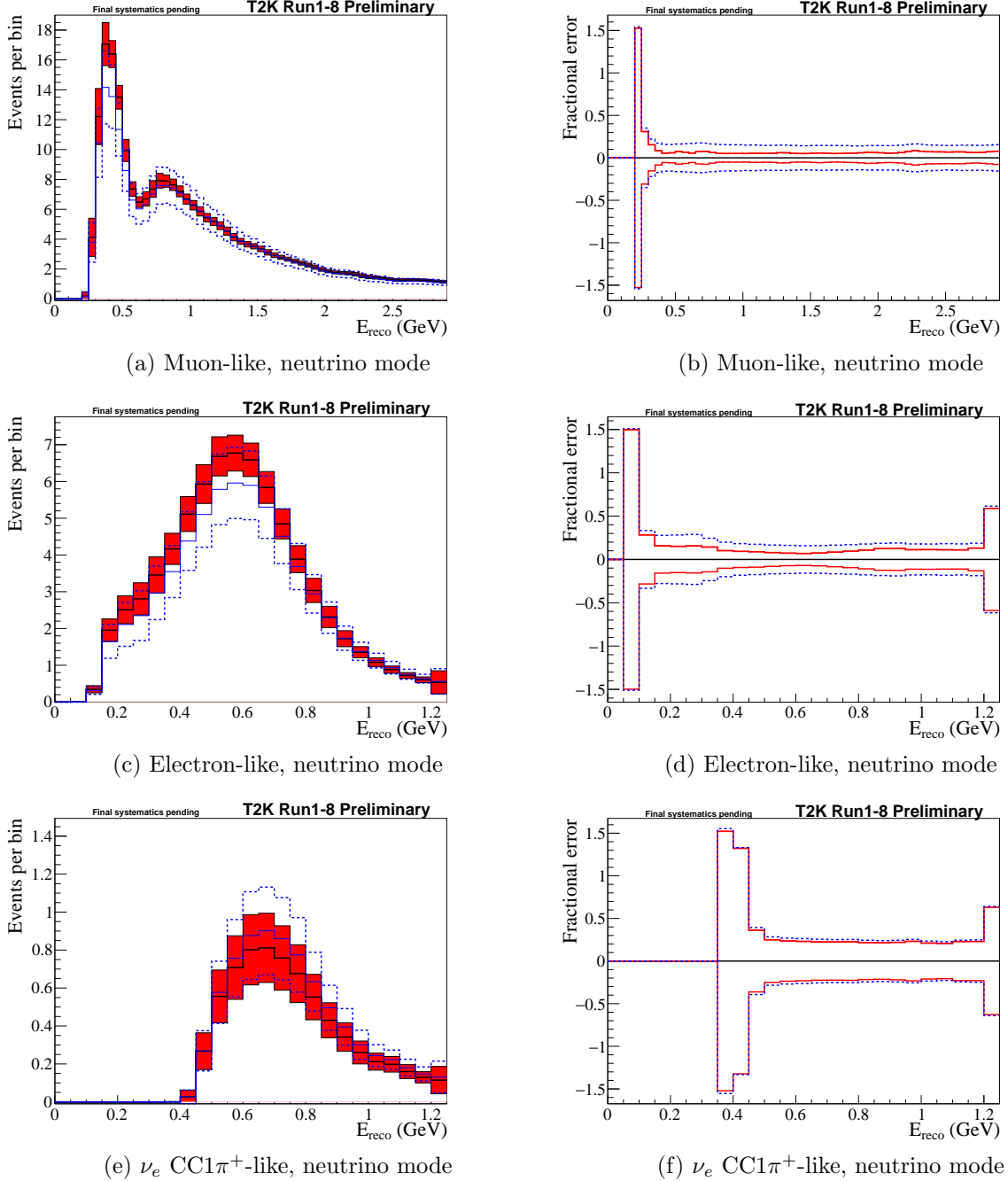


Figure 6: Error envelopes (left) and fractional errors (right) for the reconstructed neutrino energy spectrum for all systematic parameters for pre-BANFF (blue) and post-BANFF (red) errors. 1×10^4 toys are generated for the Asimov data set A with randomized systematic parameters with correlations taken into account. Since δ_{CP} , $\sin^2 \theta_{23}$, Δm_{32}^2 and the mass hierarchy will be measured, only the uncertainty on $\sin^2 \theta_{13}$, $\sin^2 \theta_{12}$ and Δm_{21}^2 are taken into account.

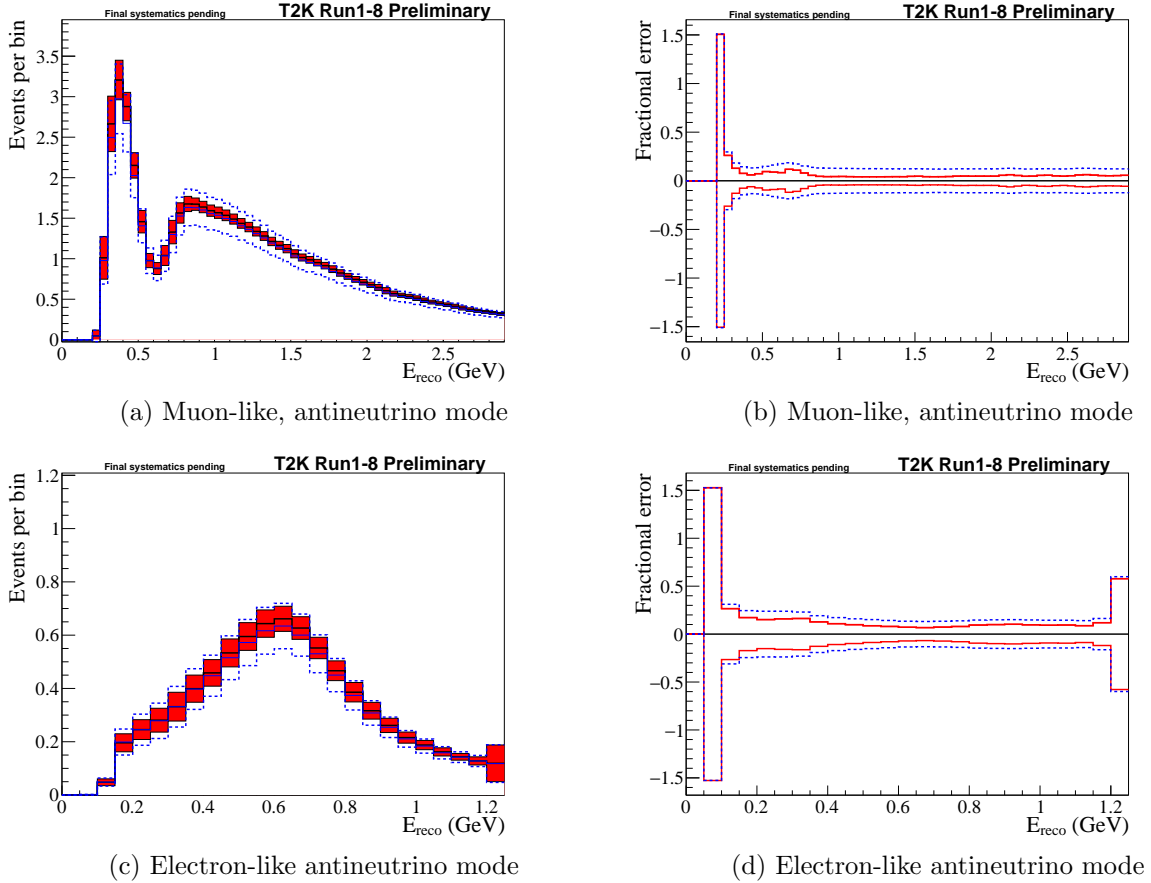


Figure 7: Error envelopes (left) and fractional errors (right) for the reconstructed neutrino energy spectrum for all systematic parameters for pre-BANFF (blue) and post-BANFF (red) errors. 1×10^4 toys are generated for the Asimov data set A with randomized systematic parameters with correlations taken into account. Since δ_{CP} , $\sin^2 \theta_{23}$, Δm_{32}^2 and the mass hierarchy will be measured, only the uncertainty on $\sin^2 \theta_{13}$, $\sin^2 \theta_{12}$ and Δm_{21}^2 are taken into account.

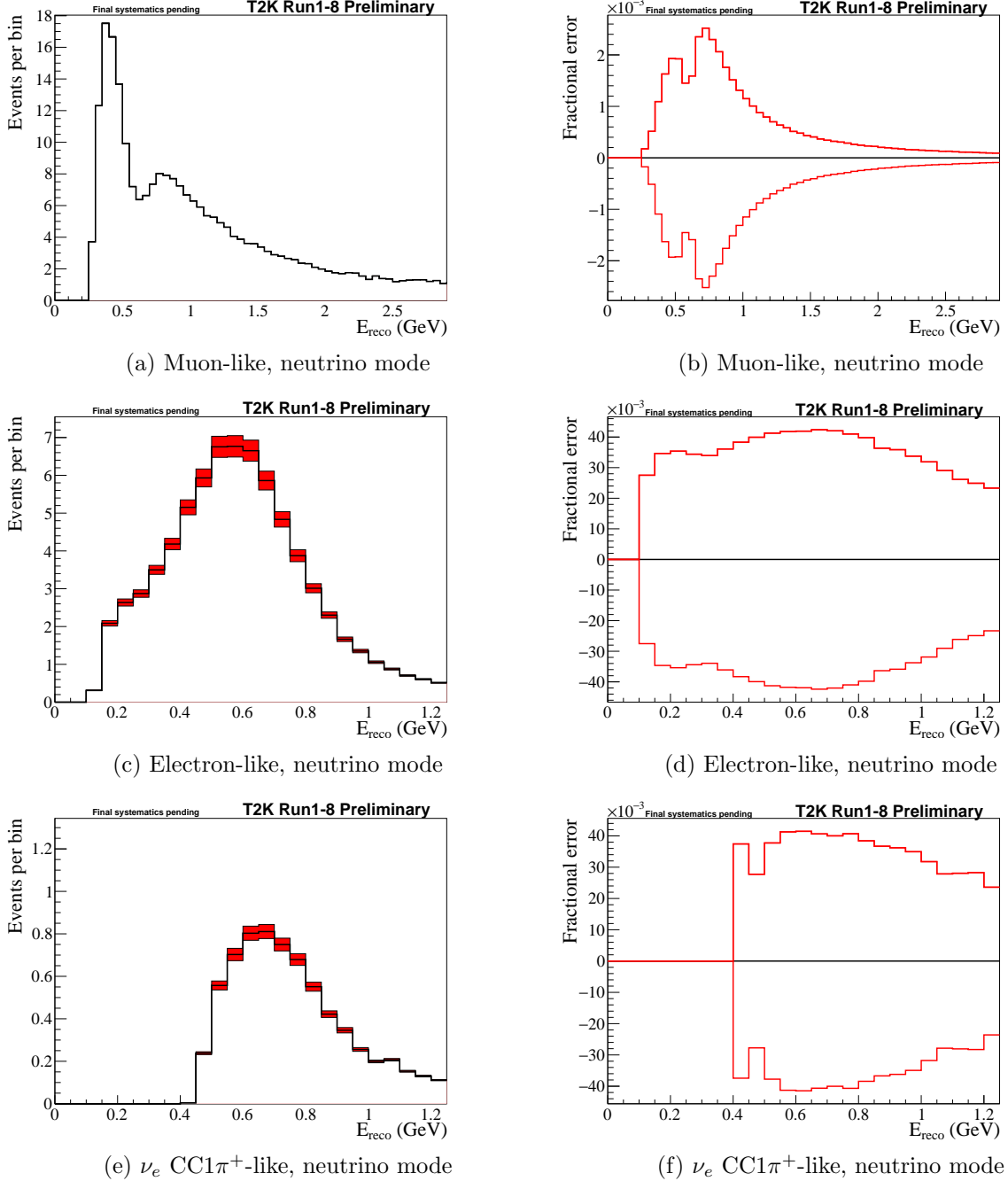


Figure 8: Error envelopes (left) and fractional errors (right) for the reconstructed neutrino energy spectrum for all oscillation nuisance parameters. 1×10^4 toys are generated for the Asimov data set A with randomized systematic parameters with correlations taken into account. Since δ_{CP} , $\sin^2 \theta_{23}$, Δm_{32}^2 and the mass hierarchy will be measured, only the uncertainty on $\sin^2 \theta_{13}$, $\sin^2 \theta_{12}$ and Δm_{21}^2 are taken into account.

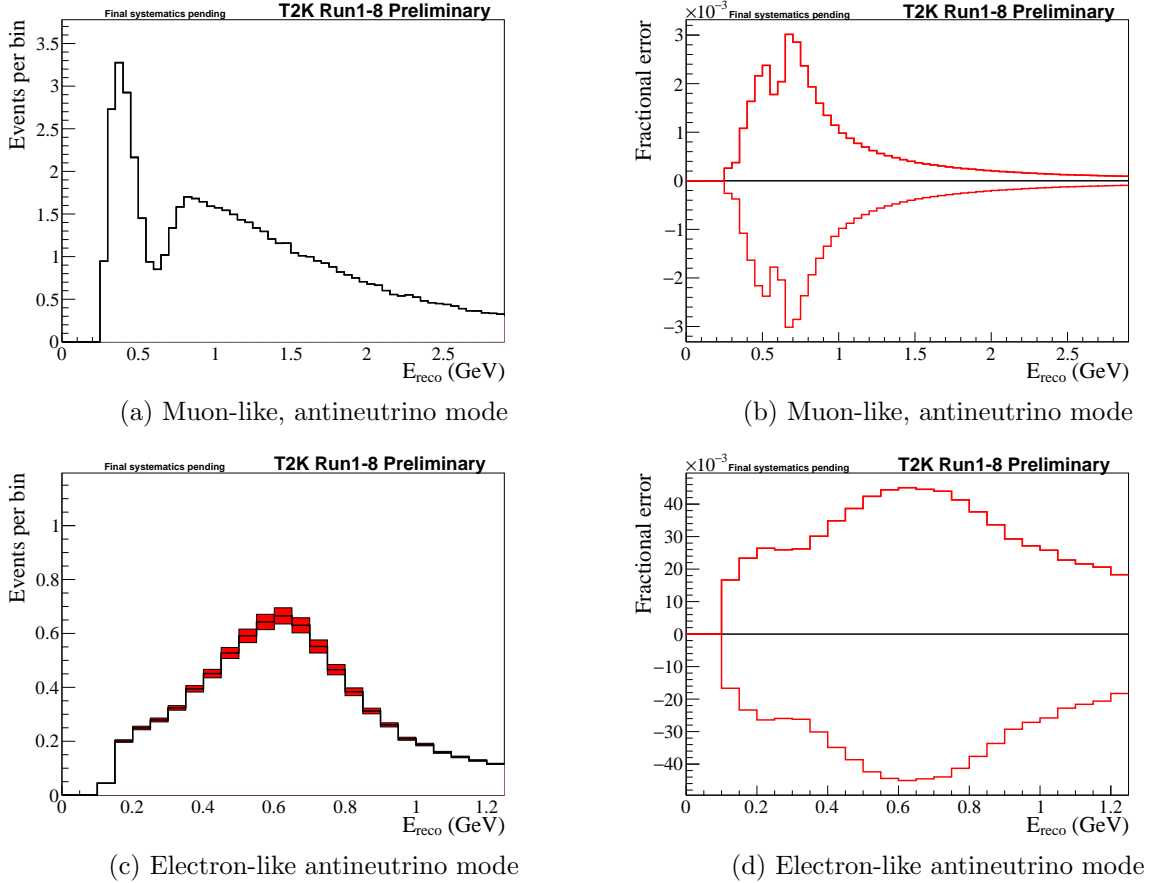


Figure 9: Error envelopes (left) and fractional errors (right) for the reconstructed neutrino energy spectrum for all oscillation nuisance parameters. 1×10^4 toys are generated for the Asimov data set A with randomized systematic parameters with correlations taken into account. Since δ_{CP} , $\sin^2 \theta_{23}$, Δm_{32}^2 and the mass hierarchy will be measured, only the uncertainty on $\sin^2 \theta_{13}$, $\sin^2 \theta_{12}$ and Δm_{21}^2 are taken into account.

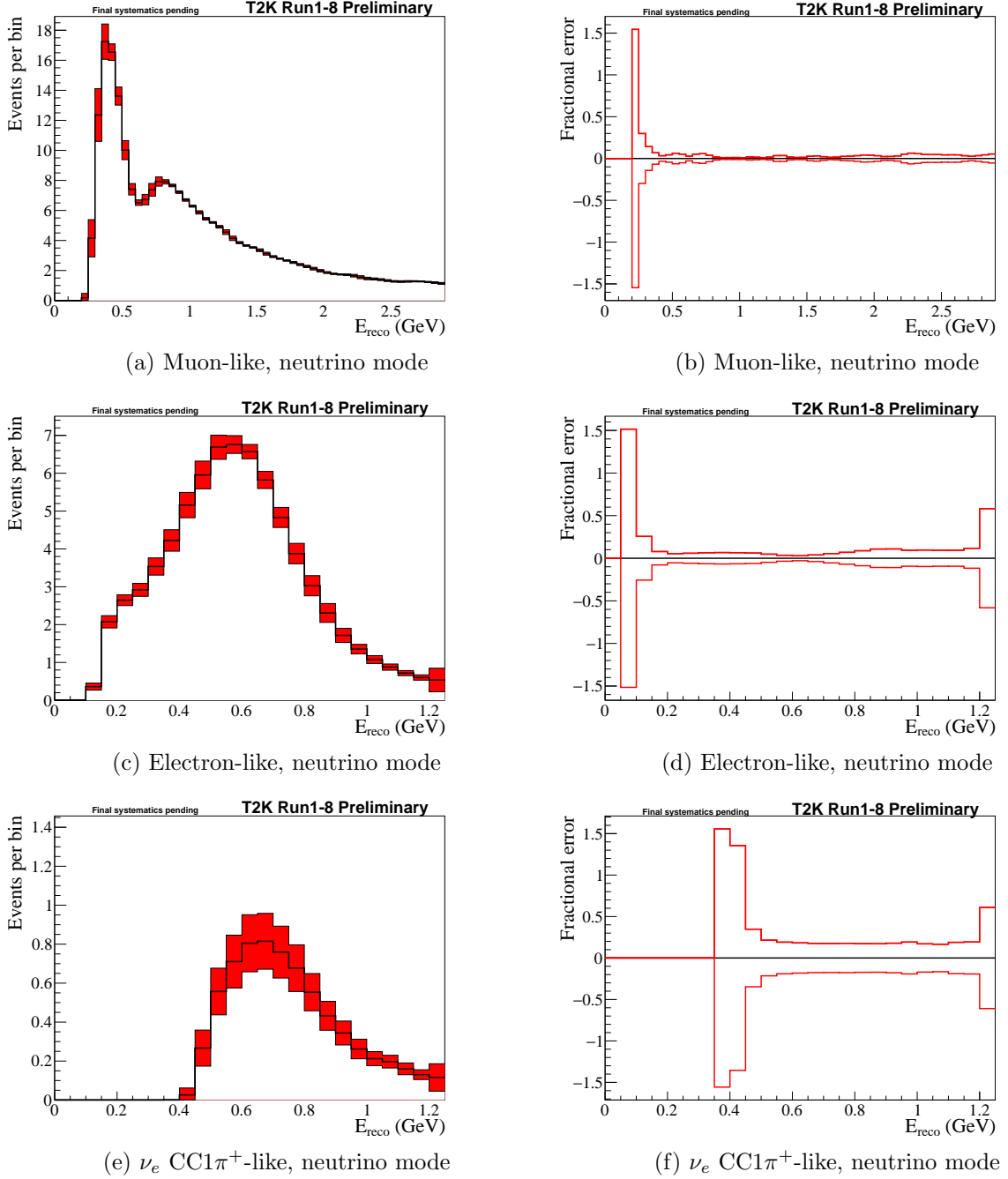


Figure 10: Error envelopes (left) and fractional error (right) for the reconstructed neutrino energy spectrum for Super-K detector systematic parameters. 1×10^4 toys are generated for the Asimov data set A with randomized systematic parameters with correlations taken into account.

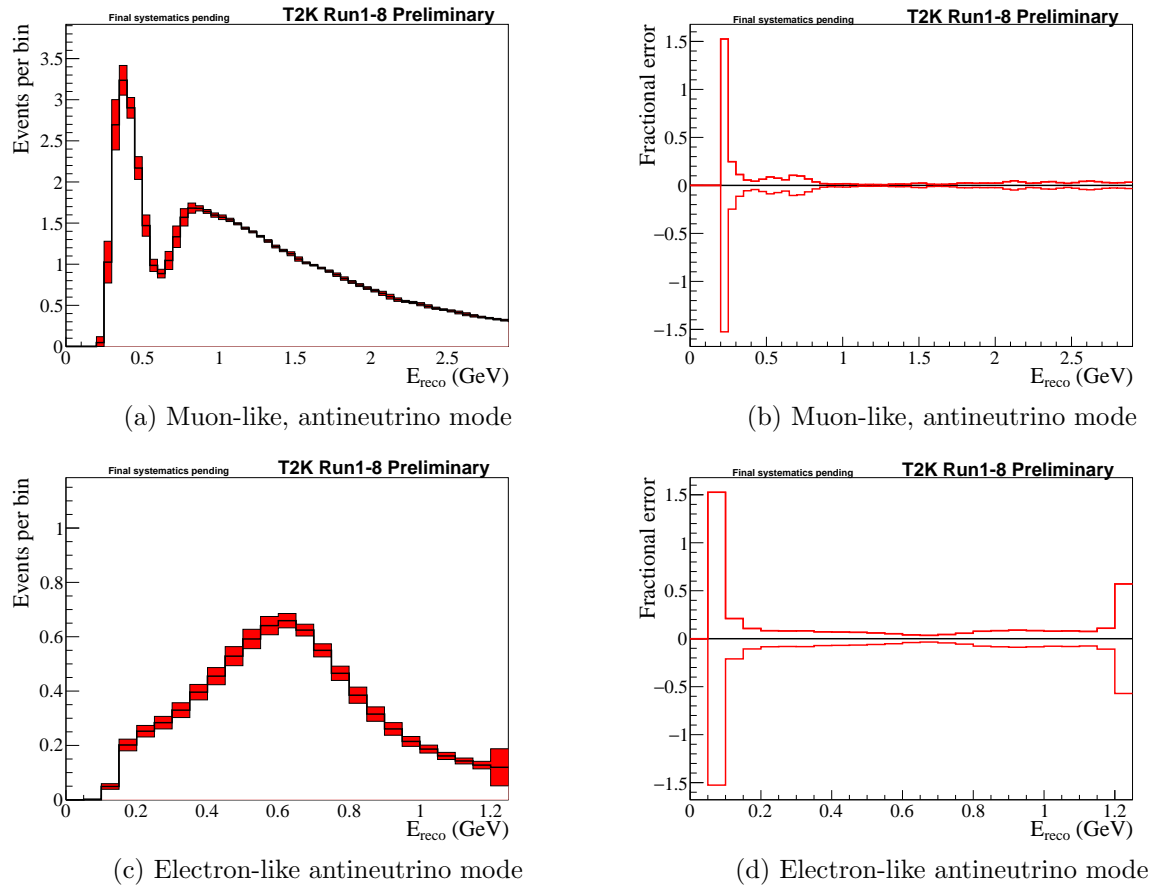


Figure 11: Error envelopes (left) and fractional error (right) for the reconstructed neutrino energy spectrum for Super-K detector systematic parameters. 1×10^4 toys are generated for the Asimov data set A with randomized systematic parameters with correlations taken into account.

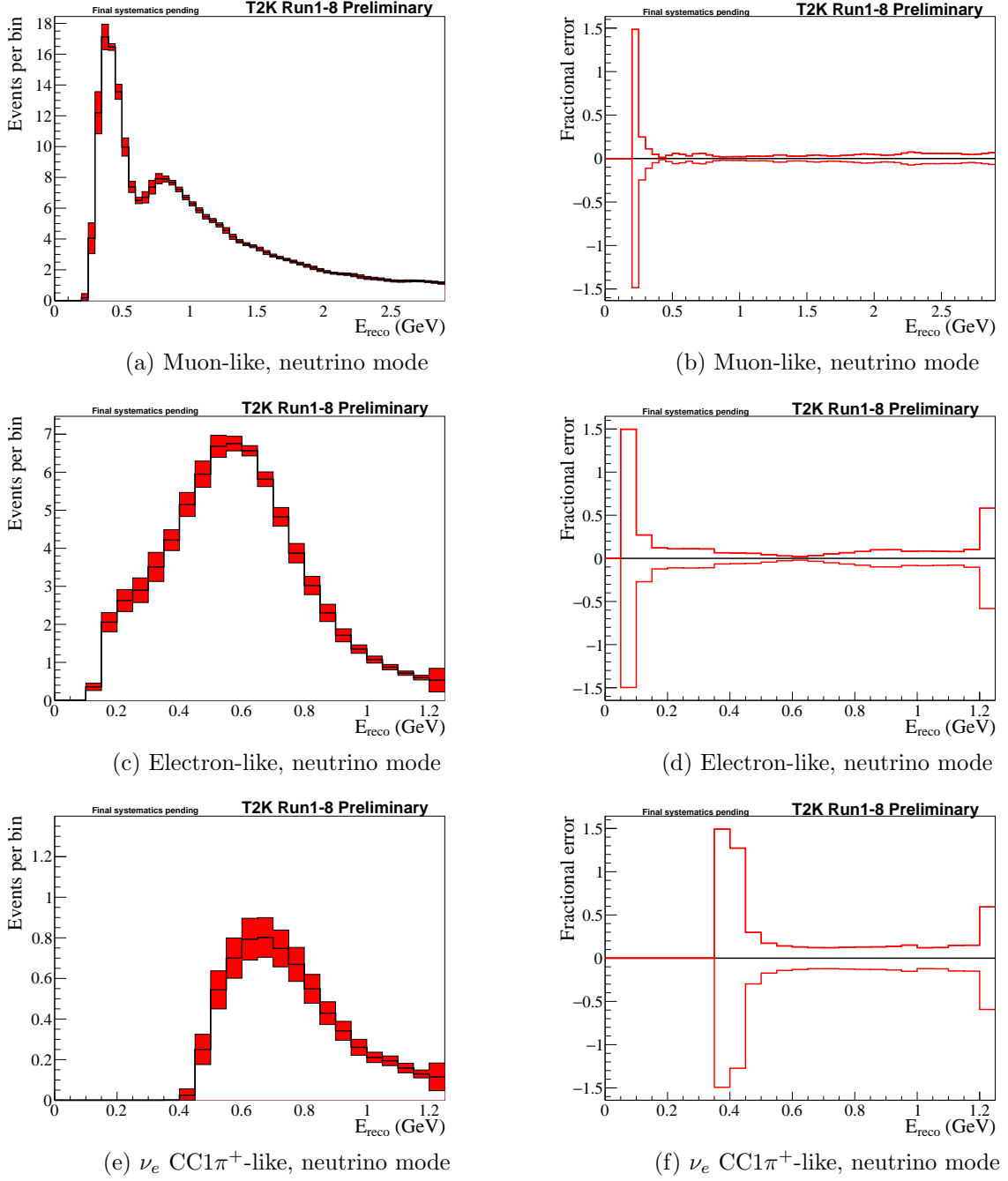


Figure 12: Error envelopes (left) and fractional error (right) for the reconstructed neutrino energy spectrum for Super-K FSI+SI+PN systematic parameters. 1×10^4 toys are generated for the Asimov data set A with randomized systematic parameters with correlations taken into account.

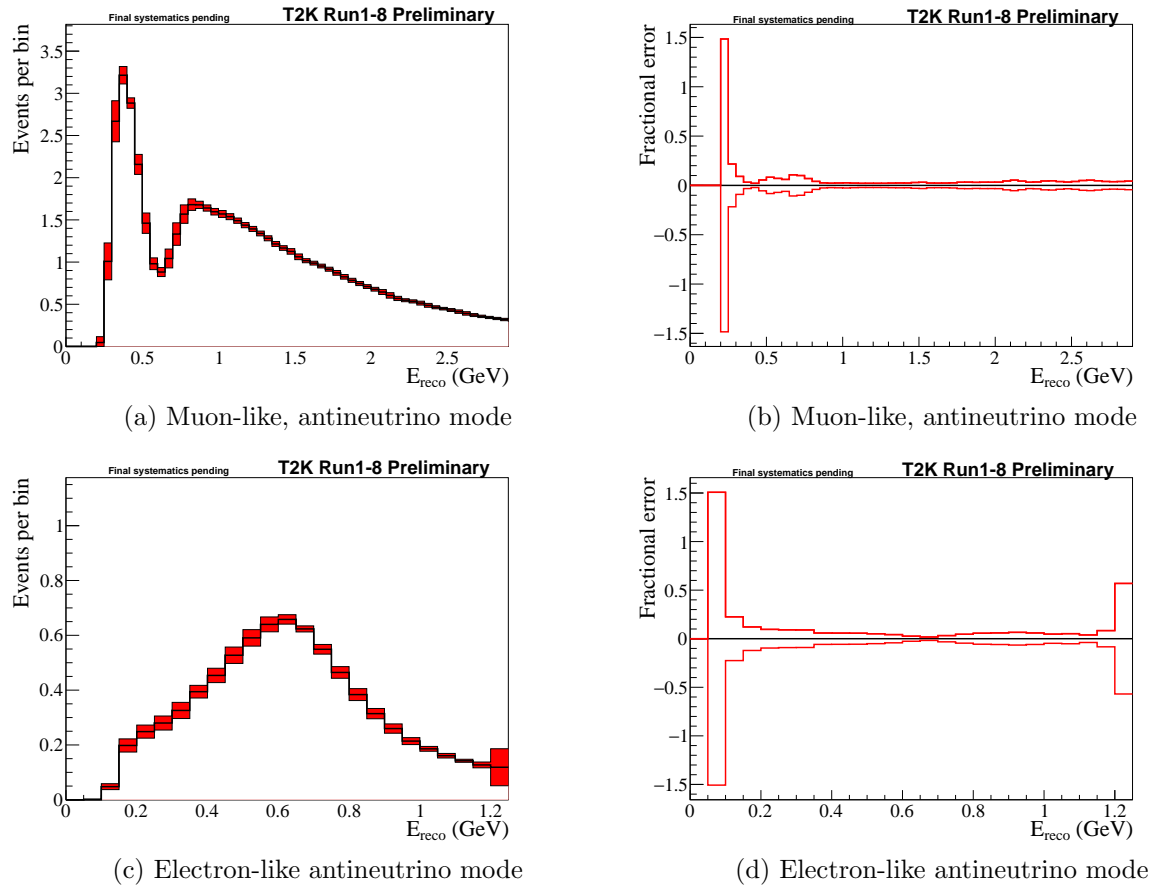


Figure 13: Error envelopes (left) and fractional errors (right) for the reconstructed neutrino energy spectrum for Super-K FSI+SI+PN systematic parameters. 1×10^4 toys are generated for the Asimov data set A with randomized systematic parameters with correlations taken into account.

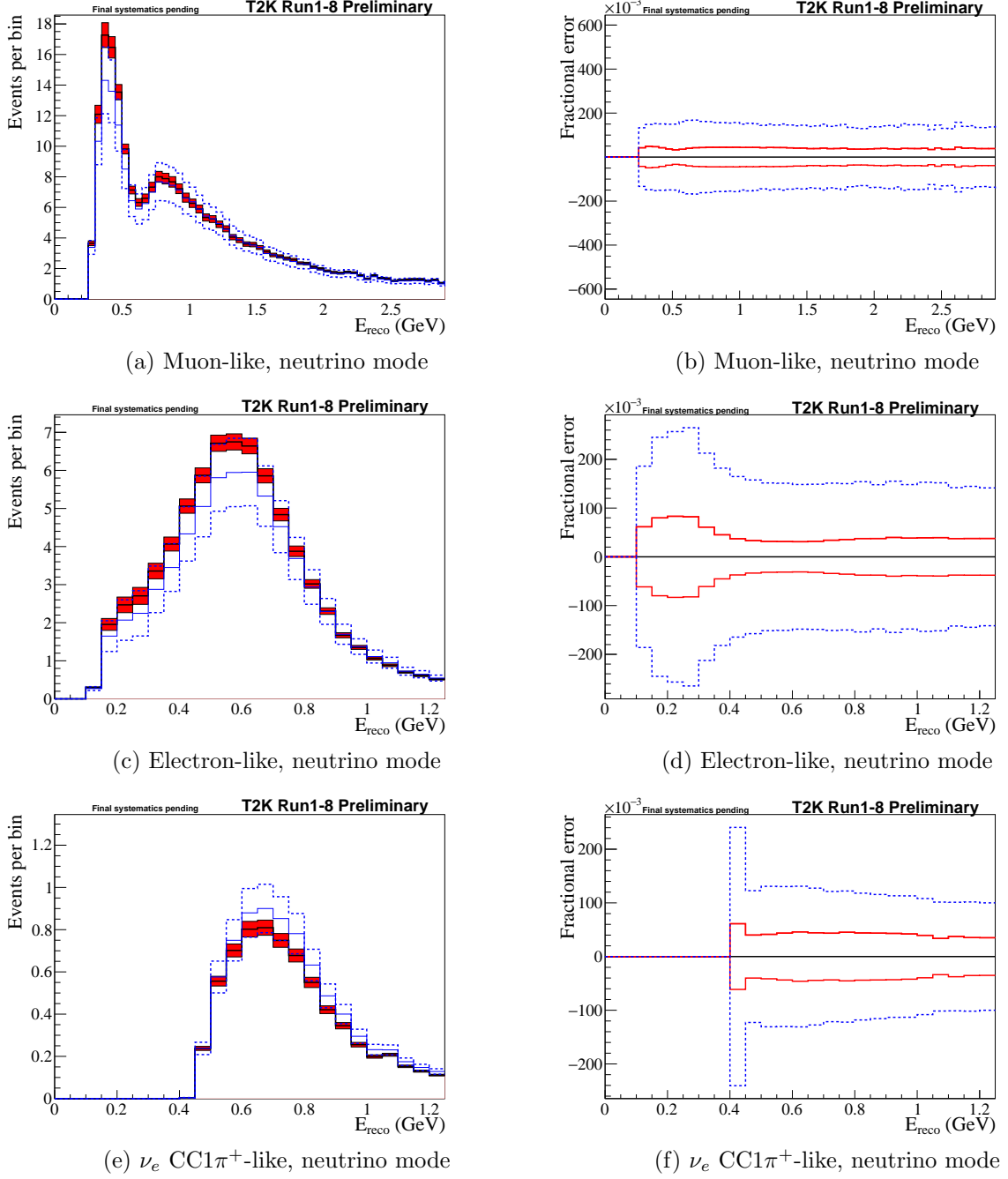


Figure 14: Error envelopes (left) and fractional errors (right) for the reconstructed neutrino energy spectrum for the flux and constrained cross-section systematic parameters for pre-BANFF (blue) and post-BANFF (red) errors. 1×10^4 toys are generated for the Asimov data set A with randomized systematic parameters with correlations taken into account.

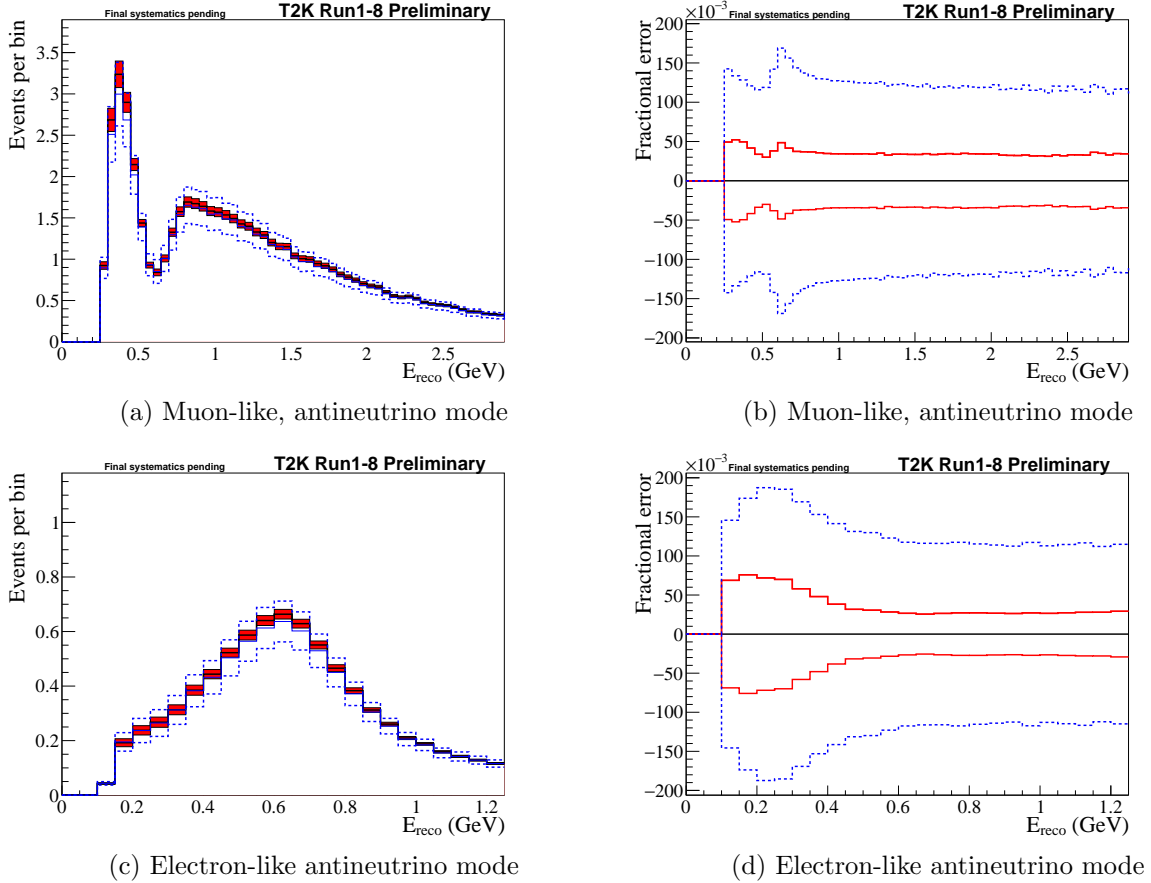


Figure 15: Error envelopes (left) and fractional error (right) for the reconstructed neutrino energy spectrum for the flux and constrained cross-section systematic parameters for pre-BANFF (blue) and post-BANFF (red) errors. 1×10^4 toys are generated for the Asimov data set A with randomized systematic parameters with correlations taken into account.

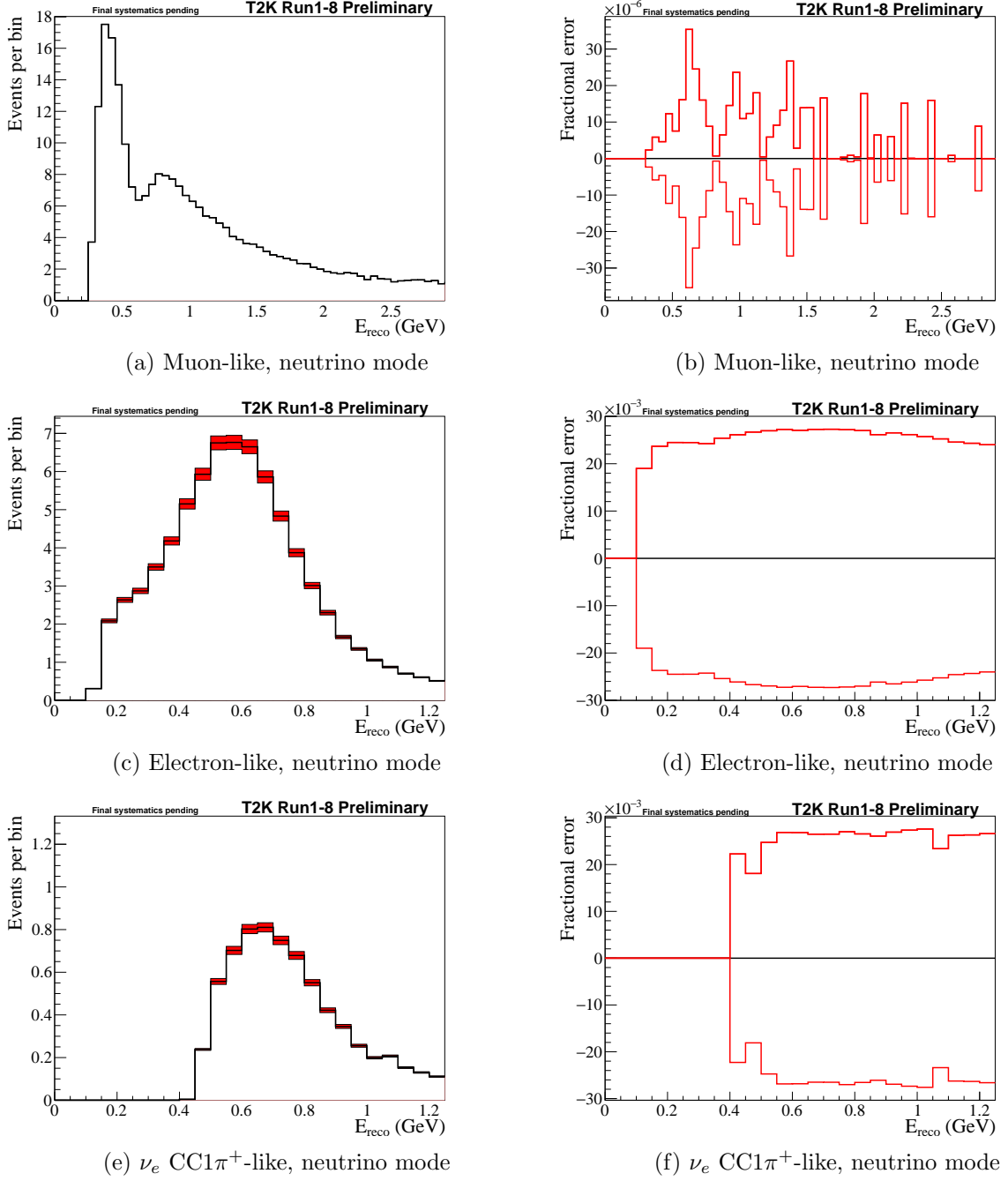


Figure 16: Error envelopes (left) and fractional errors (right) for the reconstructed neutrino energy spectrum for the unconstrained electron neutrino cross-section systematic parameters. 1×10^4 toys are generated for the Asimov data set A with randomized systematic parameters with correlations taken into account.

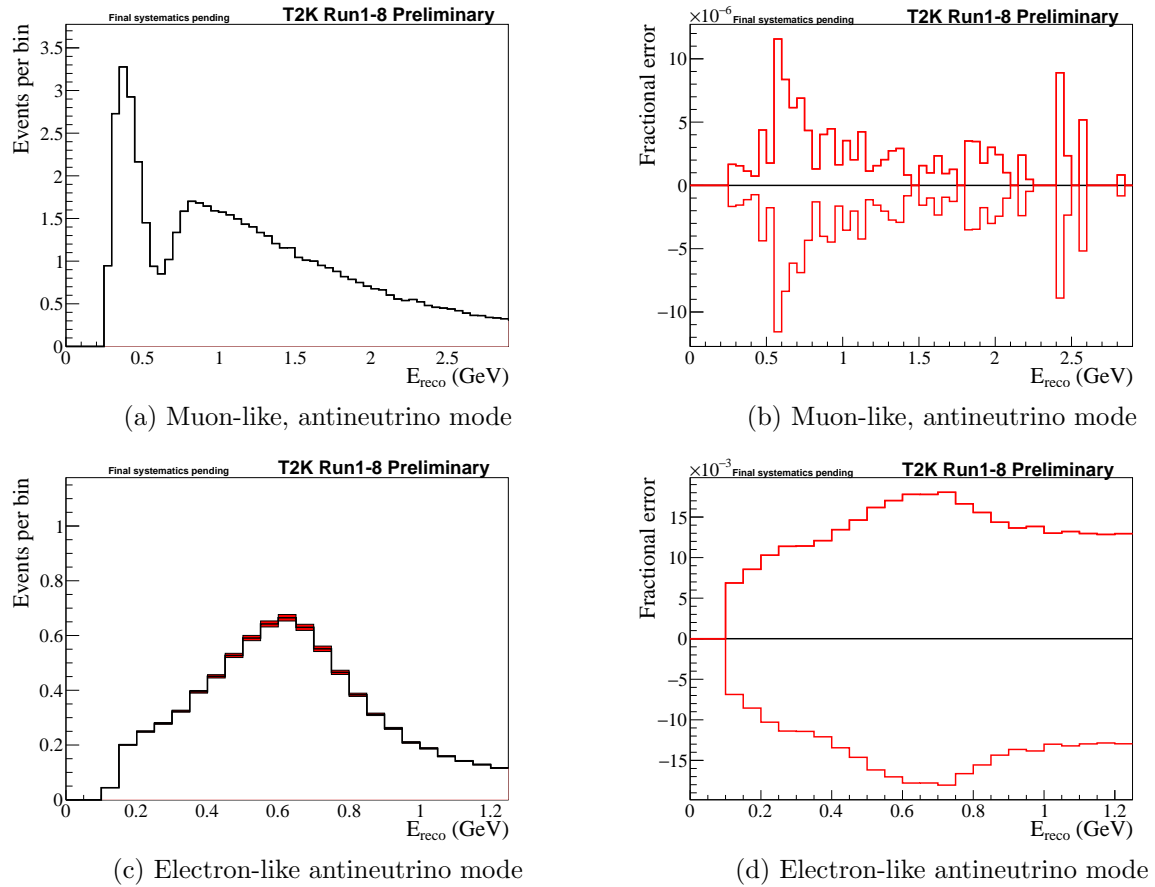


Figure 17: Error envelopes (left) and fractional errors (right) for the reconstructed neutrino energy spectrum for the unconstrained electron neutrino cross-section systematic parameters. 1×10^4 toys are generated for the Asimov data set A with randomized systematic parameters with correlations taken into account.

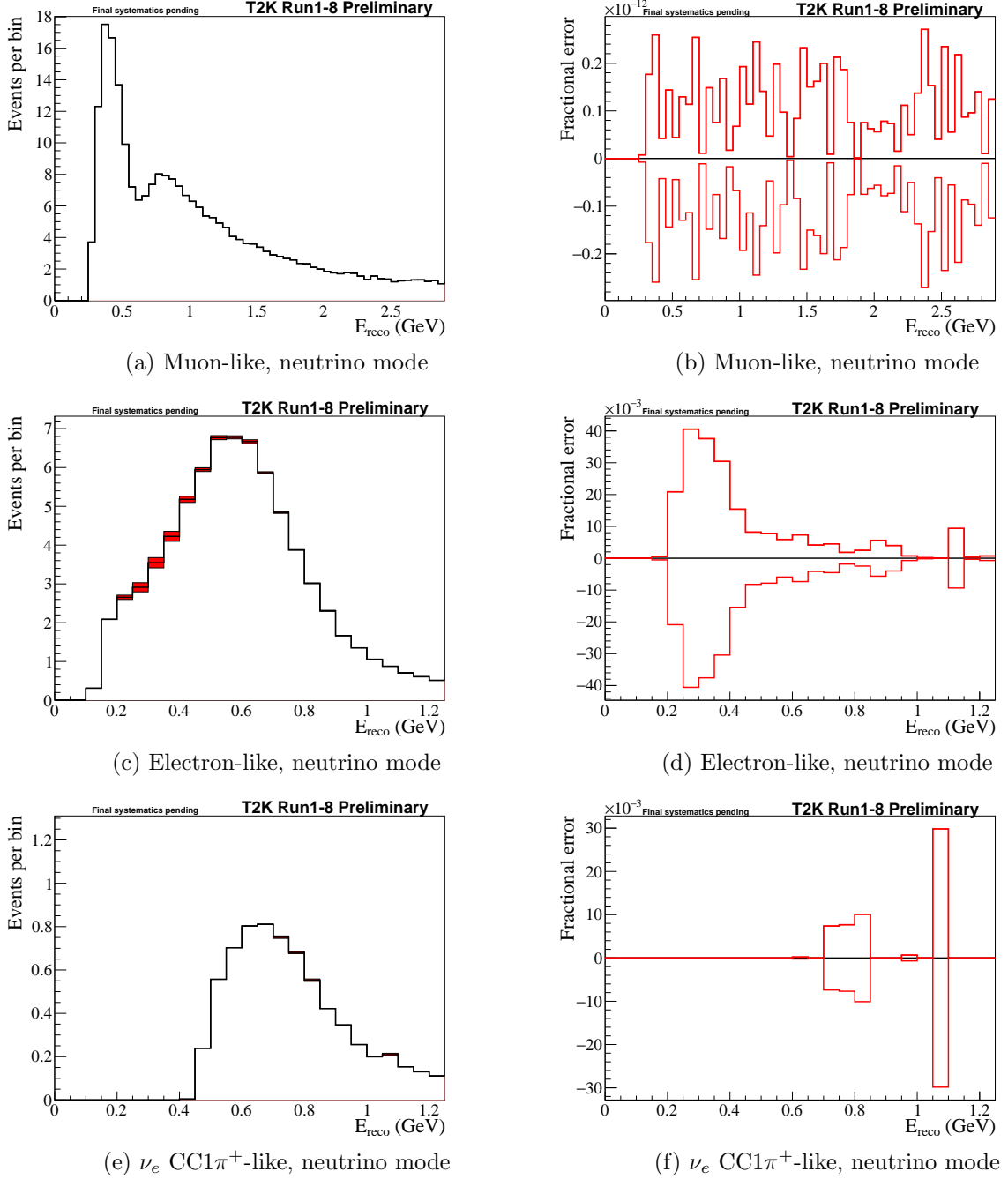


Figure 18: Error envelopes (left) and fractional error (right) for the reconstructed neutrino energy spectrum for the unconstrained NC1 γ systematic parameters. 1×10^4 toys are generated for the Asimov data set A with randomized systematic parameters with correlations taken into account.

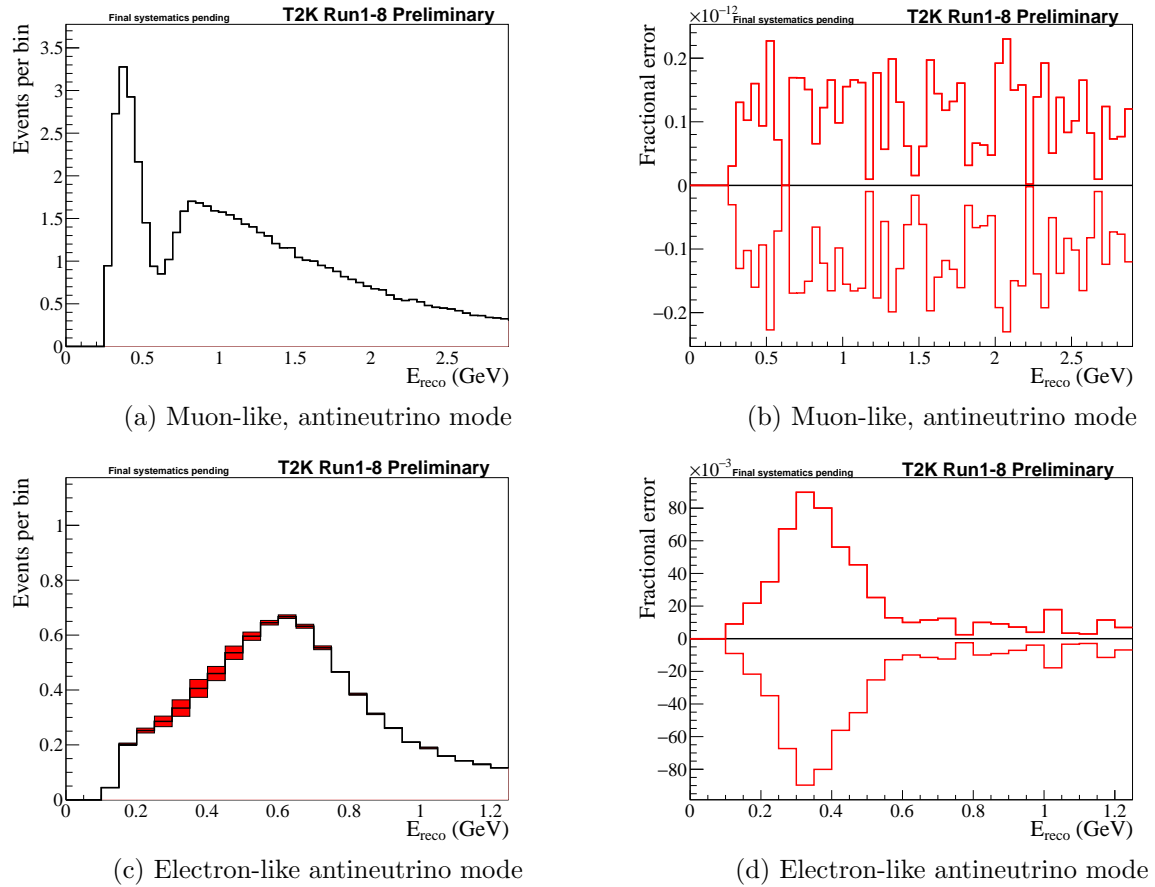


Figure 19: Error envelopes (left) and fractional errors (right) for the reconstructed neutrino energy spectrum for the unconstrained NC1 γ systematic parameters. 1×10^4 toys are generated for the Asimov data set A with randomized systematic parameters with correlations taken into account.

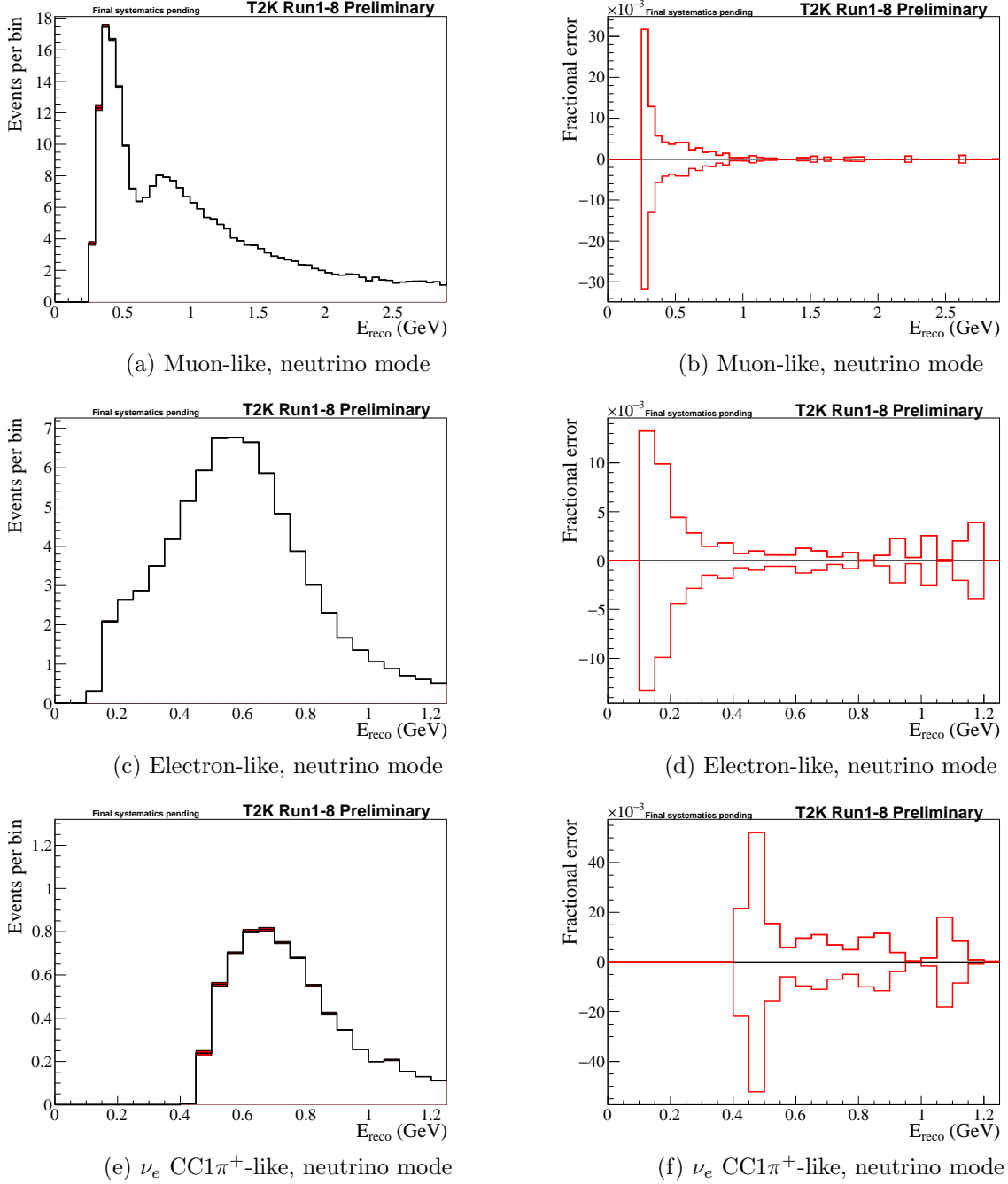


Figure 20: Error envelopes (left) and fractional errors (right) for the reconstructed neutrino energy spectrum for the unconstrained NCother systematic parameters. 1×10^4 toys are generated for the Asimov data set A with randomized systematic parameters with correlations taken into account.

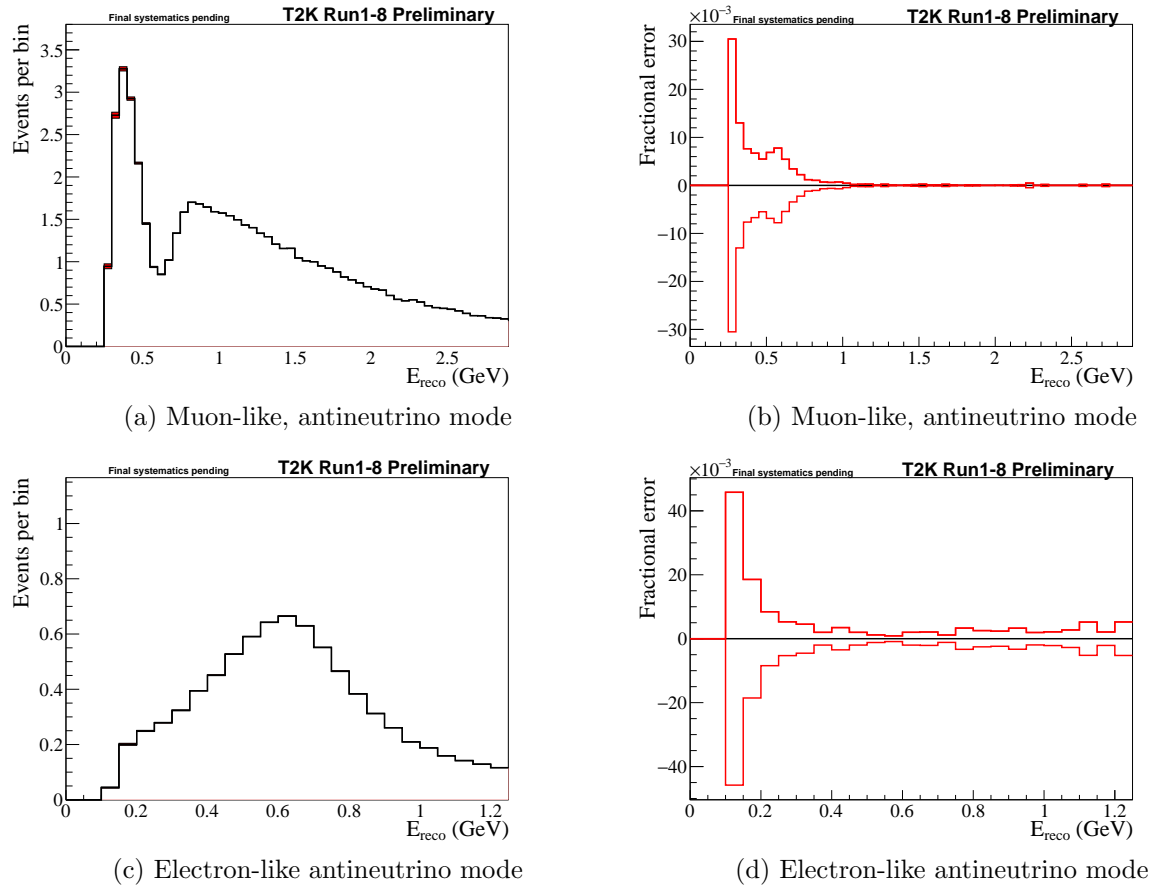


Figure 21: Error envelopes (left) and fractional errors (right) for the reconstructed neutrino energy spectrum for the unconstrained NCother systematic parameters. 1×10^4 toys are generated for the Asimov data set A with randomized systematic parameters with correlations taken into account.

351 **4. Sensitivity studies**

352 To determine the sensitivity of the analysis a number of fits were performed using Asimov
 353 data set A, the contours for which indicate the ability of the analysis to measure the oscillation
 354 parameters in the absence of statistical fluctuations and under the assumption that their true values
 355 correspond to the Asimov A values. Fits of single parameters are performed for each of $\sin^2 \theta_{13}$,
 356 δ_{CP} , $\sin^2 \theta_{23}$ and Δm_{32}^2 , with two-dimensional fits being performed for δ_{CP} vs $\sin^2 \theta_{13}$ and Δm_{32}^2
 357 vs $\sin^2 \theta_{23}$. Fits are performed for each of normal and inverted hierarchy, and also with and without
 358 the reactor constraint on $\sin^2 \theta_{13}$.

359 *4.1. Asimov data sets*

360 The definitions of the Asimov data sets given in section 2.1.1 are repeated here for reference.

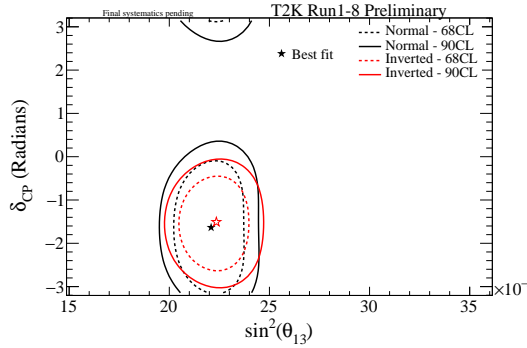
Parameter(s)	Asimov A	Asimov B
$\sin^2 \theta_{23}$	0.528	0.450
$\sin^2 \theta_{13}$ reactors	0.0219	0.0219
$\sin^2 \theta_{12}$	0.304	0.304
$ \Delta m_{32}^2 $ (NH) / $ \Delta m_{31}^2 $ (IH)	$2.509 \times 10^{-3} \text{ eV}^2/\text{c}^4$	$2.509 \times 10^{-3} \text{ eV}^2/\text{c}^4$
Δm_{21}^2	$7.53 \times 10^{-5} \text{ eV}^2/\text{c}^4$	$7.53 \times 10^{-5} \text{ eV}^2/\text{c}^4$
δ_{CP}	-1.601	0
Mass Hierarchy	Normal	Normal

Table 14: Values of oscillation parameters used to compute the event rates, systematic effects and sensitivity studies. Each set of oscillation parameters correspond to a different Asimov data set, which is the MC expected distribution in a certain oscillation hypothesis. In the Asimov data set A the nominal values of $\sin^2 2\theta_{13}$, $\sin^2 2\theta_{12}$ and Δm_{21}^2 are from [81], while all the other oscillation parameter values corresponds to the most probable values obtained by the Bayesian analysis on the T2K run 1-4 neutrino mode data [20]. The mass hierarchy is not marginalised but fixed to either NH or IH.

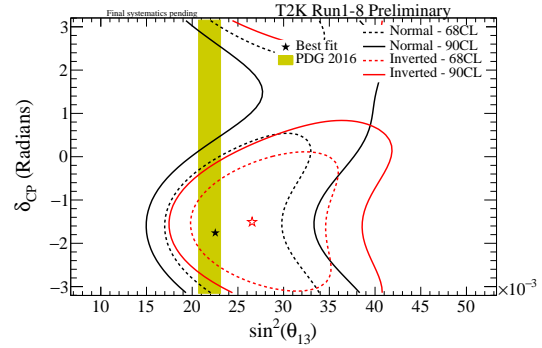
361 4.2. Results for Asimov sets A and B

362 4.2.1. Results for δ_{CP} vs $\sin^2 \theta_{13}$

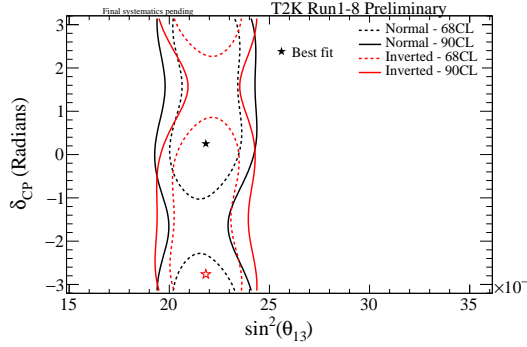
363 In fig. 22 the sensitivity to δ_{CP} vs $\sin^2 \theta_{13}$ with reactor constraint and T2K only is shown for
 364 the Asimov data sets A and B. Note that in the Asimov B case it can be seen that the best-fit point
 365 is shifted away from the true δ_{CP} value of zero towards $-\pi$. In addition to best-fit points being
 366 moved from the true value due to marginalisation of oscillation and systematic parameters there are
 367 additional contributing effects. There is a lack of sensitivity to distinguish $\delta_{CP} = 0$ and $\delta_{CP} = \pi$ for
 368 due to the spectra for $\delta_{CP} = 0$ in inverted hierarchy being similar to the spectra for $\delta_{CP} = \pi$ in
 369 normal hierarchy and vice versa (see fig. 51 in Appendix H), leading to similar $\Delta\chi^2$ values for the
 370 two points. This can be seen in fig. 24(c) and fig. 24(d), with the difference in $\Delta\chi^2_{true}$ and $\Delta\chi^2_{best-fit}$
 371 being only ~ 0.2 . Furthermore, degeneracy between δ_{CP} and mass hierarchy can cause $\delta_{CP} = 0$ to
 372 behave more like $\delta_{CP} = \pi/2$ in inverted hierarchy, and more like $\delta_{CP} = -\pi/2$ in normal hierarchy,
 373 shifting the best-fit for inverted hierarchy away from zero to a value between $-\pi$ and $-\pi/2$.



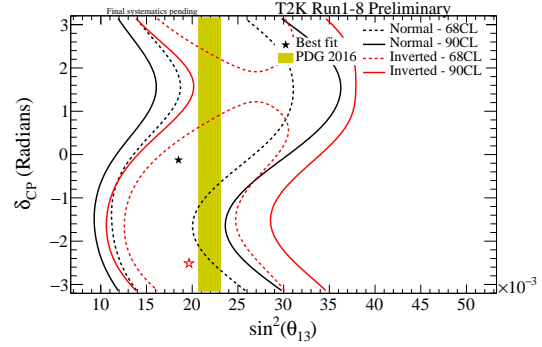
(a) Asimov A δ_{CP} vs $\sin^2 \theta_{13}$ with reactor constraint



(b) Asimov A δ_{CP} vs $\sin^2 \theta_{13}$ T2K only



(c) Asimov B δ_{CP} vs $\sin^2 \theta_{13}$ with reactor constraint

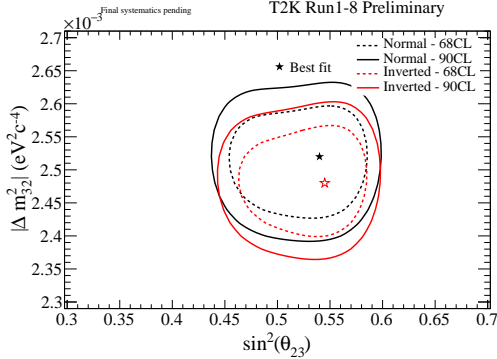


(d) Asimov B δ_{CP} vs $\sin^2 \theta_{13}$ T2K only

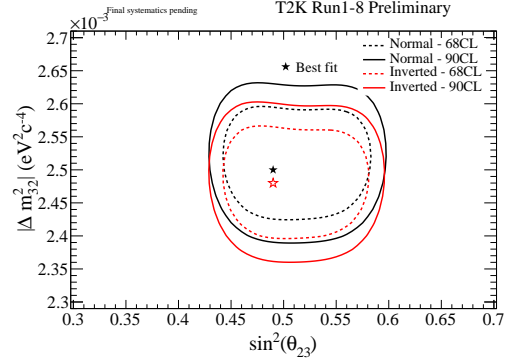
Figure 22: Contours at 68% and 90% CL for δ_{CP} vs $\sin^2 \theta_{13}$ with and without reactor constraint for Asimov data sets A and B. Normal and inverted hierarchy contours are independent. All 5 samples were used to produce these fits.

374 4.2.2. Results for Δm_{32}^2 vs $\sin^2 \theta_{23}$

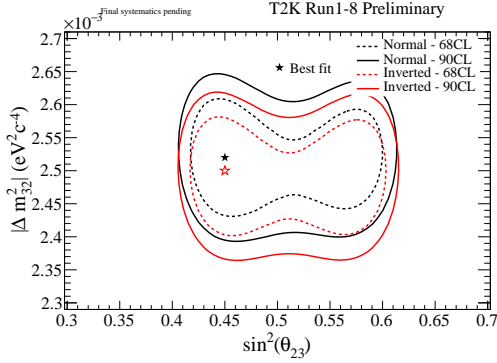
375 The sensitivity to Δm_{32}^2 vs $\sin^2 \theta_{23}$ with reactor constraint and T2K only is shown for the Asimov
 376 data sets A and B in fig. 23.



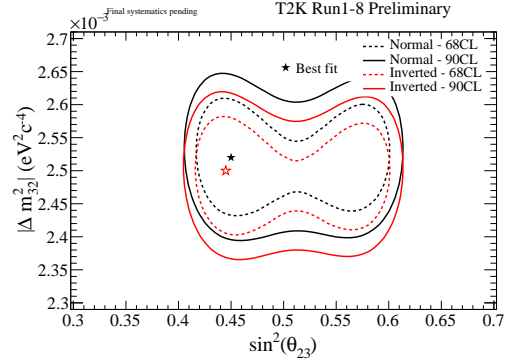
(a) Asimov A Δm_{32}^2 vs $\sin^2 \theta_{23}$ with reactor constraint



(b) Asimov A Δm_{32}^2 vs $\sin^2 \theta_{23}$ T2K only



(c) Asimov B Δm_{32}^2 vs $\sin^2 \theta_{23}$ with reactor constraint



(d) Asimov B Δm_{32}^2 vs $\sin^2 \theta_{23}$ T2K only

Figure 23: Contours at 68% and 90% CL for Δm_{32}^2 vs $\sin^2 \theta_{23}$ with and without reactor constraint for Asimov data sets A and B. Normal and inverted hierarchy contours are independent. All 5 samples were used to produce these fits.

377 4.2.3. Results for δ_{CP}

378 The sensitivity to δ_{CP} with reactor constraint and T2K only is shown for the Asimov data sets
 379 A and B in fig. 24.

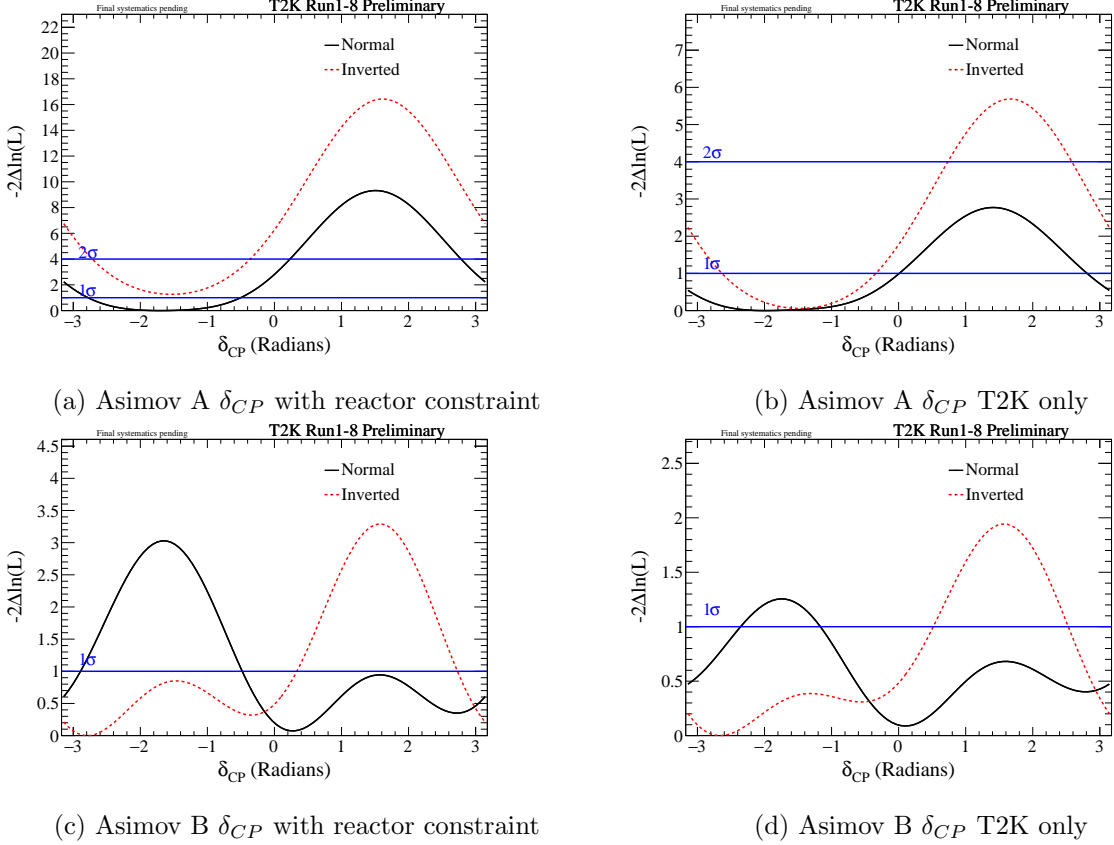


Figure 24: The expected $\Delta\chi^2$ distribution as a function of δ_{CP} with and without reactor constraint for Asimov data sets A and B. The mass hierarchy is minimized, with normal and inverted hierarchy $\Delta\chi^2$ distributions shifted to the same global best-fit χ^2 value, which is taken to be the minimum between normal and inverted hierarchy. All 5 samples were used to produce these fits.

380 4.2.4. Results for $\sin^2 \theta_{13}$

381 The sensitivity to $\sin^2 \theta_{13}$ (without reactor constraint) is shown for the Asimov data sets A and
 382 B in fig. 25.

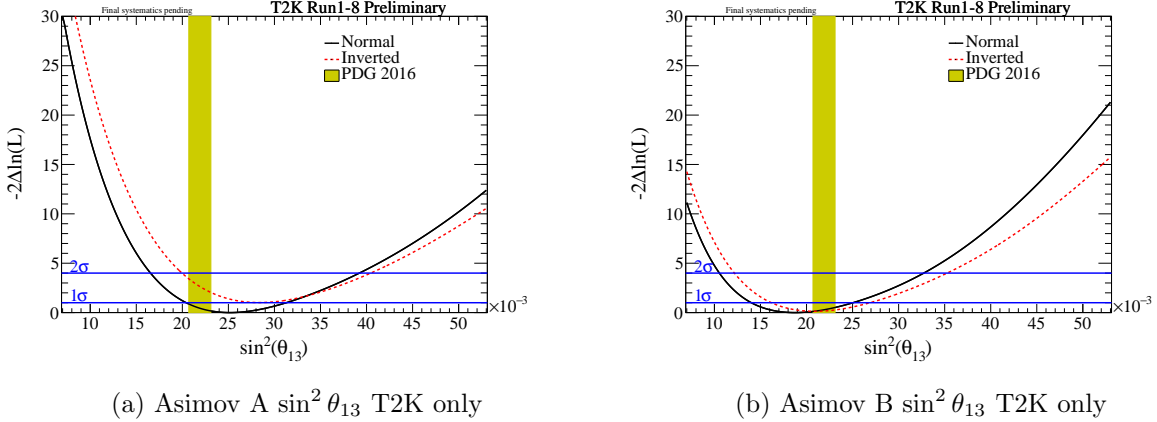


Figure 25: The expected $\Delta\chi^2$ distribution as a function of $\sin^2 \theta_{13}$ without reactor constraint for Asimov data sets A and B. The mass hierarchy is minimized, with normal and inverted hierarchy $\Delta\chi^2$ distributions shifted to the same global best-fit χ^2 value, which is taken to be the minimum between normal and inverted hierarchy. All 5 samples were used to produce these fits.

383 4.2.5. Results for $\sin^2 \theta_{23}$

384 The sensitivity to $\sin^2 \theta_{23}$ with reactor constraint and T2K only is shown for the Asimov data
 385 sets A and B in fig. 26.

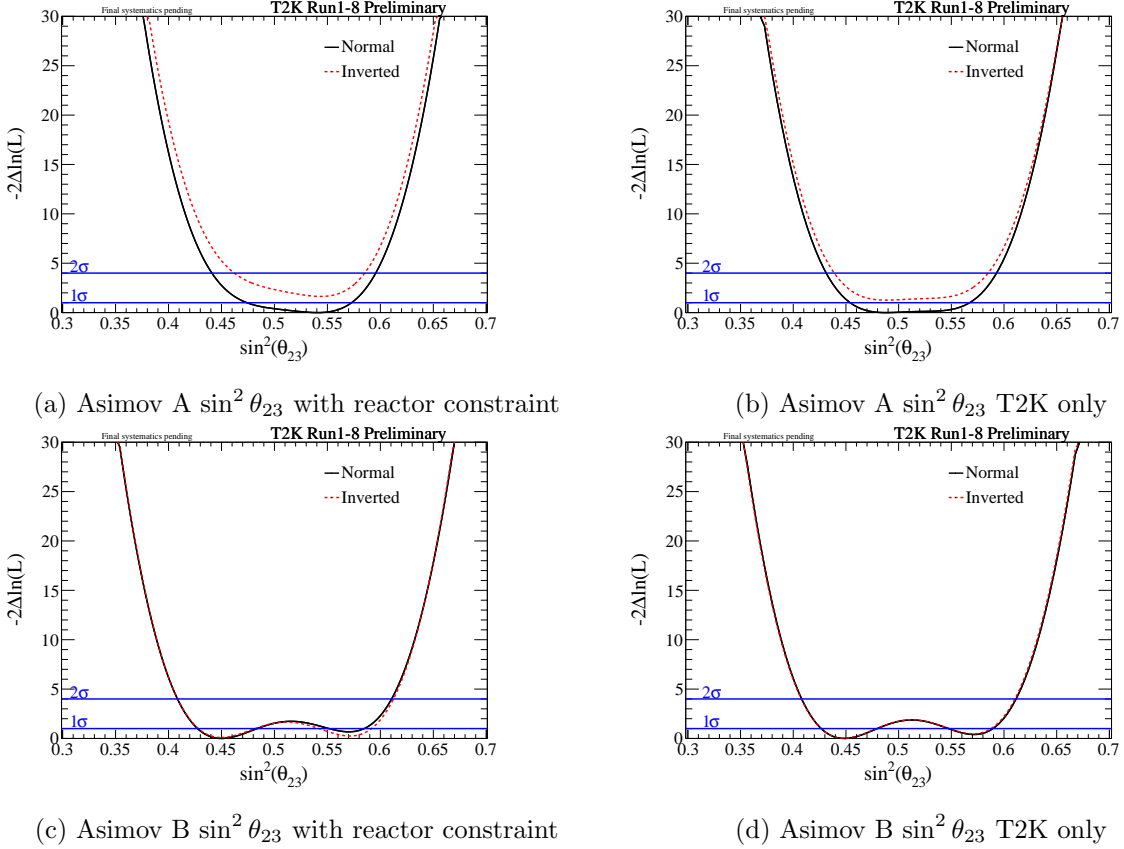


Figure 26: The expected $\Delta\chi^2$ distribution as a function of $\sin^2 \theta_{23}$ with and without reactor constraint for Asimov data sets A and B. The mass hierarchy is minimized, with normal and inverted hierarchy $\Delta\chi^2$ distributions shifted to the same global best-fit χ^2 value, which is taken to be the minimum between normal and inverted hierarchy. All 5 samples were used to produce these fits.

386 4.2.6. Results for Δm_{32}^2

387 The sensitivity to Δm_{32}^2 with reactor constraint and T2K only is shown for the Asimov data
 388 sets A and B in fig. 27.

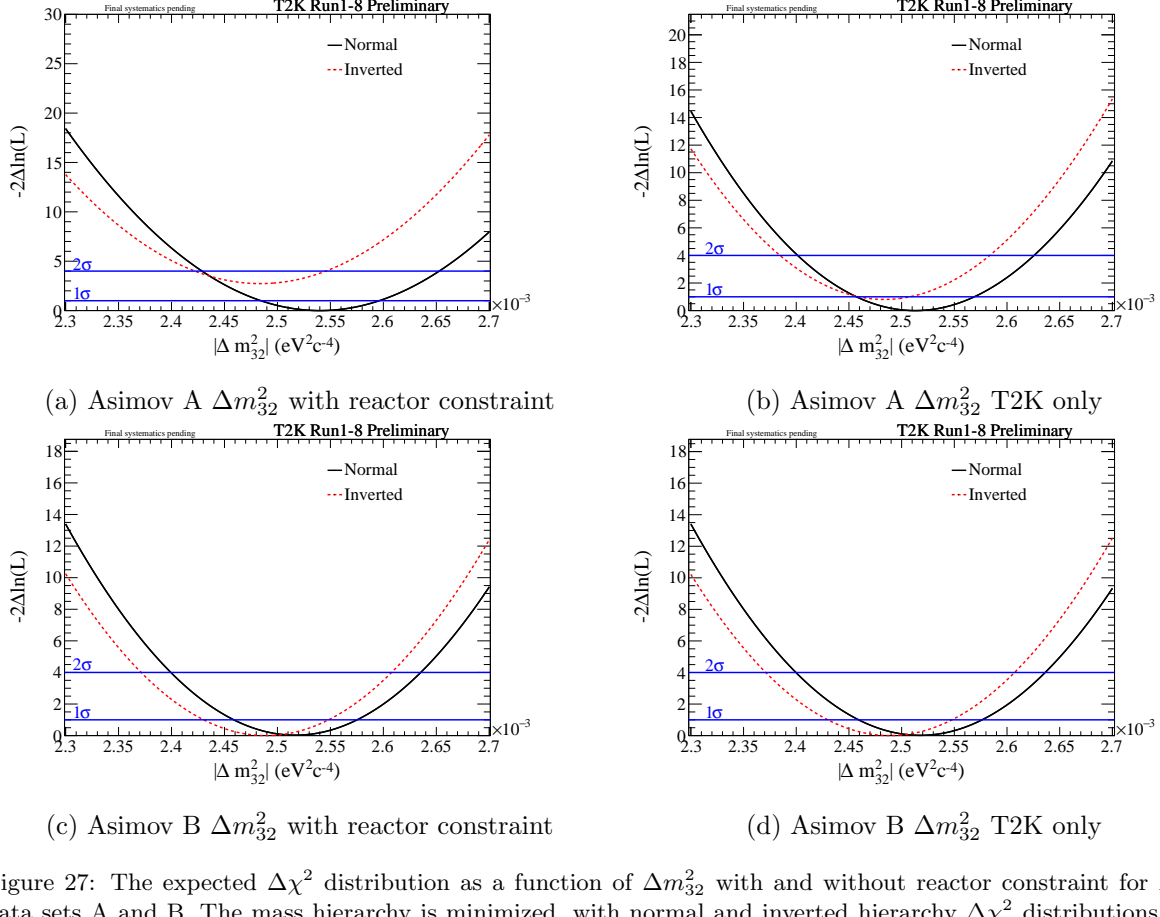


Figure 27: The expected $\Delta\chi^2$ distribution as a function of Δm_{32}^2 with and without reactor constraint for Asimov data sets A and B. The mass hierarchy is minimized, with normal and inverted hierarchy $\Delta\chi^2$ distributions shifted to the same global best-fit χ^2 value, which is taken to be the minimum between normal and inverted hierarchy. All 5 samples were used to produce these fits.

389 4.2.7. Comparison with previous analysis

390 Not available yet.

³⁹¹ **5. Results of the $\nu\bar{\nu}$ joint analysis with the Run 1-8 dataset**

³⁹² The results of the Run 1-8 data set fit, for an exposure of 1.4734×10^{21} POT in neutrino mode
³⁹³ and of 7.558×10^{20} POT in antineutrino mode, are shown in this chapter. In fig. 28 the predicted
³⁹⁴ spectra of μ -like and e -like samples are compared to the observed data. In table 15 the expected
³⁹⁵ and observed number of events in Run 1-8 data set are shown. The predicted number of events are
³⁹⁶ shown for the oscillation parameters of Asimov data sets A and B. The comparison of the confidence
³⁹⁷ intervals obtained by the fit of the Run 1-8 data set among all the oscillation analysis groups is
³⁹⁸ shown in [88].

Beam mode	Sample	Exp. Asimov A	Exp. Asimov A ($\delta_{CP} = 0$)	Exp. Asimov B	Exp. Not Osc	Observed
ν	μ -like	268.415	268.053	280.994	1209.918	240
ν	e -like	73.476	61.434	54.684	15.356	74
$\bar{\nu}$	μ -like	64.278	64.123	66.010	211.548	68
$\bar{\nu}$	e -like	7.911	9.023	8.187	3.243	7
ν	ν_e CC1 π^+ -like	6.919	6.009	5.389	2.543	15

Table 15: The observed, expected and best-fit number of events in Run 1-8 data set for an exposure of 1.4734×10^{21} POT in neutrino mode and of 7.558×10^{20} POT in antineutrino mode are shown for each selected sample. The prediction is produced using the BANFF tuning and the oscillation parameters shown in table 1.

³⁹⁹ The predicted and observed spectra are shown for each of the samples in fig. 28. The e -like
⁴⁰⁰ samples are broken down into E_{rec} and θ projections in fig. 29.

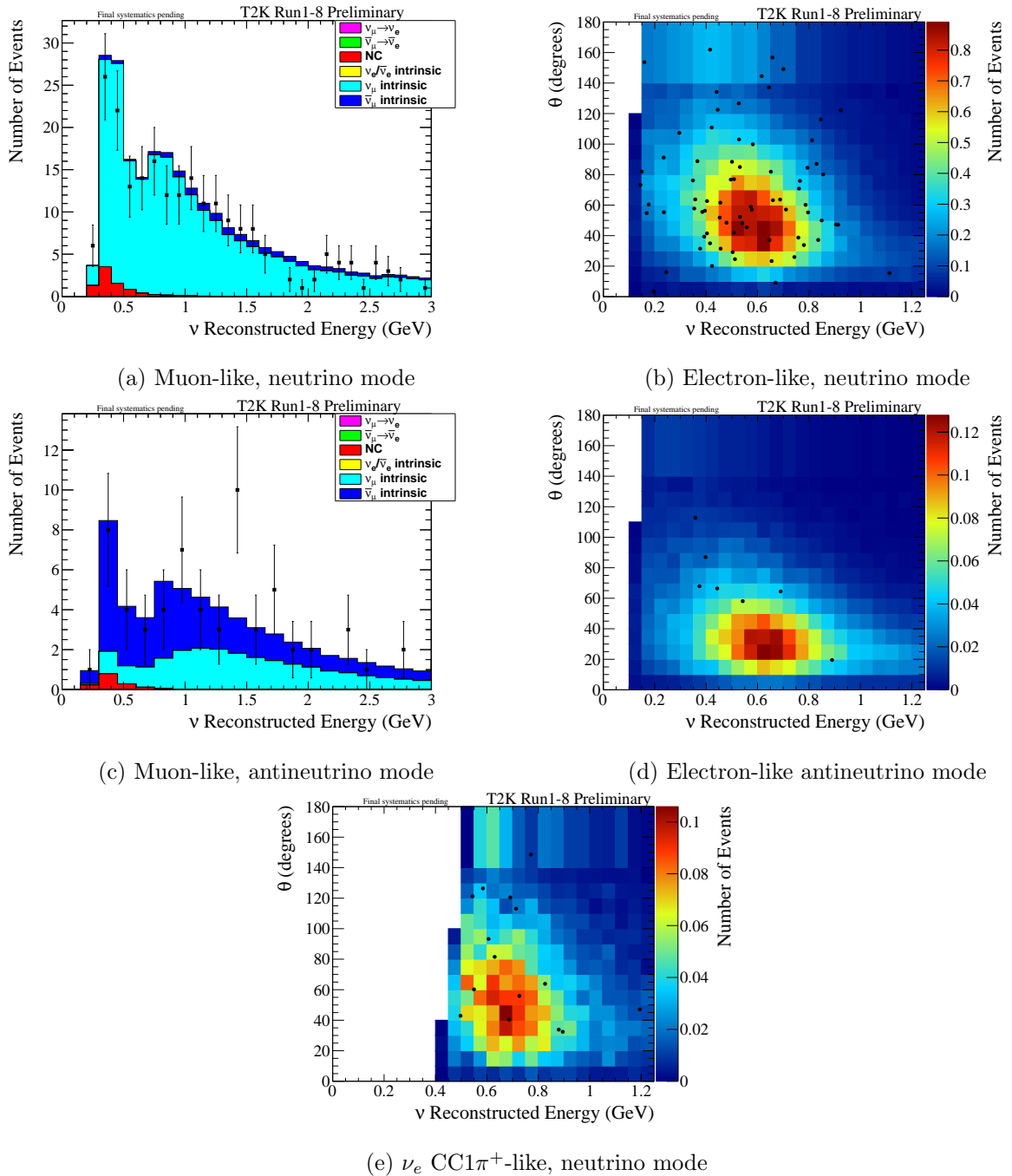


Figure 28: Predicted spectra and observed events (points). μ -like distributions are a function of the reconstructed neutrino energy, while the e -like, including ν_e CC1 π^+ , distributions are functions of both the reconstructed neutrino energy and the reconstructed angle between the outgoing lepton and the neutrino direction. The distributions correspond to the statistics collected in the full Run 1-8 data set. The spectra are generated with the systematic parameters described in section 3 and the oscillation parameters corresponding to the best-fit values from the data fit (solar parameters at PDG 2016).

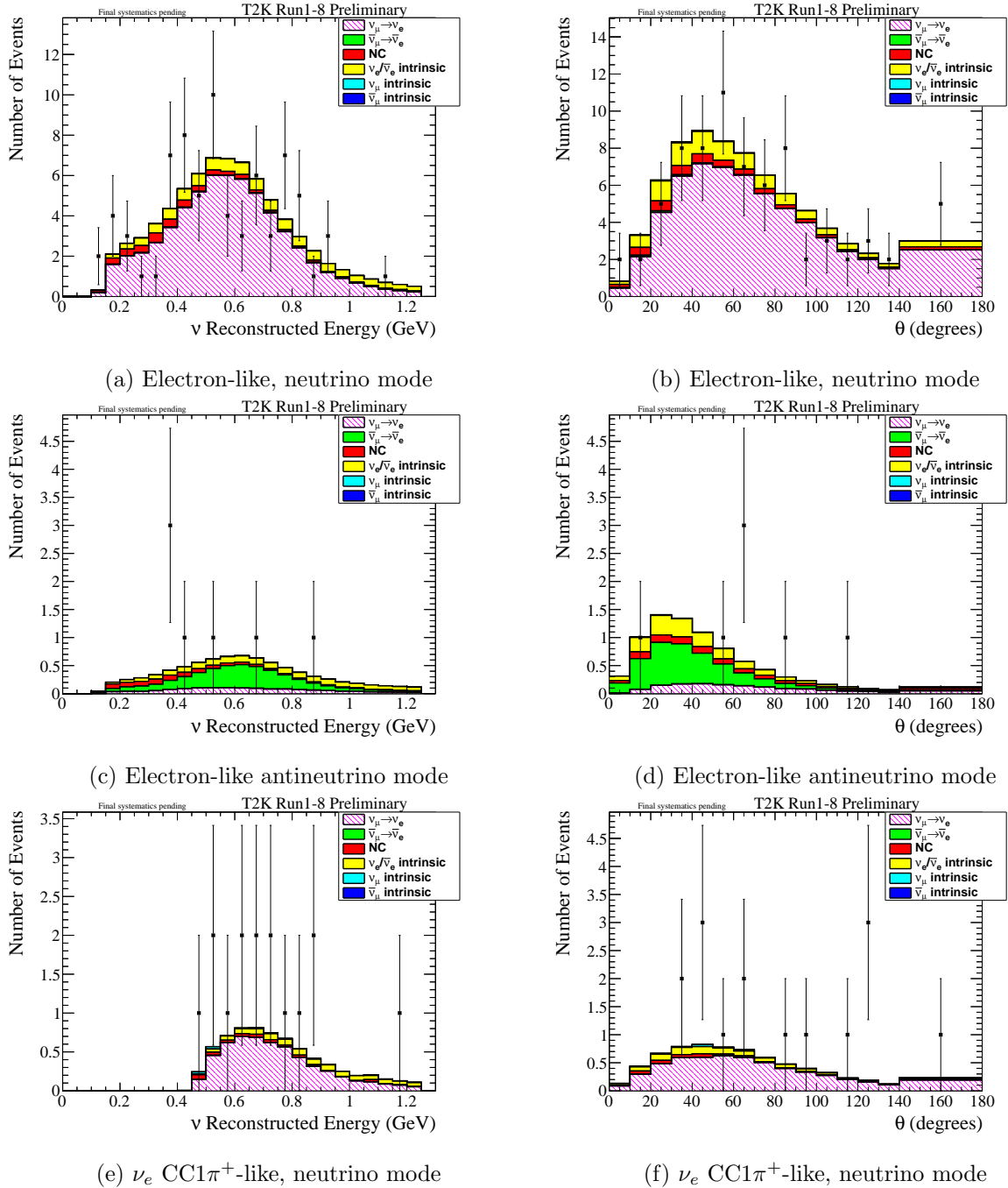


Figure 29: Predicted spectra and observed events (points). The e -like, including ν_e CC1 π^+ , distributions are functions of both the reconstructed neutrino energy and the reconstructed angle between the outgoing lepton and the neutrino direction, with the projections in each variable shown here. The distributions correspond to the statistics collected in the full Run 1-8 data set. The spectra are generated with the systematic parameters described in section 3 and the oscillation parameters corresponding to the best-fit values from the data fit (solar parameters at PDG 2016).

Parameter	Reactor	Best-fit (NH)	$\pm 1\sigma$ (NH)	Best-fit (IH)	$\pm 1\sigma$ (IH)
δ_{CP}	Yes	-1.833	[-2.476,-1.151]	-1.374	[-1.947,-0.886]
δ_{CP}	No	-2.083	[-2.972,-1.151]	-1.157	[-1.965,-0.403]
$\sin^2 \theta_{13}$	No	0.0277	[0.0230,0.0331]	0.0331	[0.0265,0.0378]
$\sin^2 \theta_{23}$	Yes	0.530	[0.493,0.561]	0.530	[0.496,0.559]
Δm_{32}^2 or Δm_{13}^2 (10^{-3} eV 2 /c 4)	Yes	2.462	[2.407,2.519]	2.436	[2.383,2.491]

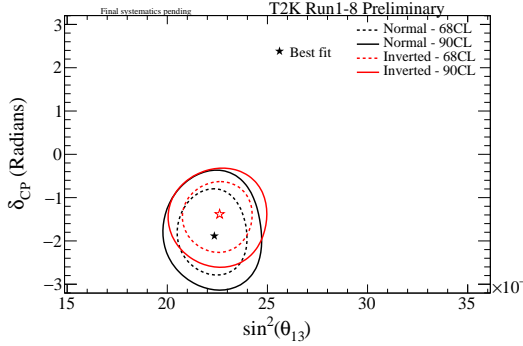
Table 16: The Run 1-8 measured oscillation parameter best-fit and the $\pm 1\sigma$ intervals are shown for normal and inverted hierarchies with respect to the hierarchy best-fit. The $\pm 1\sigma$ interval is obtained by using the constant $\Delta\chi^2$ method. For each parameter normal hierarchy is the global best-fit.

401 The best-fit values and 1σ ranges for each oscillation parameter are shown in table 16 for normal
 402 hierarchy (which is preferred in all data fits). The 1σ ranges are extracted for each oscillation
 403 parameter from the 1-dimensional $\Delta\chi^2$ distributions shown in figs. 32 to 35.

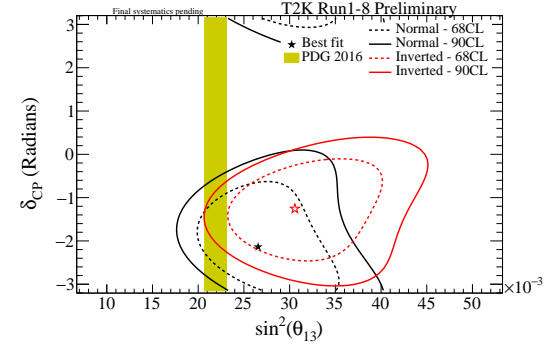
404 The 1-dimensional contours are plotted with respect to the global minimum from normal and
 405 inverted hierarchies, while the 2-dimensional confidence intervals are shown drawing the normal and
 406 inverted hierarchy contours independently, i.e. each contour is produced with respect to the global
 407 minimum under that hierarchy hypothesis.

408 5.1. Results for δ_{CP} vs $\sin^2 \theta_{13}$

409 In fig. 30 the result for δ_{CP} vs $\sin^2 \theta_{13}$ with reactor constraint and T2K only is shown.



(a) δ_{CP} vs $\sin^2 \theta_{13}$ with reactor constraint

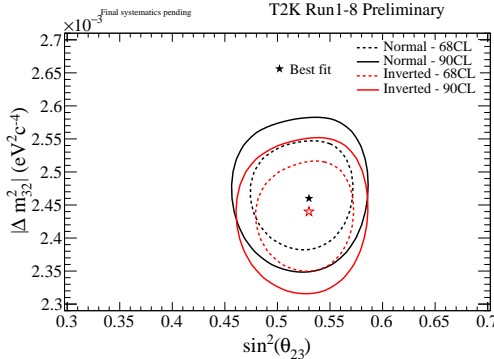


(b) δ_{CP} vs $\sin^2 \theta_{13}$ T2K only

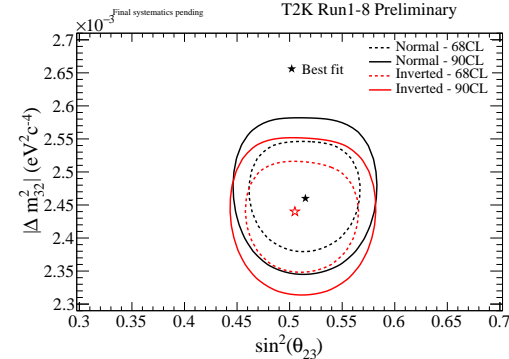
Figure 30: Contours at 68% and 90% CL for δ_{CP} vs $\sin^2 \theta_{13}$ with and without reactor constraint. Normal and inverted hierarchy contours are independent. All 5 samples were used to produce these fits.

410 5.2. Results for Δm_{32}^2 vs $\sin^2 \theta_{23}$

411 The result for Δm_{32}^2 vs $\sin^2 \theta_{23}$ with reactor constraint and T2K only is shown in fig. 31.



(a) Δm_{32}^2 vs $\sin^2 \theta_{23}$ with reactor constraint



(b) Δm_{32}^2 vs $\sin^2 \theta_{23}$ T2K only

Figure 31: Contours at 68% and 90% CL for Δm_{32}^2 vs $\sin^2 \theta_{23}$ with and without reactor constraint. Normal and inverted hierarchy contours are independent. All 5 samples were used to produce these fits.

412 5.3. Results for δ_{CP}

413 The result for δ_{CP} with reactor constraint and T2K only is shown in fig. 32.

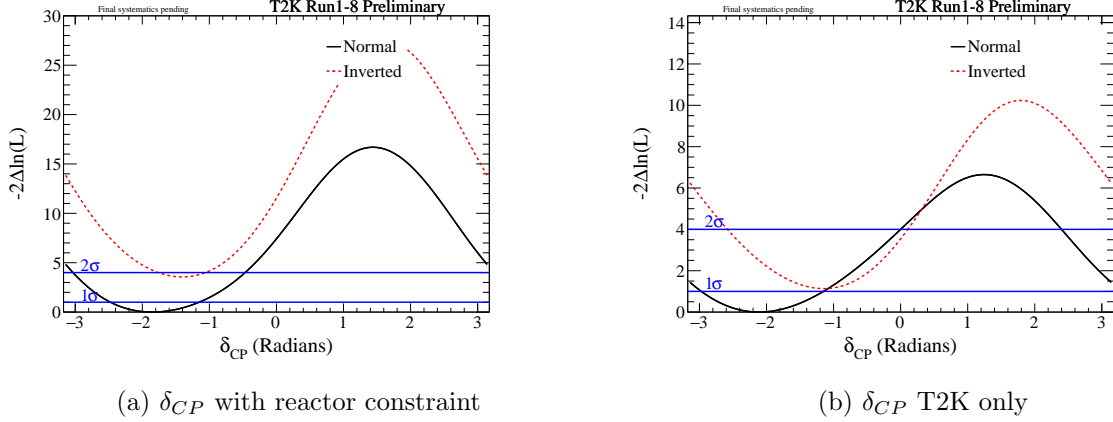


Figure 32: The expected $\Delta\chi^2$ distribution as a function of δ_{CP} with and without reactor constraint. The mass hierarchy is minimized, with normal and inverted hierarchy $\Delta\chi^2$ distributions shifted to the same global best-fit χ^2 value, which is taken to be the minimum between normal and inverted hierarchy. All 5 samples were used to produce these fits.

414 5.4. Results for $\sin^2 \theta_{13}$

415 The result for $\sin^2 \theta_{13}$ (without reactor constraint) is shown in fig. 33.

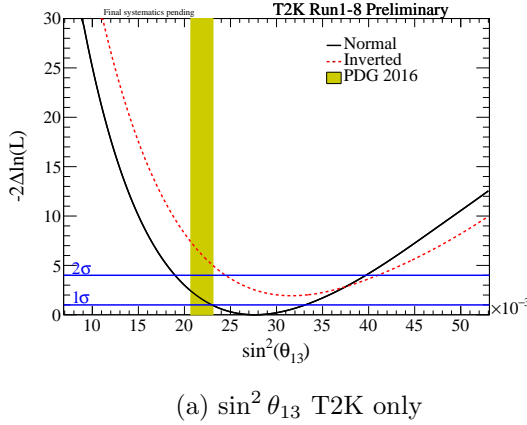


Figure 33: The expected $\Delta\chi^2$ distribution as a function of $\sin^2 \theta_{13}$ without reactor constraint. The mass hierarchy is minimized, with normal and inverted hierarchy $\Delta\chi^2$ distributions shifted to the same global best-fit χ^2 value, which is taken to be the minimum between normal and inverted hierarchy. All 5 samples were used to produce these fits.

416 5.5. Results for $\sin^2 \theta_{23}$

417 The result for $\sin^2 \theta_{23}$ with reactor constraint and T2K only is shown in fig. 34.

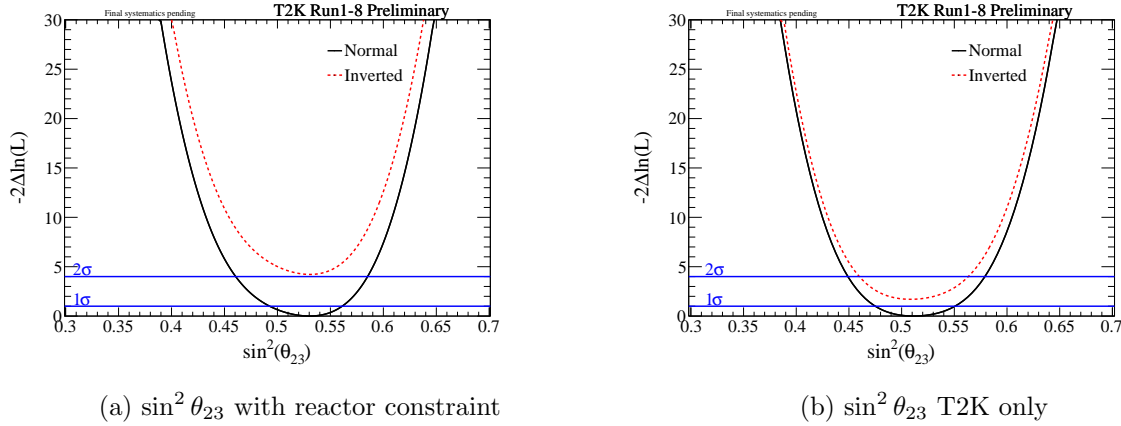


Figure 34: The expected $\Delta\chi^2$ distribution as a function of $\sin^2 \theta_{23}$ with and without reactor constraint. The mass hierarchy is minimized, with normal and inverted hierarchy $\Delta\chi^2$ distributions shifted to the same global best-fit χ^2 value, which is taken to be the minimum between normal and inverted hierarchy. All 5 samples were used to produce these fits.

418 5.6. Results for Δm_{32}^2

419 The result for Δm_{32}^2 with reactor constraint and T2K only is shown in fig. 35.

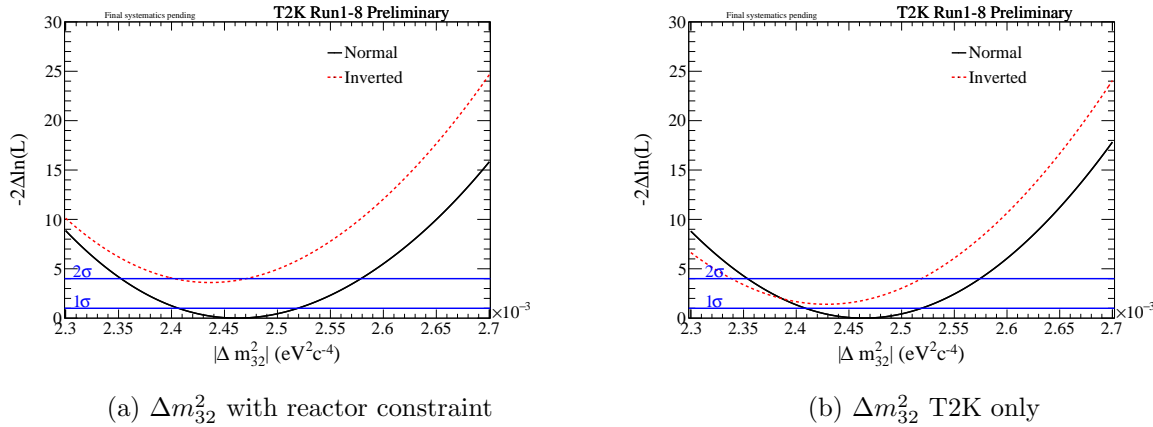


Figure 35: The expected $\Delta\chi^2$ distribution as a function of Δm_{32}^2 with and without reactor constraint. The mass hierarchy is minimized, with normal and inverted hierarchy $\Delta\chi^2$ distributions shifted to the same global best-fit χ^2 value, which is taken to be the minimum between normal and inverted hierarchy. All 5 samples were used to produce these fits.

420 5.7. Feldman-Cousins simultaneous fit of δ_{CP} and mass hierarchy

421 This section presents the results of the Feldman-Cousins fit of δ_{CP} and mass hierarchy. Throws
 422 of oscillation parameters are made according to PDG 2016 best-fit values and errors for $\sin^2 \theta_{13}$,
 423 $\sin^2 \theta_{12}$ and Δm_{21}^2 , whilst $\sin^2 \theta_{23}$ and Δm_{32}^2 are thrown according to the likelihood distribution
 424 produced by an Asimov fit using the best-fit from data for these parameters, this is an updated

method from the previous analysis and the proposal is given in [89]. δ_{CP} is fixed at one of 9 evenly specified values on the range $[-\pi, \pi]$.

5.7.1. Input oscillation parameters

The distributions of oscillation parameters (for normal hierarchy) are shown in fig. 36. Note that whilst the distributions of the atmospheric parameters are shown independently they are generated jointly from the likelihood distribution shown in fig. 37.

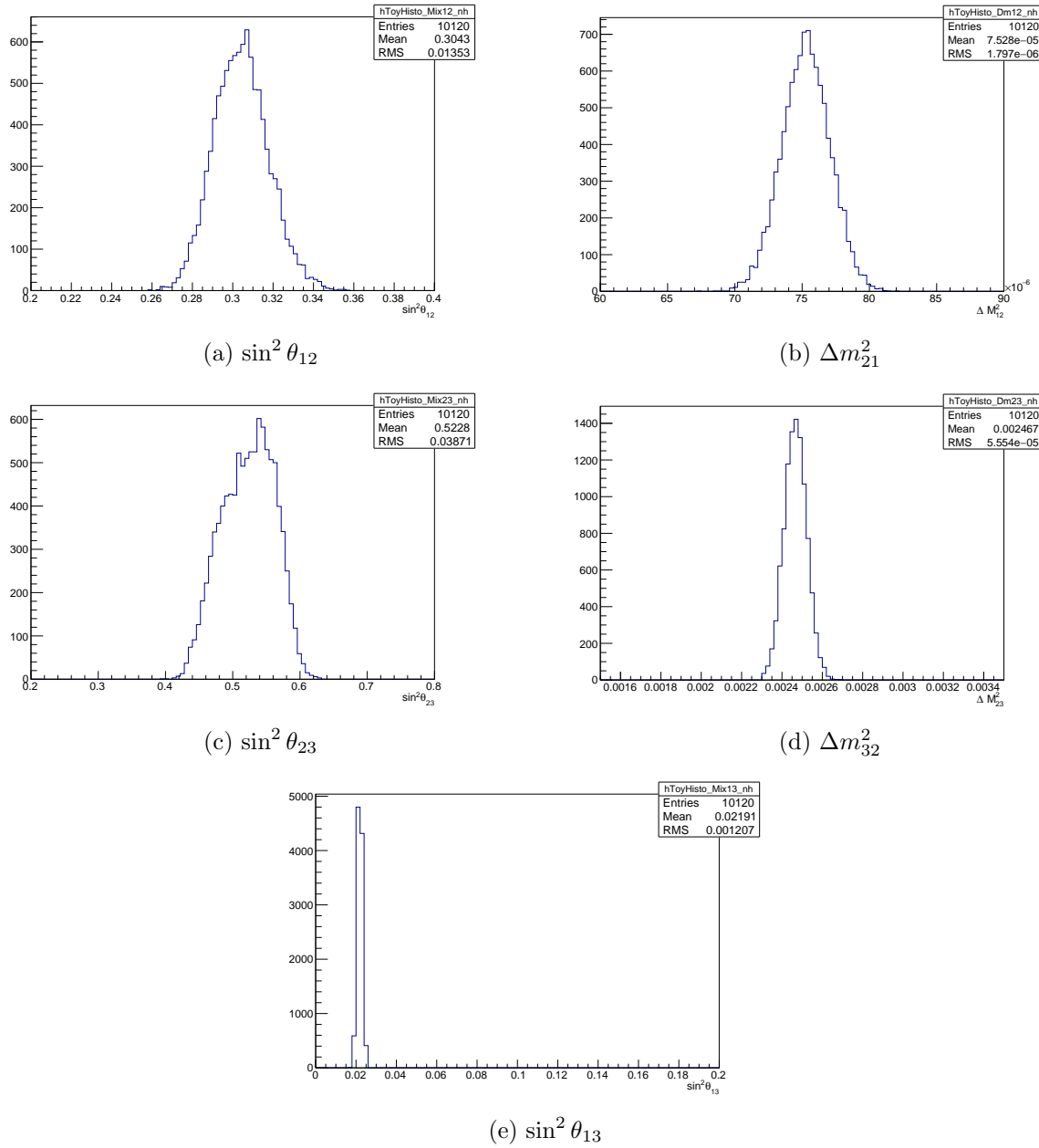
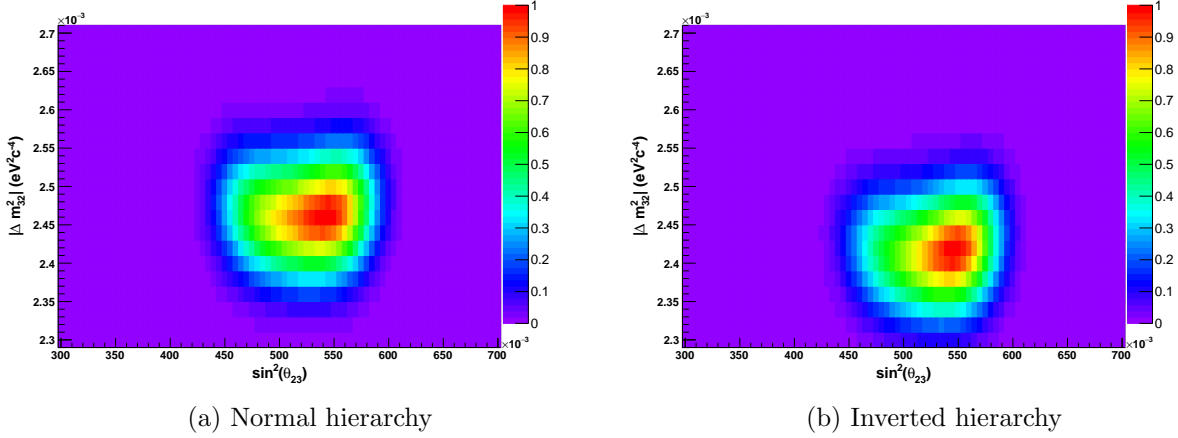


Figure 36: Distribution of oscillation parameter throws for Feldman-Cousins fits.



(a) Normal hierarchy

(b) Inverted hierarchy

Figure 37: Likelihood surfaces for throws of the disappearance parameter.

431 5.7.2. *Feldman-Cousins critical values and confidence intervals*

432 In fig. 38 the confidence intervals obtained with the ‘Feldman-Cousins’ method are shown for
 433 δ_{CP} and mass hierarchy with reactor constraint for the Run 1-8 data set. The critical values at
 434 90%, 2σ and 3σ CL are computed for both the mass hierarchies at the following true values of δ_{CP} ;
 435 $-\pi, -3\pi/4, -\pi/2, -\pi/4, 0, +\pi/4, +\pi/2, +3\pi/4$, and $+\pi$. Inverted hierarchy is almost excluded at
 436 2σ , except for a small interval around $\delta_{CP} = -\pi/2$. Both $\delta_{CP} = 0$ and $\delta_{CP} = \pi$ are excluded at 2σ .
 437 In table 17 the 2σ CL intervals for δ_{CP} versus mass hierarchy, obtained with the Feldman-Cousins
 438 method, are shown.

Parameter	Reactor	CL	Normal hierarchy	Inverted hierarchy
δ_{CP}	Yes	90%	$[-2.805, -0.830]$	-
δ_{CP}	Yes	2σ	$[-2.981, -0.600]$	$[-1.531, -1.184]$

Table 17: The confidence intervals at 90% CL and 2σ CL obtained with the Feldman-Cousins method for the Run 1-8 data set is shown for the measurement of δ_{CP} versus mass hierarchy.439 5.8. *Discussion of the Run 1-8 data fit results*

440 The ν_e CC1 π^+ data set shows an excess in the number of observed appearance events, observing
 441 15 events compared to an Asimov A expectation of 7. Unlike in our previous analysis, an excess is
 442 not observed in the neutrino mode one ring e -like sample, rather in this analysis we see a deficit in
 443 the number of observed events in neutrino mode one ring μ -like sample, observing 240 against an
 444 Asimov A expectation of 268.

445 The value of δ_{CP} favoured by the joint fit analysis, when the reactor constraint is applied, is
 446 -1.833 and corresponds to normal hierarchy. If the reactor constraint is not applied, the best-fit
 447 value of δ_{CP} is -2.083 and $\delta_{CP} = 0$ is still excluded at 2σ CL.

448 When considering the constant $\Delta\chi^2$ method, we see that the constraint on δ_{CP} is stronger than
 449 expected. To investigate the source of this difference a number of fits were undertaken using hybrids
 450 of data and MC. In particular fig. 39 shows the expected sensitivity from the Asimov A data set

451 (dashed), the data fit (solid black) and then a number of additional fits where one of the data
 452 samples was replaced by the corresponding Asimov A sample (e.g. Data x1Rmu indicates a fit of 4
 453 data samples, with the one-ring μ -like sample being replaced by the Asimov A prediction). From
 454 this one can see that the largest contribution to the stronger constraint comes from the upward
 455 fluctuation observed in the ν_e CC1 π^+ sample, but contributions are also evident from the FHC
 456 one-ring μ -like sample, where a deficit in events is seen, and from the two one-ring e -like samples.
 457 This results in the exclusion of CP-conservation at more than 2σ with the reactor constraint applied
 458 and the inverted hierarchy is disfavoured at 90%CL. The effect is also apparent in the appearance
 459 contour.

460 A stronger than expected constraint is also evident in the disappearance contour, with greater
 461 exclusion in $\sin^2 \theta_{23}$. Similarly to the δ_{CP} hybrid fits above, fig. 40 shows the expected sensitivity
 462 from the Asimov A data set (red), the data fit (black) and then a number of additional fits where
 463 one of the data samples was replaced by the corresponding Asimov A sample. From this one can
 464 see that the stronger constraint can be explained by the deficit in the observed number of events in
 465 the one-ring μ -like sample.

466 The value of $\sin^2 \theta_{13}$ favoured by the analysis is 0.0277 and corresponds to normal hierarchy,
 467 with the 1D contours in agreement with the PDG 2016 reactor constraint (0.0219 ± 0.0012) at
 468 $\sim 1.2\sigma$ (see table 16).

469 The value of $\sin^2 \theta_{23}$ favoured by the analysis is 0.530 (0.510) with (without) the reactor con-
 470 straint and corresponds to normal hierarchy, with the 1D contours in agreement with and without
 471 the reactor constraint at 1σ , favouring maximal mixing as seen in our previous analyses.

472 The value of Δm_{32}^2 favoured by the analysis is 2.462×10^{-3} eV $^2/c^4$ (2.466×10^{-3} eV $^2/c^4$) with
 473 (without) the reactor constraint and corresponds to normal hierarchy, with the 1D contours in
 474 agreement with and without the reactor constraint at 1σ .

475 5.9. Comparison of δ_{CP} versus mass hierarchy result with sensitivity

476 In order to provide a better understanding of the results of the Run 1-8 data fit, the result has
 477 been compared with the expected sensitivity obtained from a large number (10k) of toy experiments
 478 for different true value of δ_{CP} (currently only $\delta_{CP} = -\pi/2$ is included) and the mass hierarchy.

479 5.9.1. Expected sensitivity method

480 This section outlines the procedure to produce the expected sensitivity comparison plots. The
 481 example given is for true normal hierarchy and $\delta_{CP} = -\pi/2$.

- 482 • 1×10^4 fake data sets are generated following the Feldman-Cousins method for a true value
 483 of δ_{CP} and mass hierarchy, in this case $\delta_{CP} = -\pi/2$ and normal hierarchy.
- 484 • A χ^2 distribution is computed with respect to the marginalisation toys as a function of δ_{CP}
 485 and mass hierarchy.
- 486 • For each fake data set, the minimum value of χ^2 for each bin of δ_{CP} , $\chi^2_{bin,min}$ is found with
 487 respect to both normal and inverted hierarchy.

- 488 • The test statistic is then computed as $\Delta\chi^2_{bin} = \chi^2_{bin} - \chi^2_{bin,min}$, which is slightly different to
 489 the Feldman-Cousins method, where $\Delta\chi^2_{FC} = \chi^2_{true} - \chi^2_{best-fit}$. The distributions of $\Delta\chi^2_{bin}$
 490 and $\Delta\chi^2_{FC}$ coincide if the bin is $\delta_{CP} = -\pi/2$ and normal hierarchy, i.e. the true point used
 491 to generate the toy experiments.
- 492 • This results in a $\Delta\chi^2$ distribution from which we can draw conclusions about the expected
 493 $\Delta\chi^2$ for each value of δ_{CP} given a hypothesised true value and hierarchy.
- 494 • The spread of the $\Delta\chi^2$ distribution for each point of δ_{CP} and mass hierarchy is obtained as
 495 the range of the $\Delta\chi^2_{bin}$ distribution that contains respectively the 68.27% and 95.45% of the
 496 toy experiments on its left side. The test statistic $\Delta\chi^2_{bin}$ is assumed to be 1-sided because by
 497 construction $\chi^2_{bin,min} \leq \chi^2_{bin}$.
- 498 • A plot is also produced to show the fraction of toy experiments which exclude each value of
 499 δ_{CP} to greater than 2σ significance in the Feldman-Cousins corrected critical values along
 500 with the probabilities to exclude $\delta_{CP} = 0$ and $\delta_{CP} = \pi$ for a given true value of δ_{CP} .

501 *5.9.2. $\delta_{CP} = -\pi/2$ - normal hierarchy*

502 In fig. 41 the Run 1-8 data result for δ_{CP} versus mass hierarchy is compared to the 1σ and 2σ
 503 uncertainties on the $\Delta\chi^2$ distributions corresponding to $\delta_{CP} = -\pi/2$ and (a) normal hierarchy and
 504 (b) inverted hierarchy. We see that the data contour is contained within the 2σ band for inverted
 505 hierarchy, whilst the data contour falls just outside the 2σ band for normal hierarchy in the region
 506 around $\delta_{CP} = 0$. This suggests that the data constraint is consistent with the PMNS matrix at
 507 around the 2σ level.

508 We also see an interesting feature near $\delta_{CP} = -\pi/2$ where the $\Delta\chi^2$ values have a wider distri-
 509 bution. This is due to the boundary at $\delta_{CP} = -\pi/2$ which causes a wider distribution when the
 510 parameter δ_{CP} would like to be pushed beyond the boundary in the fit.

511 Finally from fig. 41(c) we see that $\delta_{CP} = 0$ and $\delta_{CP} = \pi$ are excluded at 90% confidence level
 512 in around 40% (see table 18) of the toy experiments and excluded at 2σ confidence level in between
 513 25% and 30% of the toy experiments, with $\delta_{CP} = \pi$ excluded in slightly fewer toy experiments in
 514 each case.

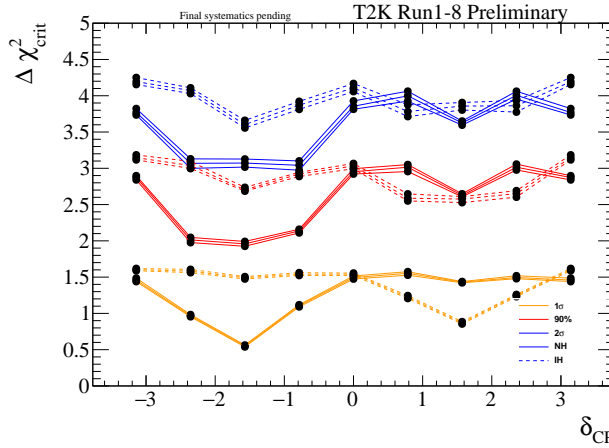
δ_{CP}	Hierarchy	90%	2σ
0	NH	0.430	0.300
π	NH	0.383	0.250
0	IH	0.760	0.656
π	IH	0.769	0.667

Table 18: The fraction of toy experiments for which $\delta_{CP} = 0, \pi$ and normal and inverted hierarchy are excluded at 90% and 2σ CL is shown. 10k toy experiments are used.

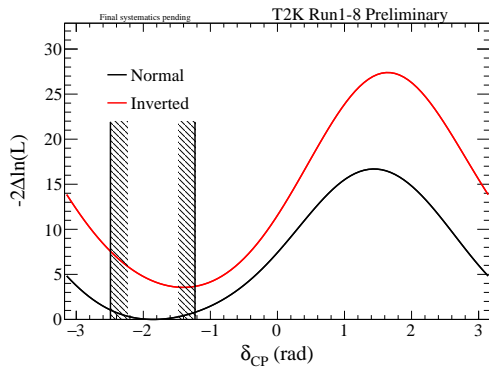
515 *5.10. Comparison of e-like event rates with expectation*

516 It is valuable to see how different values of δ_{CP} , $\sin^2 \theta_{23}$ and hierarchy affect the predicted
 517 event rates. Figure 42 shows the predicted $\bar{\nu}_e$ event rate vs ν_e event rate for best-fit values of

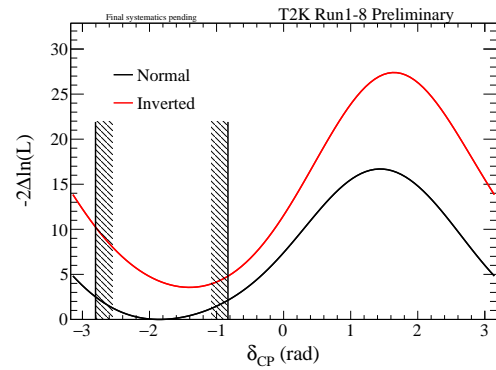
518 oscillation parameters where δ_{CP} is varied between CP conserving and maximally CP violating
519 values, and $\sin^2 \theta_{23}$ is varied around its best-fit, for both hierarchies. Event rates for a given value
520 of $\sin^2 \theta_{23}$ and mass hierarchy are linearly interpolated between those computed for the different
521 values of δ_{CP} to indicate the behaviour produced by varying δ_{CP} . The observed event rates with
522 1σ errors are also shown. Figure 42(a) shows e -like event rates where the FHC sample includes the
523 ν_e CC1 π^+ sample, while fig. 42(b) shows e -like event rates where the FHC sample does not include
524 the ν_e CC1 π^+ sample.



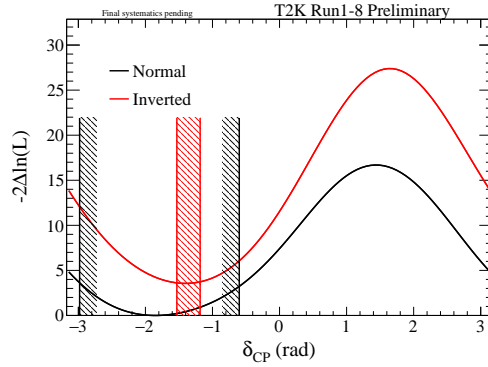
(a) Critical $\Delta\chi^2$ values



(b) 90% CL exclusion region



(c) 90% CL exclusion region



(d) 2 σ CL exclusion region

Figure 38: $\Delta\chi^2$ critical values and confidence intervals for the measured $\Delta\chi^2$ distributions for Run 1-8. Critical values obtained with the Feldman-Cousins method for Run 1-8 for 9 evenly spaced values on the range $[-\pi, \pi]$. Critical values are shown for 1σ , 2σ and 90% CL for normal (solid lines) and inverted (dashed lines) hierarchies. At least 1×10^4 toy experiments are performed for each point. The three bands of lines show the $\pm 1\sigma$ uncertainty on the critical values. Also shown are the measured $\Delta\chi^2$ distributions shifted with respect to the same global minimum and the 1σ , 90% and 2σ exclusion regions for both mass hierarchies.

NH comparison

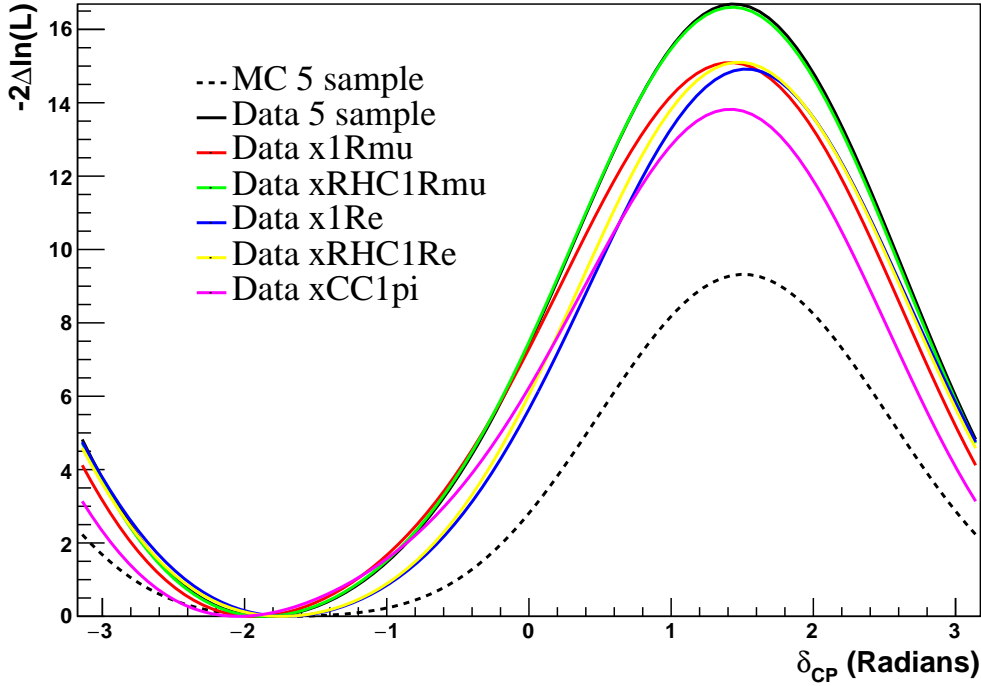


Figure 39: The expected $\Delta\chi^2$ distribution as a function of δ_{CP} with reactor constraint for MC, data and data/MC hybrid data sets.

Disappearance Comparison

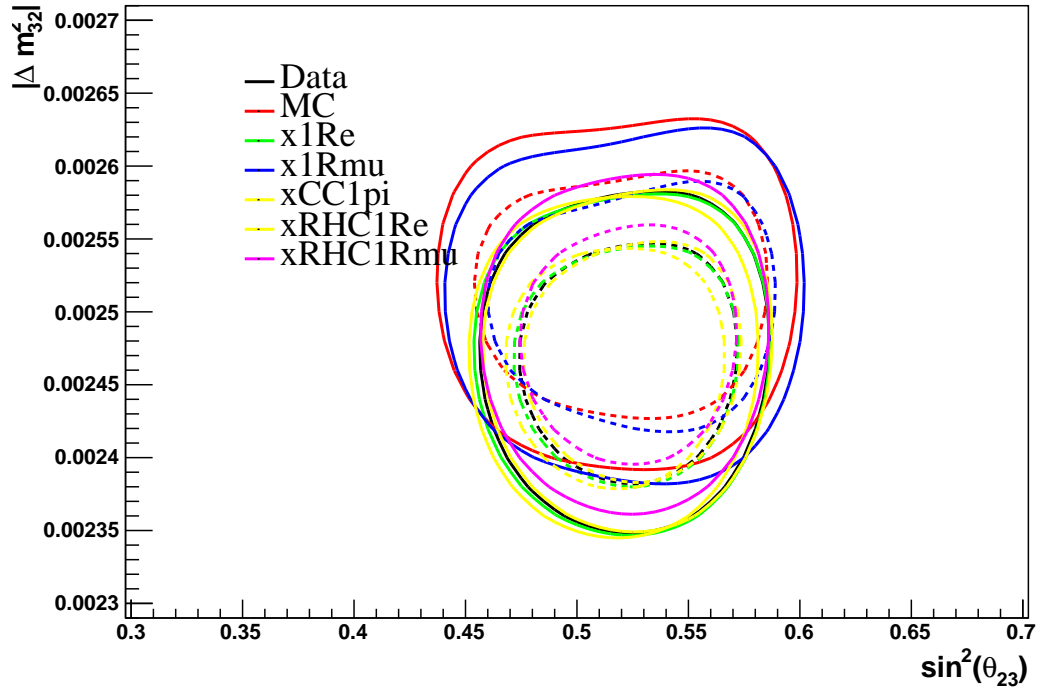


Figure 40: The expected disappearance contours with reactor constraint for normal hierarchy for MC, data and data/MC hybrid data sets.

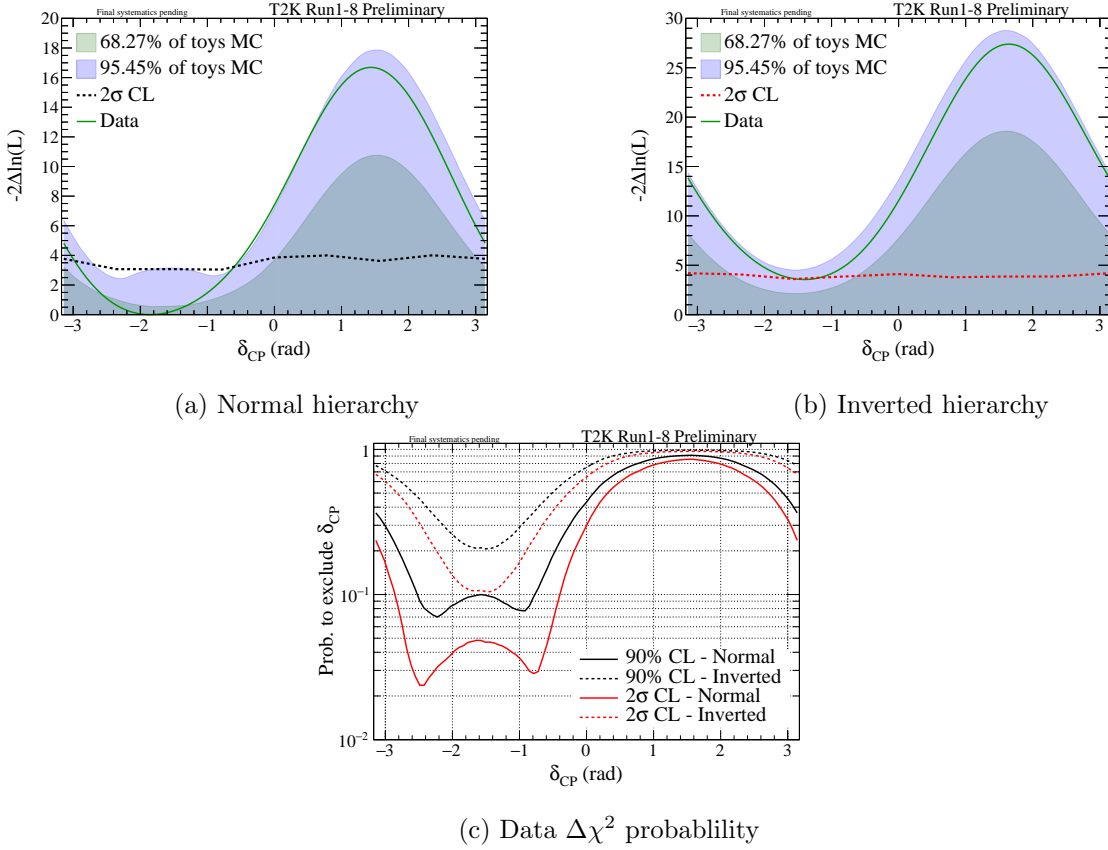


Figure 41: The distribution of $\Delta\chi^2$ vs δ_{CP} obtained with 1×10^4 toy experiments generated with $\delta_{CP} = -\pi/2$ and normal hierarchy is shown. The $\Delta\chi^2$ distributions obtained by fixing the mass hierarchy to normal (left) and inverted (right) are shown, along with the $\Delta\chi^2$ values corresponding to 68.27% and 95.45% of the toy experiments and the average $\Delta\chi^2$ values from all experiments. Also shown are the fractions of toys which exclude each value of δ_{CP} to 90% and 2σ using the Feldman-Cousins corrected critical values (bottom).

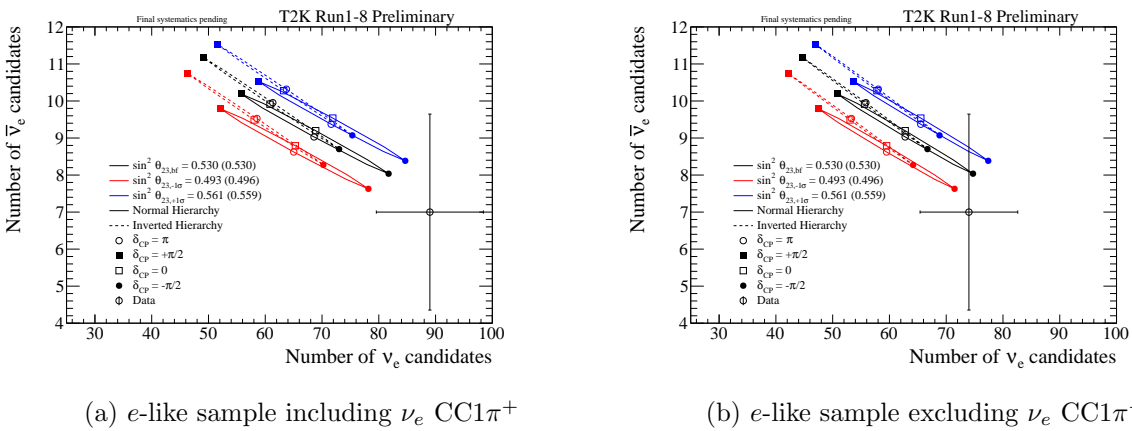


Figure 42: These plots show $\bar{\nu}_e$ event rate vs ν_e event rate for a variety of different oscillation parameter values. Predictions are generated for best-fit values of oscillation parameters for different values of δ_{CP} , $\sin^2 \theta_{23}$ and mass hierarchy. In particular the FHC and RHC event rates are plotted for the CP conserving and maximally CP violating values of δ_{CP} , with $\sin^2 \theta_{23}$ set at the best-fit value and $\pm 1\sigma$ values in both normal and inverted hierarchy. Rates for one-ring e -like including ν_e CC1 π^+ (left) and one-ring e -like excluding ν_e CC1 π^+ (right) are shown. The observed rates with statistical error shown are also included.

525 **6. Summary**

526 In this technical note, we have presented the results of the 3-flavour $\bar{\nu}/\nu$ joint analysis performed
527 by the *VALOR* group, on the combined Run 1-8 data set. The goal of the analysis was to search
528 for CP violation in the leptonic sector and determine limits on δ_{CP} as well as measure all the other
529 oscillation parameters to which T2K is sensitive: $\sin^2 \theta_{13}$, $\sin^2 \theta_{23}$, Δm_{32}^2 (Δm_{13}^2) and partially mass
530 hierarchy, to which T2K has little sensitivity.

531 This analysis predicts 268.4 ± 11.8 (syst) for neutrino μ -like, 64.3 ± 2.4 (syst) for antineutrino
532 μ -like, 73.5 ± 5.3 (syst) for neutrino e -like, 7.9 ± 0.6 (syst) for antineutrino e -like and 6.9 ± 1.5
533 (syst) for neutrino ν_e CC1 π^+ events in Super K and observes respectively 240 for neutrino μ -like,
534 68 for antineutrino μ -like, 74 for neutrino e -like, 7 for antineutrino e -like and 15 for neutrino ν_e
535 CC1 π^+ .

536 The $\bar{\nu}/\nu$ analysis was performed in a framework of 3-flavour oscillations including matter effects
537 in constant-density matter. The observed reconstructed energy spectrum of single μ -like ring events
538 and reconstructed energy versus lepton angle of single e -like ring events in addition to e -like events
539 with an additional decay electron were used to compute the confidence intervals. All 110 systematic
540 parameters as well as the oscillation parameters which were not parameters of interest considered
541 in this analysis were marginalised.

542 From the fit of the Run 1-8 data we can see that the favoured value of δ_{CP} is -1.833, close to
543 $-\pi/2$. The Feldman-Cousins method is used to construct confidence intervals with neither over or
544 under coverage from which the significance to exclude the hypothesis of CP conservation is greater
545 than 2 standard deviations.

- 546 [1] C.Andreopoulos, T.Dealtry, J.Dobson, N.Grant, M.Haigh, J.Ilic, G.Pearce and A.Weber, T2K
 547 3.23×10^{19} -POT Muon-Neutrino Disappearance Analysis, T2K-TN-036(v4),
 548 <http://www.t2k.org/docs/technotes/036>
- 549 [2] C.Andreopoulos, T.Dealtry, J.Dobson, N.Grant, M.Haigh, J.Ilic, G.Pearce and A.Weber, T2K
 550 1.431×10^{20} -POT Muon-Neutrino Disappearance Analysis T2K-TN-064(v3),
 551 <http://www.t2k.org/docs/technotes/064>
- 552 [3] C.Andreopoulos, T.Dealtry, L.Escudero, N.Grant and A.Weber, T2K 1.431×10^{20} -POT 3-
 553 Flavour Muon-Neutrino Disappearance Analysis T2K-TN-087(v1),
 554 <http://www.t2k.org/docs/technotes/087>
- 555 [4] C.Andreopoulos, T.Dealtry, L.Escudero, N.Grant and A.Weber, T2K 3.010×10^{20} -POT 3-
 556 Flavour Muon-Neutrino Disappearance Analysis T2K-TN-141(v10),
 557 <http://www.t2k.org/docs/technotes/141>
- 558 [5] C.Andreopoulos, T.Dealtry, L.Escudero, N.Grant and A.Weber, T2K 6.3933×10^{20} -POT 3-
 559 Flavour Muon-Neutrino Disappearance Analysis T2K-TN-155(v2),
 560 <http://www.t2k.org/docs/technotes/155>
- 561 [6] C.Andreopoulos, T.Dealtry, L.Escudero, N.Grant and A.Weber, T2K 6.57×10^{20} -POT 3-Flavour
 562 Muon-Neutrino Disappearance Analysis T2K-TN-183(v3),
 563 <http://www.t2k.org/docs/technotes/183>
- 564 [7] C.Andreopoulos et al., T2K 3.010×10^{20} -POT Joint 3-Flavour Oscillation Analysis T2K-TN-
 565 154(v3),
 566 <http://www.t2k.org/docs/technotes/154>
- 567 [8] C.Andreopoulos et al., T2K 6.57×10^{20} -POT Joint 3-Flavour Oscillation Analysis T2K-TN-175,
 568 <http://www.t2k.org/docs/technotes/175>
- 569 [9] C.Andreopoulos et al., T2K 2.315×10^{20} -POT 3-Flavour Muon-Antineutrino Disappearance
 570 Analysis T2K-TN-243,
 571 <http://www.t2k.org/docs/technotes/243>
- 572 [10] C.Andreopoulos et al., T2K 4.0108×10^{20} -POT 3-Flavour Electron-Antineutrino Appearance
 573 Analysis T2K-TN-252,
 574 <http://www.t2k.org/docs/technotes/252>
- 575 [11] C.Andreopoulos et al., T2K Neutrino and Anti-Neutrino 3-Flavour Joint Analysis of
 576 Run 1-6 (6.914×10^{20} -POT ν 4.011×10^{20} -POT $\bar{\nu}$),
 577 Run 1-7b (7.002×10^{20} -POT ν 7.471×10^{20} -POT $\bar{\nu}$) and
 578 Run 1-7c (7.482×10^{20} -POT ν 7.471×10^{20} -POT $\bar{\nu}$) data sets T2K-TN-266,
 579 <http://www.t2k.org/docs/technotes/266>

- 580 [12] C.Andreopoulos et al., T2K 7.482×10^{20} -POT FHC and 7.471×10^{20} -POT RHC (1-7c) Join
 581 3-Flavour $\nu_\mu/\bar{\nu}_\mu$ Disappearance and $\nu_e/\bar{\nu}_e$ Appearance Analysis with
 582 additional ν_e CC1 π^+ -like sample T2K-TN-306,
 583 <http://www.t2k.org/docs/technotes/306>
- 584 [13] C.Andreopoulos, T.Dealtry, L.Escudero and N.Grant, T2K 6.5700×10^{20} -POT 3-Flavour Muon-
 585 Neutrino Disappearance Analysis: Supplementary material on the effect of systematics, T2K-
 586 TN-183 supplement,
 587 <http://www.t2k.org/docs/technotes/183>
- 588 [14] S. Bolognesi, M. Dunkman, P. Dunne, Y. Hayato, A. Kaboth, K. Mahn, K. McFarland, J.
 589 Morrison, M. Scott, P. Stowell, C. Wilkinson, and C. Wret Updates to T2KReWeight for the
 590 2017 analysis T2K-TN-309,
 591 <http://www.t2k.org/docs/technotes/309>
- 592 [15] S. Bolognesi, C. Bronner, A. Cudd, M. Dunkman, P. Dunne, Y.Hayato, A. Kaboth, M.
 593 Kabirnezhad, K. Mahn, P. Martins, K.McFarland, J. Morrison, E.S. Pinzon Guerra, M.Scott,
 594 P.Stowell, C. Wilkinson, and C. Wret Updated recommendation of the 2017 NIWG parameters
 595 T2K-TN-315,
 596 <http://www.t2k.org/docs/technotes/315>
- 597 [16] X. Li, M. Wilking FiTQun Event Selection Optimization T2K-TN-319
 598 <http://www.t2k.org/docs/technotes/319>
- 599 [17] S. Berkman, P. de Perio, A. Konaka, A. Missert, H. Tanaka, S. Tobayama, M. J.
 600 Wilking, E. D. Zimmerman fitQun: A New Reconstruction Algorithm for Super-K
 601 <http://www.t2k.org/docs/technotes/146>
- 602 [18] T2K Collaboration (K.Abe et al.), First Muon-Neutrino Disappearance Study with an Off-Axis
 603 Beam, Phys.Rev.D85:031103, 2012; arXiv:1201.1386
- 604 [19] T2K Collaboration (K.Abe et al.), Measurement of Neutrino Oscillation Parameters from Muon
 605 Neutrino Disappearance with an Off-axis Beam, arXiv:1308.0465 [hep-ex], 2013.
 606 t2k neutrino
- 607 [20] T2K Collaboration (K.Abe et al.), Measurement of neutrino oscillation in appearance
 608 and disappearance channels by the T2K experiment with 6.6×10^{20} protons on target
 609 <http://www.t2k.org/comm/pubboard/JournalPapers/oa2014prd/draft3>
- 610 [21] J. Imber et al., Four Sample Joint Oscillation Analysis with T2K Run1-6 Data, T2K-TN-267,
 611 <http://www.t2k.org/docs/technotes/267>
- 612 [22] Y.Hayato, A neutrino interaction simulation program library NEUT, Acta
 613 Phys.Polon.B40:2477-2489,2009.

- 614 [23] Beam WG, Flux tuning (11b v3.2), <http://www.t2k.org/beam/NuFlux/FluxRelease/11brelease/11btuned-v3.2>
- 615
- 616 [24] M.Otani and J.Kameda, Super-K events and Updated systematic errors for ν_μ disappearance
617 analysis with T2K 1.431×10^{20} POT T2K-TN-065(v6), <http://www.t2k.org/docs/technotes/065>
- 618 [25] P. de Perio et al., NEUT nuclear effects (FSI) T2K-TN-033(v2.0),
619 <http://www.t2k.org/docs/technotes/033>
- 620 [26] P. de Perio et al., Cross section parameters for the 2012a oscillation analysis T2K-TN-108(v1.3),
621 <http://www.t2k.org/docs/technotes/108>
- 622 [27] P. de Perio et al., Implementation of the NIWG cross-section parametrization, T2K-TN-
623 113(v1.2)
- 624 [28] Y.Hayato, K.McFarland, and M.Wascko (Private communication)
- 625 [29] P. de Perio et al., Pion Hadronic Secondary Interactions in Super-Kamiokande, T2K-TN-
626 105(v1.1) <http://www.t2k.org/docs/technotes/105>
- 627 [30] Y. Ashie et al., Phys. Rev. Lett. 93, 101801 (2004); Y. Ashie et al., Phys. Rev. D71, 112005
628 (2005); J. Hosaka et al., Phys. Rev. D 74, 032002 (2006).
- 629 [31] Beam group, <http://www.t2k.org/beam/NuFlux/FluxRelease/11arelease/11atuned-v2.3>.
- 630 [32] M. Wilking, Status of the 2013 ND280 ν_μ analysis,
631 <http://www.t2k.org/asg/meeting/20130411/nd280numustatus/view>.
- 632 [33] M. Hartz, A. Kaboth, and K. Mahn, Constraining the Flux and Cross Section Models
633 with Data from the ND280 Detector for the 2013 Oscillation Analysis, T2K-TN-166(v3.0)
634 <http://www.t2k.org/docs/technotes/166>.
- 635 [34] M. Hartz, A. Kaboth, K. Mahn, Jordan Myslik, Christine Nielsen and Mark Scott, Constraining
636 the Flux and Cross Section Models with Data from the ND280 Detector for the 2014/2015
637 Oscillation Analysis, T2K-TN-220(v1.0) <http://www.t2k.org/docs/technotes/220>.
- 638 [35] M. Hartz, A. Kaboth, K. Mahn, Jordan Myslik, Christine Nielsen and Mark Scott, ND280 Flux and Cross Section Constraint (BANFF) for 2015/16, T2K-TN-230(v.1.0)
639 <http://www.t2k.org/docs/technotes/230>.
- 640
- 641 [36] M. Hartz, A. Kaboth, K. Mahn, Mark Scott and Clarence Wret, ND280 Analysis (BANFF)
642 for 2017 Oscillation Analyses, T2K-TN-324(v.1.0) <http://www.t2k.org/docs/technotes/324>.
- 643 [37] J. Kameda, “Updated study of the systematic error in ν_μ disappearance analysis from Super-
644 Kamiokande”, T2K-TN-159

- 645 [38] J. Albert et al., "Study on SK ν_e candidates and systematic errors with T2K 3.23×10^{19} POT
 646 data" T2K-TN-157
- 647 [39] J. Hignight et al., Super-Kamiokande events and data quality studies for T2K Run4 T2K-TN-
 648 148(v2r3), <http://www.t2k.org/docs/technotes/148>.
- 649 [40] A. Himmel et al., "Super-Kamiokande events and data quality studies for T2K Runs 5 and 6"
 650 T2K-TN-219
- 651 [41] J. Imber et al., "Super-Kamiokande events and data quality studies for T2K Run 7" T2K-TN-
 652 284
- 653 [42] R. Akutsu et al., "Super-Kamiokande events and data quality studies for T2K Run 8" T2K-
 654 TN-317
- 655 [43] 14a data and MC info [http://www.t2k.org/t2ksk/documentation-
 656 page/MCWeighting/MCReweighting14a](http://www.t2k.org/t2ksk/documentation-page/MCWeighting/MCReweighting14a)
- 657 [44] E. Wang, L. Alvarez-Ruso, Y. Hayato, K. Mahn, J. Nieves "Photon emission in neutral current
 658 interactions at the T2K experiment" <http://arxiv.org/pdf/1507.02446v1.pdf>
- 659 [45] 2015 SK splines <http://www.t2k.org/asg/oagroup/inputs/201415/2015SKsplines>
- 660 [46] Super-K 13a flux release <http://www.t2k.org/beam/NuFlux/FluxRelease/13arelease>
- 661 [47] M. Friend et al. Flux Tuning and Uncertainty Updates for the 13a Flux T2K-TN-217
 662 <http://www.t2k.org/docs/technotes/217>
- 663 [48] A. Bercellie et al. Cross section parameters for 2014 oscillation analysis. T2K-TN-192 (v2.1)
 664 <http://www.t2k.org/docs/technotes/192>
- 665 [49] M. Dunkman et al. Updated Recommendation of the 2015 NIWG Parameters. T2K-TN-265
 666 <http://www.t2k.org/docs/technotes/265>
- 667 [50] <http://www.t2k.org/asg/xsec/niwgdocs/neut/NEUT5.3.2>
- 668 [51] K. Iwamoto et al. Inelastic Single Pion Signal Study in ν_e Appearance using Modified Decay
 669 Electron Cut T2K-TN-233 <http://www.t2k.org/docs/technotes/233>
- 670 [52] T. Wongjirad, A. Minamino and J. Kameda, Muon neutrino disappearance analysis with T2K
 671 6.57×10^{20} POT data, T2K-TN-164(v4), <http://www.t2k.org/docs/technotes/164>
- 672 [53] C. Bronner et al., Run1-4 p-theta electron neutrino appearance analysis, T2K-TN-161(v2.6),
 673 <http://www.t2k.org/docs/technotes/161>
- 674 [54] Y. Nishimura, J. Hignight, and S. Nakayama ν_e appearance analysis of RUN1-4 data with
 675 neutrino energy spectrum, T2K-TN-162(v2.2), <http://www.t2k.org/docs/technotes/162>

- 676 [55] A. Kaboth, R. Calland and D. Payne (Mach3) A Joint ND280-SK 1R _{μ} -SK 1R_e Fit using
 677 MCMC T2K-TN-171 <http://www.t2k.org/docs/technotes/171>
- 678 [56] K. Duffy and A. Kaboth (Mach3) A Joint ND280-SK 1R _{μ} -SK 1R_e of neutrino and antineutrino-
 679 mode data using MCMC T2K-TN-269 <http://www.t2k.org/docs/technotes/269>
- 680 [57] K. Duffy for the Mach3 group, http://www.t2k.org/asg/meeting/2015-06-18/mach3_nuebarapp
- 681 [58] H. Tanaka for the p-θ group, http://www.t2k.org/asg/meeting/2015-06-18/nuebar_appearance_study
- 683 [59] N Abgrall et al. Measurements of production properties of K_S⁰ mesons and Λ hyperons in
 684 proton-carbon interactions at 31 GeV/c Phys. Rev. C 89, 025205
- 685 [60] N Abgrall et al. Measurements of Cross Sections and Charged Pion Spectra in Proton-Carbon
 686 Interactions at 31 GeV/c. Phys.Rev., C84:034604, 2011; N. Abgrall et al. Measurement of
 687 production properties of positively charged kaons in proton-carbon interactions at 31 GeV/c.
 688 arXiv:hep-ex/1112.0150, 2011.
- 689 [61] J. Beringer et al. (Particle Data Group), Phys. Rev. D86, 010001 (2012)
- 690 [62] Lorena Escudero Sanchez for the VALOR group, <http://www.t2k.org/asg/oagroup/meeting/20121219/VaLOR>
- 691 [63] Tom Dealtry for the VALOR group, <http://www.t2k.org/asg/meeting/2012/20121015/valornumudisapp/view>
- 692 [64] Davide Sgalaberna for the VALOR group, <http://www.t2k.org/asg/meeting/2015-05-14/view>
- 693 [65] G.Cowan, K.Cranmer, E.Gross, O.Vitells, "Asymptotic formulae for likelihood-based tests of
 694 new physics" arXiv:1007.1727v2
- 695 [66] G. Cowan (1998) Statistical data analysis, Oxford University Press, ISBN 0-19-850155-2.
- 696 [67] F.James, M.Roos, Minuit: A System for Function Minimization and Analysis of the Parameter
 697 Errors and Correlations, Comput.Phys.Commun. 10:343 (1975)
- 698 [68] https://en.wikipedia.org/wiki/Gradient_descent
- 699 [69] G.J. Feldman and R.D. Cousins, A Unified approach to the classical statistical analysis of small
 700 signals, Phys.Rev.D57:3873-3889,1998; physics/9711021
- 701 [70] R.D. Cousins and V.L.Highland, Nucl.Instr. and Meth. A320:331035, 1992.
- 702 [71] J. Stuart, A. Ord and S.Arnold, Kendall's Advanced Theory of Statistics, Vol 2A (6th Ed.)
 703 (Oxford University Press, New York, 1994).
- 704 [72] N.Grant for the VALOR group, <http://www.t2k.org/asg/meeting/2011/20111124/pvalues/view>
- 705 [73] D.Karlen, p-values, distributions and low statistics, <http://www.t2k.org/asg/oagroup/meeting/20120416/lows>

- 706 [74] X. Qian, A. Tan, W. Wang, J. J. Ling, R. D. McKeown and C. Zhang, Statistical evaluation
 707 of experimental determinations of neutrino mass hierarchy, Phys.Rev.D86, 113011 (2012)
- 708 [75] K. McFarland for the T2K ν_μ -disappearance contour committee (C.Andreopoulos, N.Grant,
 709 J.Kameda, D.Karlen, E.Kearns, K.McFarland, M.Otani, M.Zito) Report to ASG conveners
 710 meeting, 17 May 2011, <http://www.t2k.org/asg/contour/ASG-Conveners-Report/view>
- 711 [76] R.Nichol, Talk at Neutrino 2012
- 712 [77] P. Adamson, et al., Measurement of Neutrino and Antineutrino Oscillations Using Beam and
 713 Atmospheric Data in MINOS, arXiv:1304.6335 [hep-ex], 2013
- 714 [78] A. Radovic, Talk at DPF 2013
- 715 [79] Y. Itow, Recent results in atmospheric neutrino oscillations in the light of large θ_{13} , Nucl. Phys.
 716 B (Proc. Suppl.) 235 79 (2013).
- 717 [80] J. Beringer et al. (Particle Data Group with 2013 update), Phys. Rev. D86, 010001 (2012)
- 718 [81] K.A. Olive et al. (Particle Data Group 2014 with 2015 update), Chin. Phys. C, 38, 090001
- 719 [82] G. Cowan, PDG statistical review (Particle Data Group with 2013 update),
 720 <http://pdg.lbl.gov/2013/reviews/rpp2013-rev-statistics.pdf>
- 721 [83] G.L.Fogli, E.Lisi et al., Evidence of theta(13)>0 from global neutrino data analysis,
 722 Phys.Rev.D84:053007, 2011; arXiv:1106.6028 [hep-ph]
- 723 [84] M.C.Gonzalez-Garcia, M.Maltoni, J.Salvado and T.Schwetz, Global fit to three neutrino mix-
 724 ing: critical look at present precision, arXiv:1209.3023 [hep-ph]
- 725 [85] Prob3++ 3-flavour oscillation probability software, <http://www.phy.duke.edu/raw22/public/Prob3++/>
- 726 [86] P. Adamson *et al.* [MINOS Collaboration], Phys. Rev. Lett. **110** (2013) 25, 251801
 727 [arXiv:1304.6335 [hep-ex]].
- 728 [87] P. Adamson *et al.* [NOvA Collaboration], Measurement of the Neutrino Mixing Angles θ_{23} in
 729 NOvA, Phys. Rev. Lett. **118** (2017) 151802 [arXiv:1701.05891 [hep-ex]]
- 730 [88] K. Duffy, P. Dunne, L. Haegel, A. Kaboth , E. Pinzon and C. Wret, A Joint ND280-
 731 SK 1R $_\mu$ -SK 1R $_e$ fit of neutrino and antineutrino-mode data using MCMC, T2K-TN-320,
 732 <http://www.t2k.org/docs/technotes/320>
- 733 [89] D. Sgalaberna, Proposal for Feldman & Cousins method,
 734 <https://www.t2k.org/asg/oagroup/meeting/2017/2017-07-06/>
- 735 [90] K. Hagiwara *et al.*, The earth matter effects in neutrino oscillation experiments from Tokai to
 736 Kamioka and Korea, Journal of High Energy Physics **9** (2011) 82, [arXiv:1107.5857 [hep-ph]]

737 Appendices

738 A. Fitter details

739 A.1. Spectra prediction methodology

740 In this analysis a comparison of the reconstructed energy (E_r) and reconstructed lepton angle
 741 (θ) spectrum of single ring events, including the ν_e CC1 π^+ -like sample, observed at Super-K with
 742 the predicted spectrum is used to build the test statistic to quote confidence intervals for neutrino
 743 oscillation parameters. For μ -like samples the templates are built as a function of the reconstructed
 744 neutrino energy, as in previous analyses, and a single θ bin is used. The predicted number $N_{SK;r,\theta}$
 745 of single ring events in the r -th and θ -th bin is computed for each selected sample as follows:

$$N_{SK;r,\theta} = \sum_m \sum_t \sum_{r'} P_{m;t} \cdot T_{r;r';f_{E;r}^{SK}} \cdot S_{m;t;r',\theta;\vec{f}} \cdot N_{SK;m;r',\theta;t}^{MC} \quad (6)$$

746 In 6, $N_{SK;m;r',\theta;t}^{MC}$ is the input Super-K Monte Carlo (MC) template containing the number of
 747 events in the single ring MC sample with true reaction mode m in the true energy bin t , the
 748 reconstructed energy bin r' and reconstructed lepton angle bin θ . $S_{m;t;r',\theta;\vec{f}}$ is an overall, multiplica-
 749 tive, systematic error factor depending on a vector of nuisance (systematic) parameters \vec{f} , which
 750 is function of the reaction mode m , the true energy bin t , the reconstructed energy bin r' , and
 751 the reconstructed lepton angle bin θ . $T_{r;r';f_{E;r}^{SK}}$ is a transfer function describing the migration of
 752 events between the reconstructed energy bins r and r' due to uncertainty in the Super-K recon-
 753 structed energy scale, expressed here in terms of the nuisance parameter $f_{E;r}^{SK}$. Finally, $P_{m;t}$ is the
 754 3-flavour oscillation probability applied to the true energy bin t of the Super-K MC template which
 755 corresponds to mode m ; application of the term $P_{m;t}$ is discussed in A.3.

756 A.2. Construction of the nominal Super-K Monte Carlo templates

757 The nominal Super-K single ring and ν_e CC1 π^+ MC analysis templates $N_{SK;m;r',\theta;t}^{MC}$ are con-
 758 structed by applying the single e -like ring selection cuts, the ν_e CC1 π^+ selection cuts, or the single
 759 μ -like ring selection cuts to the official Super-K MC samples [42]. The calculation of the normalisa-
 760 tion of each MC sample is described in section A.2.1. The list of MC templates used in this analysis
 761 is shown in section A.2.2, while the true and reconstructed energy as well as the reconstructed
 762 lepton angle binning of the templates are discussed in section A.2.3.

763 A.2.1. Normalisation of Monte Carlo samples

764 The normalisation (integrated exposure in terms of POT) of each event sample is calculated
 765 from the number of events with a MC truth interaction vertex within the 22.5 kt fiducial volume.

$$N = \int dS dIdE \cdot \frac{d^3\Phi_{SK}}{dS dIdE_\nu} \cdot \sigma_{H_2O} \cdot \frac{N_A}{A} \cdot \rho \cdot L \quad (7)$$

766 where $d^3\Phi_{SK}/dS dIdE$ is the number of flux particles for the given neutrino species per neutrino
 767 energy bin dE_ν , per unit area dS and per POT, σ_{H_2O} is the total interaction cross section on water

768 for the given neutrino species, I is the beam exposure in terms of POT, N_A is Avogadro's number,
 769 A is the mass number for water, ρ is the water density and L is the neutrino path length in the
 770 water volume.

771 The Super-K MC samples are normalised to the Run 1-8 POT. Assuming that all the MC files
 772 are used, each sample is first normalised to 10^{21} POT by weighting it with the ratio of the number
 773 of events per 22.5 kt per 10^{21} POT to the number of generated events in the true fiducial volume
 774 in all the available MC. Then each sample is normalised to 1.4734×10^{21} POT for neutrino and
 775 7.558×10^{20} for antineutrino mode, by weighting the result respectively by 1.4734 and 0.7558 (the
 776 Run 1-8 POT in units of 10^{21} POT).

777 *A.2.2. List of Monte Carlo templates*

778 For each Super-K MC sample, a number of different MC templates is constructed corresponding
 779 to different true reaction modes. The template number depends on the type of oscillation analysis
 780 and the specific systematic parameters considered in the analysis. 50 are used for the current
 781 analysis, these are the same templates as in our 2016 analysis [12]. In particular

- 782 • $\bar{\nu}_\mu$ CCQE,
- 783 • $\bar{\nu}_\mu$ CC1 π ,
- 784 • $\bar{\nu}_\mu$ CC coherent,
- 785 • $\bar{\nu}_\mu$ CC 2p-2h,
- 786 • $\bar{\nu}_\mu$ CC other,
- 787 • $\bar{\nu}_\mu$ (and $\rightarrow \bar{\nu}_e, \bar{\nu}_\tau$) NC1 π^0 ,
- 788 • $\bar{\nu}_\mu$ (and $\rightarrow \bar{\nu}_e, \bar{\nu}_\tau$) NC1 π^\pm ,
- 789 • $\bar{\nu}_\mu$ (and $\rightarrow \bar{\nu}_e, \bar{\nu}_\tau$) NC coherent,
- 790 • $\bar{\nu}_\mu$ (and $\rightarrow \bar{\nu}_e, \bar{\nu}_\tau$) NC other,
- 791 • $\bar{\nu}_\mu$ (and $\rightarrow \bar{\nu}_e, \bar{\nu}_\tau$) NC 1 γ ,
- 792 • ν_μ CCQE,
- 793 • ν_μ CC1 π ,
- 794 • ν_μ CC coherent,
- 795 • ν_μ CC 2p-2h,
- 796 • ν_μ CC other,
- 797 • ν_μ (and $\rightarrow \nu_e, \nu_\tau$) NC1 π^0 ,

- 798 • ν_μ (and $\rightarrow \nu_e, \nu_\tau$) NC1 π^\pm ,
- 799 • ν_μ (and $\rightarrow \nu_e, \nu_\tau$) NC coherent,
- 800 • ν_μ (and $\rightarrow \nu_e, \nu_\tau$) NC other,
- 801 • ν_μ (and $\rightarrow \nu_e, \nu_\tau$) NC 1 γ ,
- 802 • $\bar{\nu}_e$ CCQE,
- 803 • $\bar{\nu}_e$ CC1 π ,
- 804 • $\bar{\nu}_e$ CC coherent,
- 805 • $\bar{\nu}_e$ CC 2p-2h,
- 806 • $\bar{\nu}_e$ CC other,
- 807 • $\bar{\nu}_e$ (and $\rightarrow \bar{\nu}_\mu, \bar{\nu}_\tau$) NC1 π^0 ,
- 808 • $\bar{\nu}_e$ (and $\rightarrow \bar{\nu}_\mu, \bar{\nu}_\tau$) NC1 π^\pm ,
- 809 • $\bar{\nu}_e$ (and $\rightarrow \bar{\nu}_\mu, \bar{\nu}_\tau$) NC coherent,
- 810 • $\bar{\nu}_e$ (and $\rightarrow \bar{\nu}_\mu, \bar{\nu}_\tau$) NC other,
- 811 • $\bar{\nu}_e$ (and $\rightarrow \bar{\nu}_\mu, \bar{\nu}_\tau$) NC 1 γ ,
- 812 • ν_e CCQE,
- 813 • ν_e CC1 π ,
- 814 • ν_e CC coherent,
- 815 • ν_e CC 2p-2h,
- 816 • ν_e CC other,
- 817 • ν_e (and $\rightarrow \nu_\mu, \nu_\tau$) NC1 π^0 ,
- 818 • ν_e (and $\rightarrow \nu_\mu, \nu_\tau$) NC1 π^\pm ,
- 819 • ν_e (and $\rightarrow \nu_\mu, \nu_\tau$) NC coherent,
- 820 • ν_e (and $\rightarrow \nu_\mu, \nu_\tau$) NC other,
- 821 • ν_e (and $\rightarrow \nu_\mu, \nu_\tau$) NC 1 γ ,
- 822 • oscillated $\nu_\mu \rightarrow \nu_e$ CCQE,
- 823 • oscillated $\nu_\mu \rightarrow \nu_e$ CC1 π ,

- 824 • oscillated $\nu_\mu \rightarrow \nu_e$ CC coherent,
- 825 • oscillated $\nu_\mu \rightarrow \nu_e$ CC 2p-2h,
- 826 • oscillated $\nu_\mu \rightarrow \nu_e$ CC other,
- 827 • oscillated $\bar{\nu}_\mu \rightarrow \bar{\nu}_e$ CCQE,
- 828 • oscillated $\bar{\nu}_\mu \rightarrow \bar{\nu}_e$ CC1 π ,
- 829 • oscillated $\bar{\nu}_\mu \rightarrow \bar{\nu}_e$ CC coherent,
- 830 • oscillated $\bar{\nu}_\mu \rightarrow \bar{\nu}_e$ CC 2p-2h,
- 831 • oscillated $\bar{\nu}_\mu \rightarrow \bar{\nu}_e$ CC other.

832 *A.2.3. Binning of Monte Carlo templates*

833 The binning scheme for the current analysis remains unchanged from the previous analysis [12].
 834 For μ -like samples the templates are built as a function of the reconstructed neutrino energy, having
 835 84 true energy bins and 73 reconstructed energy bins. e -like templates have 84 true energy bins, 25
 836 reconstructed energy bins and 15 reconstructed lepton angle bins.

837 For all templates the 84 true energy bins of constant width are:

- 838 • 6 50-MeV bins from 0-0.3 GeV,
- 839 • 28 25-MeV bins from 0.3-1 GeV,
- 840 • 40 50-MeV bins from 1-3 GeV,
- 841 • 5 100-MeV bin from 3-3.5 GeV,
- 842 • 1 bin from 3.5-4 GeV,
- 843 • 1 bin from 4-5 GeV,
- 844 • 1 bin from 5-7 GeV,
- 845 • 1 bin from 7-10 GeV and
- 846 • 1 bin from 10-30 GeV

847 For μ -like samples the 73 reconstructed energy bins are:

- 848 • 60 50-MeV bins from 0-3 GeV,
- 849 • 4 250-MeV bins from 3-4 GeV,
- 850 • 4 500-MeV bins from 4-6 GeV,
- 851 • 4 1000-MeV bins from 6-10 GeV and

852 • 1 bin from 10-30 GeV.

853 For e -like samples the 25 reconstructed energy bins with constant width are the following:

854 • 25 50-MeV bins from 0-1.25 GeV.

855 The θ binning used for e -like samples is

856 • 14 10° bins from 0° to 140°,

857 • 1 bin for the range 140° – 180°.

858 For μ -like samples a single θ bin, that covers the whole range 0° - 180°, is used. The predicted
859 e -like 2-dimensional spectra were studied in detail in [11] for each flavour component and were
860 compared with the 1-dimensional reconstructed energy spectra.

861 A study was performed to decide the optimum binning scheme for reconstructing neutrino
862 energy, balancing the needs for accuracy and speed. Details are given in Appendix I of Ref. [4].

863 *A.3. Applying neutrino oscillations*

864 The MC templates are constructed from the unoscillated MC samples and must be weighted
865 with the appropriate oscillation probability. Oscillations are applied as a function of true energy to
866 the MC templates for all CC interactions.

867 The MC templates calculated from the $\bar{\nu}_\mu$ MC sample are weighted with $P(\bar{\nu}_\mu \rightarrow \bar{\nu}_\mu)$, with
868 this survival probability being calculated using the oscillation parameters, namely $\sin^2 \theta_{23}$, $\sin^2 \theta_{12}$,
869 $\sin^2 \theta_{13}$, $|\Delta m_{32}^2|$ (normal hierarchy) or $|\Delta m_{31}^2|$ (inverted hierarchy), Δm_{21}^2 and δ_{CP} . The $\bar{\nu}_e$ templates
870 are weighted with $P(\bar{\nu}_e \rightarrow \bar{\nu}_e)$, while the oscillated $\bar{\nu}_\mu \rightarrow \bar{\nu}_e$ templates are weighted with $P(\bar{\nu}_\mu \rightarrow \bar{\nu}_e)$
871 (the sample was generated assuming 100% of $\bar{\nu}_\mu$ transform to $\bar{\nu}_e$). All these oscillation probabilities
872 are computed in a 3-flavour framework including matter effects in constant-density matter (assuming
873 an Earth crust density of 2.6 g/cm³). Custom oscillation probability calculation code was developed
874 within the *VALOR* analysis framework. Details and estimates of the numerical accuracy of this code
875 are first presented in [3], and is also shown in Appendix A of [4]. Comparisons between the *VALOR*
876 oscillation probability calculation code and Prob3++ [85], which is typically used by the alternative
877 T2K oscillation analyses, are shown in Appendix B of [4].

878 In the standard 3-flavour oscillation framework, oscillations of $\bar{\nu}_e$ and $\bar{\nu}_\mu$ can yield $\bar{\nu}_\tau$. In this
879 analysis, we neglect contributions from ν_τ -CC and $\bar{\nu}_\tau$ -CC as their energy threshold is around 3.5 GeV
880 and their effect is negligible¹. Accordingly, this analysis uses no ν_τ -CC and $\bar{\nu}_\tau$ -CC MC templates
881 (and, in fact, no ν_τ and $\bar{\nu}_\tau$ Super-K MC samples are available).

882 It should be emphasized here that the ν_μ NC MC templates for a mode m contain the NC MC
883 templates for the mixture of $\nu_e + \nu_\mu + \nu_\tau$ resulting from 3-flavour ν_μ oscillations for that mode m .

¹A back-of-the-envelope calculation can be found in the replies to comments and revision history document of [4] that gives $\ll 1\%$ ν_τ contamination in the 1-ring μ -like Super-K sample. A Super-K MC study is required to determine whether the Super-K efficiency assumptions made there are valid.

884 The same applies to the $\bar{\nu}_\mu$, ν_e and $\bar{\nu}_e$ NC MC templates. These NC MC templates are unchanged
885 under standard 3-flavour oscillations.

886 Also it should be noted that there are no explicit NC MC templates made from the oscillated
887 $\bar{\nu}_e$ and ν_e samples. If they were used, the oscillated $\bar{\nu}_e$ (i.e. $\bar{\nu}_e$ coming from oscillations of $\bar{\nu}_\mu$) would
888 be double counted since they are already included in the $\bar{\nu}_\mu$ NC MC templates. The same applies
889 to oscillated ν_e .

890 **B. Event rates**

891 Tables 19-23 present unoscillated rates.

	ν_μ	ν_e	$\bar{\nu}_\mu$	$\bar{\nu}_e$	Osc. ν_e	Osc. $\bar{\nu}_e$	Total
CCQE	953.15505	0.00429	23.18824	0.00020	0.00000	0.00000	976.34778
CC1pi	76.40088	0.00211	4.12922	0.00010	0.00000	0.00000	80.53230
CCcoherent	0.75678	0.00000	0.17387	0.00000	0.00000	0.00000	0.93065
2p2h	134.02475	0.00161	2.51636	0.00008	0.00000	0.00000	136.54280
CCother	6.94520	0.00090	0.50167	0.00008	0.00000	0.00000	7.44785
NC1pi0	0.61495	0.01841	0.02120	0.00143	N/A	N/A	0.65599
NC1piPM	4.90783	0.09799	0.17531	0.00975	N/A	N/A	5.19089
NCcoherent	0.00000	0.00000	0.00043	0.00003	N/A	N/A	0.00047
NCother	2.05619	0.07378	0.13055	0.00912	N/A	N/A	2.26963
Total	1178.86162	0.19909	30.83686	0.02080	0.00000	0.00000	1209.91837

Table 19: Predicted number of events in the neutrino mode μ -like sample obtained after applying the BANFF weight for a total exposure of 1.4734×10^{21} POT. Oscillations are not applied.

	ν_μ	ν_e	$\bar{\nu}_\mu$	$\bar{\nu}_e$	Osc. ν_e	Osc. $\bar{\nu}_e$	Total
CCQE	36.21445	0.00089	133.92633	0.00096	0.00000	0.00000	170.14262
CC1pi	6.51012	0.00035	11.57229	0.00027	0.00000	0.00000	18.08303
CCcoherent	0.06956	0.00000	0.75838	0.00005	0.00000	0.00000	0.82799
2p2h	8.28538	0.00028	10.73613	0.00028	0.00000	0.00000	19.02208
CCother	1.18677	0.00012	0.77049	0.00000	0.00000	0.00000	1.95738
NC1pi0	0.06000	0.00222	0.06147	0.00169	N/A	N/A	0.12538
NC1piPM	0.35950	0.01527	0.46009	0.01235	N/A	N/A	0.84721
NCcoherent	0.00000	0.00000	0.00201	0.00000	N/A	N/A	0.00201
NCother	0.31580	0.01640	0.20064	0.00789	N/A	N/A	0.54073
Total	53.00159	0.03552	158.48783	0.02349	0.00000	0.00000	211.54843

Table 20: Predicted number of events in the antineutrino mode μ -like sample obtained after applying the BANFF weight for a total exposure of 7.558×10^{20} POT. Oscillations are not applied.

	ν_μ	ν_e	$\bar{\nu}_\mu$	$\bar{\nu}_e$	Osc. ν_e	Osc. $\bar{\nu}_e$	Total
CCQE	0.99622	6.79206	0.02082	0.27180	0.00000	0.00000	8.08090
CC1pi	0.18090	0.99514	0.00514	0.07082	0.00000	0.00000	1.25199
CCcoherent	0.00076	0.00885	0.00031	0.00419	0.00000	0.00000	0.01412
2p2h	0.13667	1.71219	0.00236	0.04511	0.00000	0.00000	1.89633
CCother	0.02827	0.13255	0.00057	0.00971	0.00000	0.00000	0.17111
NC1pi0	1.70203	0.03706	0.06012	0.00356	N/A	N/A	1.80278
NC1piPM	0.16854	0.00472	0.01020	0.00057	N/A	N/A	0.18404
NCcoherent	0.52817	0.00715	0.04794	0.00294	N/A	N/A	0.58619
NCother	0.31767	0.01695	0.02120	0.00128	N/A	N/A	0.35711
NC1gamma	0.94222	0.01687	0.04983	0.00233	N/A	N/A	1.01125
Total	5.00145	9.72355	0.21850	0.41231	0.00000	0.00000	15.35581

Table 21: Predicted number of events in the neutrino mode e -like sample obtained after applying the BANFF weight for a total exposure of 1.4734×10^{21} POT. Oscillations are not applied.

	ν_μ	ν_e	$\bar{\nu}_\mu$	$\bar{\nu}_e$	Osc. ν_e	Osc. $\bar{\nu}_e$	Total
CCQE	0.04096	0.54758	0.13906	0.90195	0.00000	0.00000	1.62955
CC1pi	0.01660	0.10715	0.01787	0.15254	0.00000	0.00000	0.29415
CCcoherent	0.00006	0.00105	0.00143	0.01133	0.00000	0.00000	0.01388
2p2h	0.00652	0.15324	0.00694	0.11994	0.00000	0.00000	0.28664
CCother	0.00568	0.02184	0.00232	0.01193	0.00000	0.00000	0.04177
NC1pi0	0.13849	0.00541	0.17659	0.00468	N/A	N/A	0.32516
NC1piPM	0.02475	0.00127	0.02001	0.00080	N/A	N/A	0.04683
NCcoherent	0.04776	0.00221	0.20260	0.00317	N/A	N/A	0.25574
NCother	0.05664	0.00221	0.02672	0.00097	N/A	N/A	0.08654
NC1gamma	0.07943	0.00439	0.17490	0.00383	N/A	N/A	0.26255
Total	0.41688	0.84635	0.76842	1.21115	0.00000	0.00000	3.24280

Table 22: Predicted number of events in the antineutrino mode e -like sample obtained after applying the BANFF weight for a total exposure of 7.558×10^{20} POT. Oscillations are not applied.

	ν_μ	ν_e	$\bar{\nu}_\mu$	$\bar{\nu}_e$	Osc. ν_e	Osc. $\bar{\nu}_e$	Total
CCQE	0.34542	0.02646	0.00615	0.00187	0.00000	0.00000	0.37990
CC1pi	0.54696	0.82041	0.00710	0.00403	0.00000	0.00000	1.37850
CCcoherent	0.00364	0.01905	0.00021	0.00008	0.00000	0.00000	0.02298
2p2h	0.08323	0.02355	0.00176	0.00100	0.00000	0.00000	0.10953
CCother	0.17904	0.11704	0.00287	0.00289	0.00000	0.00000	0.30184
NC1pi0	0.02049	0.00076	0.00083	0.00008	N/A	N/A	0.02216
NC1piPM	0.06474	0.00165	0.00382	0.00033	N/A	N/A	0.07053
NCother	0.20584	0.00830	0.01304	0.00088	N/A	N/A	0.22807
NC1gamma	0.02844	0.00000	0.00067	0.00007	N/A	N/A	0.02918
Total	1.47780	1.01722	0.03645	0.01122	0.00000	0.00000	2.54269

Table 23: Predicted number of events in the neutrino mode e -like sample obtained after applying the BANFF weight for a total exposure of 1.4734×10^{21} POT. Oscillations are not applied.

Tables 24-28 present oscillated rates corresponding to the Asimov B data set.

	ν_μ	ν_e	$\bar{\nu}_\mu$	$\bar{\nu}_e$	Osc. ν_e	Osc. $\bar{\nu}_e$	Total
CCQE	186.41514	0.00413	11.15862	0.00019	0.01514	0.00018	197.59340
CC1pi	28.20533	0.00199	2.62809	0.00009	0.01651	0.00009	30.85209
CCcoherent	0.29385	0.00000	0.09293	0.00000	0.00000	0.00001	0.38678
2p2h	36.71916	0.00151	1.42161	0.00008	0.01693	0.00005	38.15934
CCother	5.47728	0.00086	0.40680	0.00008	0.00011	0.00001	5.88513
NC1pi0	0.61495	0.01841	0.02120	0.00143	N/A	N/A	0.65599
NC1piPM	4.90783	0.09799	0.17531	0.00975	N/A	N/A	5.19089
NCcoherent	0.00000	0.00000	0.00043	0.00003	N/A	N/A	0.00047
NCother	2.05619	0.07378	0.13055	0.00912	N/A	N/A	2.26963
Total	264.68973	0.19867	16.03554	0.02078	0.04868	0.00032	280.99373

Table 24: Predicted number of events in the neutrino mode μ -like sample obtained after applying the BANFF weight for a total exposure of 1.4734×10^{21} POT. The Asimov data set B in 1 is used.

	ν_μ	ν_e	$\bar{\nu}_\mu$	$\bar{\nu}_e$	Osc. ν_e	Osc. $\bar{\nu}_e$	Total
CCQE	15.53910	0.00085	31.15342	0.00093	0.00068	0.00181	46.69679
CC1pi	3.97662	0.00033	4.60026	0.00025	0.00043	0.00073	8.57862
CCcoherent	0.04724	0.00000	0.18223	0.00005	0.00000	0.00007	0.22959
2p2h	4.50940	0.00026	2.92853	0.00027	0.00030	0.00025	7.43900
CCother	0.94370	0.00012	0.60700	0.00000	0.00000	0.00000	1.55082
NC1pi0	0.06000	0.00222	0.06147	0.00169	N/A	N/A	0.12538
NC1piPM	0.35950	0.01527	0.46009	0.01235	N/A	N/A	0.84721
NCcoherent	0.00000	0.00000	0.00201	0.00000	N/A	N/A	0.00201
NCother	0.31580	0.01640	0.20064	0.00789	N/A	N/A	0.54073
Total	25.75135	0.03544	40.19565	0.02342	0.00142	0.00286	66.01015

Table 25: Predicted number of events in the antineutrino mode μ -like sample obtained after applying the BANFF weight for a total exposure of 7.558×10^{20} POT. The Asimov data set B in 1 is used.

	ν_μ	ν_e	$\bar{\nu}_\mu$	$\bar{\nu}_e$	Osc. ν_e	Osc. $\bar{\nu}_e$	Total
CCQE	0.17174	6.30178	0.00647	0.25566	31.20630	0.33860	38.28056
CC1pi	0.04847	0.93168	0.00282	0.06750	3.28336	0.05561	4.38943
CCcoherent	0.00012	0.00830	0.00018	0.00397	0.02515	0.00382	0.04154
2p2h	0.03143	1.59694	0.00118	0.04275	6.08289	0.04642	7.80162
CCother	0.01346	0.12803	0.00034	0.00942	0.07482	0.00374	0.22981
NC1pi0	1.70203	0.03706	0.06012	0.00356	N/A	N/A	1.80278
NC1piPM	0.16854	0.00472	0.01020	0.00057	N/A	N/A	0.18404
NCcoherent	0.52817	0.00715	0.04794	0.00294	N/A	N/A	0.58619
NCother	0.31767	0.01695	0.02120	0.00128	N/A	N/A	0.35711
NC1gamma	0.94222	0.01687	0.04983	0.00233	N/A	N/A	1.01125
Total	3.92386	9.04948	0.20030	0.38998	40.67252	0.44819	54.68432

Table 26: Predicted number of events in the neutrino mode e -like sample obtained after applying the BANFF weight for a total exposure of 1.4734×10^{21} POT. The Asimov data set B in 1 is used.

	ν_μ	ν_e	$\bar{\nu}_\mu$	$\bar{\nu}_e$	Osc. ν_e	Osc. $\bar{\nu}_e$	Total
CCQE	0.01318	0.50911	0.02513	0.84721	0.72476	3.38779	5.50718
CC1pi	0.00771	0.10111	0.00742	0.14431	0.11344	0.39683	0.77081
CCcoherent	0.00002	0.00099	0.00043	0.01066	0.00090	0.03680	0.04981
2p2h	0.00298	0.14379	0.00224	0.11301	0.17444	0.39087	0.82733
CCother	0.00392	0.02116	0.00121	0.01154	0.00920	0.00777	0.05480
NC1pi0	0.13849	0.00541	0.17659	0.00468	N/A	N/A	0.32516
NC1piPM	0.02475	0.00127	0.02001	0.00080	N/A	N/A	0.04683
NCcoherent	0.04776	0.00221	0.20260	0.00317	N/A	N/A	0.25574
NCother	0.05664	0.00221	0.02672	0.00097	N/A	N/A	0.08654
NC1gamma	0.07943	0.00439	0.17490	0.00383	N/A	N/A	0.26255
Total	0.37487	0.79164	0.63724	1.14019	1.02275	4.22006	8.18675

Table 27: Predicted number of events in the antineutrino mode μ -like sample obtained after applying the BANFF weight for a total exposure of 7.558×10^{20} POT. The Asimov data set B in 1 is used.

	ν_μ	ν_e	$\bar{\nu}_\mu$	$\bar{\nu}_e$	Osc. ν_e	Osc. $\bar{\nu}_e$	Total
CCQE	0.03298	0.02442	0.00123	0.00174	0.14531	0.00339	0.20908
CC1pi	0.08149	0.76065	0.00261	0.00383	3.47649	0.00267	4.32774
CCcoherent	0.00031	0.01765	0.00008	0.00007	0.07633	0.00013	0.09457
2p2h	0.01100	0.02195	0.00050	0.00095	0.11660	0.00125	0.15225
CCother	0.03947	0.11225	0.00117	0.00279	0.09788	0.00174	0.25531
NC1pi0	0.02049	0.00076	0.00083	0.00008	N/A	N/A	0.02216
NC1piPM	0.06474	0.00165	0.00382	0.00033	N/A	N/A	0.07053
NCother	0.20584	0.00830	0.01304	0.00088	N/A	N/A	0.22807
NC1gamma	0.02844	0.00000	0.00067	0.00007	N/A	N/A	0.02918
Total	0.48477	0.94764	0.02396	0.01075	3.91261	0.00917	5.38890

Table 28: Predicted number of events in the neutrino mode e -like sample obtained after applying the BANFF weight for a total exposure of 1.4734×10^{21} POT. The Asimov data set B in 1 is used.

⁸⁹³ **C. Systematic variations**

⁸⁹⁴ Tables table 29 through table 38 show the effect of systematic variations on the event rates for
⁸⁹⁵ pre-BANFF and post-BANFF errors.

Parameter	1 σ value	BANFF tuned -3 σ	BANFF tuned +3 σ	BANFF tuned -1 σ	BANFF tuned +1 σ	BANFF tuned +3 σ
All syst	61.9761	-74.2947(%)	143.921	-40.307 (%)	385.63	59.945(%)
BANFF 0, SK numu flux, 0.0 - 0.4 GeV	0.0987323	234.4348	-2.76012	238.884	-0.9204	247.757
BANFF 1, SK numu flux, 0.4 - 0.5 GeV	0.103488	234.337	-2.79341	238.857	-0.93114	2760.12
BANFF 2, SK numu flux, 0.5 - 0.6 GeV	0.096444	239.435	-0.691334	240.547	-0.23051	2793.41
BANFF 3, SK numu flux, 0.6 - 0.7 GeV	0.0866958	239.741	-0.564733	240.648	-0.18824	0.691534
BANFF 4, SK numu flux, 0.7 - 1.0 GeV	0.1133052	224.426	-6.91684	235.543	-2.3056	0.564733
BANFF 5, SK numu flux, 1.0 - 1.5 GeV	0.0911476	228.616	-5.17878	236.94	-1.7263	6.91684
BANFF 6, SK numu flux, 1.5 - 2.5 GeV	0.07071742	233.261	-3.25225	238.489	-0.10841	5.17878
BANFF 7, SK numu flux, 2.5 - 3.5 GeV	0.0733805	237.002	-1.70083	239.735	-0.56694	3.25225
BANFF 8, SK numu flux, 3.5 - 5.0 GeV	0.0873733	236.859	-1.76011	239.688	-0.58607	1.70083
BANFF 9, SK numu flux, 5.0 - 7.0 GeV	0.0973369	239.83	-0.527644	240.678	-0.17588	1.76011
BANFF 10, SK numu flux, 7.0 - 30.0 GeV	0.114436	240.982	-0.0498157	241.062	-0.016605	0.527644
BANFF 11, SK numubar flux, 0.0 - 0.7 GeV	0.1022576	240.821	-0.116474	241.009	-0.038825	0.0498157
BANFF 12, SK numubar flux, 0.7 - 1.0 GeV	0.0768331	240.849	-0.105028	241.018	-0.035009	0.116474
BANFF 13, SK numubar flux, 1.0 - 1.5 GeV	0.0844536	240.163	-0.389456	240.759	-0.12988	0.105028
BANFF 14, SK numubar flux, 1.5 - 2.5 GeV	0.0865683	239.779	-0.548919	240.661	-0.18297	0.38964
BANFF 15, SK numubar flux, 2.5 - 30.0 GeV	0.0864284	240.158	-0.391625	240.788	-0.13054	0.548919
BANFF 16, SK numubar flux, 0.0 - 0.5 GeV	0.0896983	241.101	-0.000449436	241.102	-0.00014981	0.391625
BANFF 17, SK num flux, 0.5 - 0.7 GeV	0.0898552	241.1	-0.000112608	241.101	-0.00037536	0.000449436
BANFF 18, SK num flux, 0.7 - 0.8 GeV	0.0859648	241.1	-0.000823573	241.102	-0.00027452	0.00112608
BANFF 19, SK num flux, 0.8 - 1.5 GeV	0.0809182	241.088	-0.00584391	241.098	-0.00195	0.00112608
BANFF 20, SK num flux, 1.5 - 2.5 GeV	0.0789719	241.085	-0.00705564	241.097	-0.0023519	0.00112608
BANFF 21, SK num flux, 2.5 - 40 GeV	0.08385	241.09	-0.00521714	241.098	-0.001739	0.0021714
BANFF 22, SK num flux, 4.0 - 30.0 GeV	0.0938843	231.751	-0.84132	241.098	-0.0009195	0.0027585
BANFF 23, SK numbar flux, 0.0 - 2.5 GeV	0.07440279	241.096	-0.000858525	241.102	-0.000250528	0.000885825
BANFF 24, SK numbar flux, 2.5 - 30.0 GeV	0.128416	241.097	-0.00209235	241.101	-0.00069745	0.00209235
BANFF; Norm; 2p2h	1	214.649	-10.972	214.649	0.00165	241.116
BANFF; Shape; CC Orth	0.148515	223.261	-7.39978	234.198	-2.8636	242.426
BANFF; Norm; BgRES Isospin 1/2	0.307692	237.768	-1.38331	238.756	-0.97328	0.007564
BANFF; Norm; Ma RES	0.026	231.751	-3.87874	238.038	-1.27111	0.00021714
BANFF; Norm; NC Orth	0.1577895	223.458	-7.31819	235.185	-2.4544	0.00109
BANFF; Norm; ν_e To ν_μ	0.05777778	246.226	2.12531	243.832	1.1323	0.00027452
BANFF; Norm; $\bar{\nu}_e$ To $\bar{\nu}_\mu$	0.4	238.696	-0.998635	240.292	-0.33617	0.00027452
BANFF; Norm; CC Coh	0.3	241.102	-0.000187994	241.102	-0.053837	0.0023519
BANFF; Norm; NC Coh	0.3	240.025	-0.000187994	240.426	-6.2665 $\times 10^{-5}$	0.0023519
BANFF; Norm; NC Orth	0.3	239.074	-0.0023235	241.1	-0.00077545	0.0023519
BANFF; Norm; ν_e To ν_μ	0.02982843	241.097	-0.00023235	241.102	-7.5091 $\times 10^{-6}$	0.0023519
BANFF; Norm; $\bar{\nu}_e$ To $\bar{\nu}_\mu$	0.02982843	241.102	-2.252723 $\times 10^{-5}$	241.102	-1.1782	0.0023519
BANFF; Norm; 2p2h Bar	1	239.969	-0.470064	239.969	-0.47006	241.102
BANFF; Norm; BerPA A	0.118	240.44	-14.1262	229.749	-4.7088	241.102
BANFF; BerPA B	0.219	208.023	-13.72	230.076	-4.5734	241.102
BANFF; BerPA D	0.1695	216.789	-10.0843	232.998	-3.3614	241.102
BANFF; BerPA E	0.352	240.035	-0.442852	240.672	-0.24116	241.102
BANFF; Shape; 2p2h	3	242.411	0.542884	241.756	0.27134	241.102
BANFF; Norm; 2p2h C to O	0.2	224.545	-6.86522	235.585	-2.2884	241.102
SKD $\nu_{\text{e}} + \text{FSI}(\text{SI}, 0)$; E_{reco} (0.00 - 0.40) GeV; $\nu_{\text{e}}/\bar{\nu}_{\mu}$ CCQE (1 R_{μ})	0.00878593	240.539	-0.22114	240.925	-0.073713	0.0073713
SKD $\nu_{\text{e}} + \text{FSI}(\text{SI}, 1)$; E_{reco} (0.40 - 1.10) GeV; $\nu_{\text{e}}/\bar{\nu}_{\mu}$ CCQE (1 R_{μ})	0.00740328	239.211	-0.784136	240.472	-0.26151	0.26151
SKD $\nu_{\text{e}} + \text{FSI}(\text{SI}, 2)$; E_{reco} (1.10 - 30.00) GeV; $\nu_{\text{e}}/\bar{\nu}_{\mu}$ CCQE (1 R_{μ})	0.0072044	239.287	-0.752812	240.497	-0.25094	0.25094
SKD $\nu_{\text{e}} + \text{FSI}(\text{SI}, 3)$; E_{reco} (0.00 - 30.00) GeV; $\nu_{\text{e}}/\bar{\nu}_{\mu}$ CCQE (1 R_{μ})	0.1691353	219.654	-8.89593	233.953	-2.9653	248.252
SKD $\nu_{\text{e}} + \text{FSI}(\text{SI}, 4)$; E_{reco} (0.00 - 30.00) GeV; $\nu_{\text{e}}/\bar{\nu}_{\mu}$ CCQE (1 R_{μ})	1.06548	240.901	-0.0835907	241.035	-0.027834	241.169
SKD $\nu_{\text{e}} + \text{FSI}(\text{SI}, 5)$; E_{reco} (0.00 - 30.00) GeV; all NC (1 R_{μ})	0.658101	222.61	-7.66938	234.938	-2.5567	247.266
SK energy scale	0.024	241.102	-2.35765 $\times 10^{-14}$	241.102	-3.5365 $\times 10^{-14}$	-1.1788 $\times 10^{-14}$

Table 29: $\pm 1\sigma$ and $\pm 3\sigma$ effect of the systematic parameters on the total number of μ -like Super-K events with Run 1-8 POT for neutrino mode pre-BANFF Asimov data set A. Only the systematic parameters which affect this sample are shown.

Parameter	1 σ value	BANFF tuned -3 σ	BANFF tuned -1 σ	BANFF tuned +1 σ	BANFF tuned +3 σ
All syst.					
BANFF 0, SK number flux, 0.0 - 0.7 GeV; RHC	0.039 682 2	19.3721	-66.0249(%)	37.6935	-35.06 (%)
BANFF 1, SK number flux, 0.7 - 1.0 GeV; RHC	0.079 343	57.0767	-0.632032	57.9213	-0.21088
BANFF 2, SK number flux, 1.0 - 1.5 GeV; RHC	0.076 727 1	57.5584	-0.835738	57.8819	-0.2786
BANFF 3, SK number flux, 1.5 - 2.5 GeV; RHC	0.080 588 7	56.1916	-2.46723	57.5701	-0.81574
BANFF 4, SK number flux, 2.5 - 3.00 GeV; RHC	0.080 289 6	56.1027	-3.19067	57.1262	-1.0636
BANFF 5, SK number flux, 0.0 - 0.4 GeV; RHC	0.104 476	56.3778	-2.31012	57.5966	-0.77004
BANFF 6, SK number flux, 0.4 - 0.5 GeV; RHC	0.101 533	57.067	-2.59124	57.5416	-0.86475
BANFF 7, SK number flux, 0.5 - 0.6 GeV; RHC	0.096 167 3	57.5301	-1.68251	57.718	-0.56084
BANFF 8, SK number flux, 0.6 - 0.7 GeV; RHC	0.084 636 6	57.8844	-0.367714	57.9724	-0.12257
BANFF 9, SK number flux, 0.7 - 1.0 GeV; RHC	0.125 091	55.6825	-0.212748	57.9005	-0.091416
BANFF 10, SK number flux, 1.0 - 1.5 GeV; RHC	0.105 291	56.3659	-0.46781	57.2565	-1.35559
BANFF 11, SK number flux, 1.5 - 2.5 GeV; RHC	0.079 987	56.4133	-3.75176	57.3177	-1.2506
BANFF 12, SK number flux, 2.5 - 3.5 GeV; RHC	0.073 938 4	57.3425	-2.04856	57.5001	-0.93622
BANFF 13, SK number flux, 3.5 - 5.0 GeV; RHC	0.063 992 3	57.1413	-1.08934	57.8099	-0.40261
BANFF 14, SK number flux, 5.0 - 7.0 GeV; RHC	0.092 512 6	57.9201	-0.212685	58.0024	-0.070895
BANFF 15, SK number flux, 7.0 - 30.0 GeV; RHC	0.130 312	58.432	-0.0198956	58.0387	-0.0636319
BANFF 16, SK number flux, 0.0 - 2.5 GeV; RHC	0.068 881 3	58.6397	-0.00669758	58.043	-0.0022325
BANFF 17, SK number flux, 2.5 - 30.0 GeV; RHC	0.084 944 6	58.0384	-0.00894923	58.0418	-0.0029831
BANFF 18, SK number flux, 0.0 - 0.5 GeV; RHC	0.094 695 4	58.0435	-0.000168308	58.0435	-5.6103 $\times 10^{-5}$
BANFF 19, SK number flux, 0.5 - 0.7 GeV; RHC	0.041 042 2	58.0432	-0.000168308	58.0435	-0.36311
BANFF 20, SK number flux, 0.7 - 0.8 GeV; RHC	0.091 012 4	58.0434	-0.000258631	58.0435	-0.078595
BANFF 21, SK number flux, 0.8 - 1.5 GeV; RHC	0.082 865 6	58.0442	-0.00277929	58.0433	-0.04747
BANFF 22, SK number flux, 1.5 - 2.5 GeV; RHC	0.079 577 6	58.0442	-0.00261759	58.0431	-0.00494
BANFF 23, SK number flux, 2.5 - 4.0 GeV; RHC	0.089 007 5	58.0416	-0.00342141	58.0429	-0.0011405
BANFF 24, SK number flux, 4.0 - 30.0 GeV; RHC	0.155 813	58.0419	-0.0029416	58.043	-0.00038053
BANFF, Norm, p2h	1	55.0471	-5.16251	55.0471	-5.1625
BANFF, Norm, CCRHS	0.148 515	54.04272	-6.91963	56.3167	-2.9751
BANFF, Norm, RegRES Isospin 1/2	0.307 692	57.1647	-1.51408	57.422	-1.0654
BANFF, Norm, MaQE	0.025	56.3858	-2.05611	57.4906	-0.95262
BANFF, Norm, Fermi Momentum	0.157 895	54.3275	-6.40221	56.6448	-2.4099
BANFF, Norm, ν_e To $\bar{\nu}_\mu$	0.028 284 3	58.0433	-0.000419022	58.0435	-0.00013967
BANFF, Norm, 2p2hBar	1	55.04778	-50.1725	57.637	-1.0224
BANFF, Norm, CC_Oth	0.4	57.4048	-1.10053	57.9291	-0.36955
BANFF, Norm, NC_Coh	0.3	57.8175	-0.389455	57.9082	-0.12982
BANFF, Norm, NC_Coh	0.3	58.0416	-0.00340446	58.0429	-0.0011348
BANFF, Norm, NC_Oth	0.3	57.5743	-0.808423	57.8872	-0.26947
BANFF, Norm, ν_e To $\bar{\nu}_\mu$	0.028 284 3	58.0433	-0.000419022	58.0435	-0.00013967
BANFF, Norm, $\bar{\nu}_e$ To $\bar{\nu}_\mu$	0.2	54.70778	-4.25365	55.57716	-4.2536
BANFF, Norm, 2p2h	0.2	55.5746	-4.64469	56.9505	-1.8832
BANFF, BarPA A	0.118	51.1456	-11.8841	55.7443	-3.9613
BANFF, BarPA B	0.241	52.401	-9.54905	56.196	-3.183
BANFF, BarPA D	0.1695	54.0755	-6.83636	56.7299	-2.2788
BANFF, BarPA E	0.352	57.3798	-0.28206	57.9772	-0.11438
BANFF, Norm, 2p2h C to O	0.2	54.7643	-0.190836	58.1007	0.098417
SXDet + FSU/SU; E_{reco} (0.00 - 0.40 GeV; $\nu_e/\bar{\nu}_\mu$; CCQE (LR_μ); RHC	0.008 512 49	57.9186	-0.215368	58.0019	-0.071789
SXDet + FSU/SU; E_{reco} (0.40 - 1.10 GeV; $\nu_e/\bar{\nu}_\mu$; CCQE (LR_μ); RHC	0.007 050 99	57.7186	-0.559823	57.9353	-0.18661
SXDet + FSU/SU; E_{reco} (0.40 - 1.10 GeV; $\nu_e/\bar{\nu}_\mu$; CCQE (LR_μ); RHC	0.006 784	57.5365	-0.0737521	57.8746	-0.29117
SXDet + FSU/SU; E_{reco} (0.00 - 30.00 GeV; $\nu_e/\bar{\nu}_\mu$; CCQE (LR_μ); RHC	1.004 54	58.0233	-0.031468	58.0375	-0.010489
SXDet + FSU/SU; E_{reco} (0.00 - 30.00 GeV; $\nu_e/\bar{\nu}_\mu$; CCQE (LR_μ); RHC	0.657 251	54.0298	-5.89682	56.9027	-1.9656
SXDet + FSU/SU; E_{reco} (0.00 - 30.00 GeV; all NC (LR_μ); RHC	0.024	58.0436	-2.44831 $\times 10^{-14}$	58.0436	-8.5691 $\times 10^{-14}$
SK energy scale					-1.2292×10^{-13}
					-6.12077×10^{-14}

Table 30: $\pm 1\sigma$ and $\pm 3\sigma$ effect of the systematic parameters on the total number of μ -like Super-K events with Run 1-8 POT for antineutrino mode pre-BANFF Asimov data set A. Only the systematic parameters which affect this sample are shown.

Parameter	1σ value	BANFF tuned -3 σ	BANFF tuned 0	BANFF tuned +3 σ	BANFF tuned -1 σ	BANFF tuned +1 σ	BANFF tuned +3 σ
All syst		13.4912	-79.0516(%)	36.0858	-43.968(%)	109.17	69.507(%)
BANFF 0, SK numu flux, 0.0 - 0.4 GeV	0.0987323	64.0102	-0.608829	64.2716	-0.20294	64.7944	0.608829
BANFF 1, SK numu flux, 0.4 - 0.5 GeV	0.103488	62.682	-2.67126	63.8289	-0.89042	64.9758	0.89042
BANFF 2, SK numu flux, 0.5 - 0.6 GeV	0.096444	60.6675	-5.73923	63.1574	-1.9331	65.6473	1.9331
BANFF 3, SK numu flux, 0.6 - 0.7 GeV	0.0866958	60.3974	-6.21864	63.0673	-2.0729	65.7373	2.0729
BANFF 4, SK numu flux, 0.7 - 1.0 GeV	0.113052	58.8035	-8.69353	62.536	-2.8978	66.2686	2.8978
BANFF 5, SK numu flux, 1.0 - 1.5 GeV	0.0917476	63.687	-1.11072	64.1639	-0.37024	64.6408	0.37024
BANFF 6, SK numu flux, 1.5 - 2.5 GeV	0.0701742	64.2733	-0.290259	64.5353	-0.066753	64.9453	0.066753
BANFF 7, SK numu flux, 2.5 - 3.5 GeV	0.0736805	64.3235	-0.122345	64.376	-0.040782	64.4286	0.040782
BANFF 8, SK numu flux, 3.5 - 5.0 GeV	0.0873733	64.2921	-0.17113	64.3656	-0.057043	64.439	0.057043
BANFF 9, SK numu flux, 5.0 - 7.0 GeV	0.0973369	64.3488	-0.08304	64.3845	-0.02768	64.4201	0.02768
BANFF 10, SK numu flux, 7.0 - 30.0 GeV	0.11436	64.3732	-0.0452789	64.3926	-0.015093	64.412	0.015093
BANFF 11, SK numubar flux, 0.0 - 0.7 GeV	0.102576	64.3597	-0.0661419	64.3881	-0.022047	64.4165	0.022047
BANFF 12, SK numubar flux, 0.7 - 1.0 GeV	0.0785331	64.3627	-0.0615239	64.3890	-0.020508	64.4155	0.020508
BANFF 13, SK numubar flux, 1.0 - 1.5 GeV	0.0844536	64.3682	-0.0530126	64.3909	-0.017671	64.4137	0.017671
BANFF 14, SK numubar flux, 1.5 - 2.5 GeV	0.0855683	64.3811	-0.0330017	64.3952	-0.011001	64.4094	0.011001
BANFF 15, SK numubar flux, 2.5 - 30.0 GeV	0.0864284	64.3817	-0.0319347	64.3955	-0.01645	64.4092	0.01645
BANFF 16, SK nue flux, 0.0 - 0.5 GeV	0.0896983	64.0426	-0.558585	64.2824	-0.1862	64.5022	0.1862
BANFF 17, SK nue flux, 0.5 - 0.7 GeV	0.089952	63.9068	-0.769331	64.2372	-0.25644	64.5675	0.25644
BANFF 18, SK nue flux, 0.7 - 0.8 GeV	0.0859648	64.1548	-0.384367	64.3198	-0.12812	64.4848	0.12812
BANFF 19, SK nue flux, 0.8 - 1.5 GeV	0.0809182	63.6486	-1.17031	64.1511	-0.3901	64.6535	0.3901
BANFF 20, SK nue flux, 1.5 - 2.5 GeV	0.0789719	64.3446	-0.0896441	64.3891	-0.029881	64.4216	0.029881
BANFF 21, SK nue flux, 2.5 - 4.0 GeV	0.08385	64.3936	-0.0134845	64.3994	-0.0044948	64.4052	0.0044948
BANFF 22, SK nue flux, 4.0 - 30.0 GeV	0.0938943	64.3987	-0.00567038	64.4011	-0.0018901	64.4035	0.0018901
BANFF 23, SK nuclebar flux, 0.0 - 2.5 GeV	0.0740279	64.3297	-0.11281	64.3781	-0.037603	64.4265	0.037603
BANFF 24, SK nuclebar flux, 2.5 - 30.0 GeV	0.028416	64.3905	-0.0043831	64.4014	-0.001461	64.4033	0.001461
BANFF; Norm; 2p2h	1	55.5264	-10.6765	57.5204	-10.677	71.2782	10.677
BANFF; CA5; RES	0.148515	60.5772	-5.93936	62.946	-2.2612	66.0398	2.5426
BANFF; Norm; BgRES Isospin 1/2	0.307692	63.1448	-0.756971	64.5053	-0.532367	64.9239	0.81302
BANFF; Ma QE	0.025	61.7753	-4.07899	63.5516	-1.3299	65.2283	1.2825
BANFF; Norm; NC; Orth	0.157895	61.1503	-5.0496	63.4044	-1.5494	65.3124	1.4132
BANFF; Fermi Momentum	0.0577778	65.765	2.11587	65.128	1.1268	63.6315	-1.1968
BANFF; Shape; CC; Oth	0.4	62.2479	-2.059744	64.3445	-0.088736	64.4601	0.088736
BANFF; Norm; CC; Coh	0.3	64.3496	-0.0818662	64.3848	-0.027289	64.4198	0.027289
BANFF; Norm; NC; Coh	0.3	63.8321	-0.885326	64.2123	-0.29511	64.5924	0.29511
BANFF; Norm; NC; Orth	0.3	64.0843	-0.493823	64.2963	-0.16461	64.5083	0.16461
BANFF; Norm; ν_e ; To ν_μ	0.0282843	54.1919	-7.619397	62.7665	-2.54	66.0381	2.54
BANFF; Norm; NC; 1; γ	1	62.3329	-3.21331	62.3329	-3.2133	66.4718	3.2133
BANFF; Norm; ν_e ; To $\bar{\nu}_\mu$	0.0282843	64.3447	-0.0858529	64.3839	-0.028618	64.4207	0.028618
BANFF; Norm; 2p2hBar	1	64.3424	-0.0930022	64.3424	-0.003002	64.4622	0.003002
BANFF; BelRA A	0.118	55.2091	-14.2747	61.3739	-4.752	67.7582	14.2747
BANFF; BelRA B	0.21	53.464	-16.9843	60.7562	-5.6614	55.6614	16.9843
BANFF; BelRA D	0.1695	58.806	60.4597	62.2951	-3.272	66.5096	3.272
BANFF; BelRA E	0.352	64.0489	63.3311	64.0452	-0.2187	64.5432	0.2187
BANFF; Shape; 2p2h	3	63.8496	-0.548743	64.2615	-0.32249	64.603	0.32249
BANFF; Norm; 2p2h C to O	0.2	60.2408	-6.644983	64.1946	-2.1539	65.7895	2.1539
SKDet + FSI/SI 11; E_{reco} (0.00 - 0.35)GeV; Osc. ν_e CC (1R _e)	0.181271	61.2702	-4.86341	63.3583	-1.6211	65.4464	1.6211
SKDet + FSI/SI 12; E_{reco} (0.35 - 0.80)GeV; Osc. ν_e CC (1R _e)	0.036083	60.3311	-6.1219	63.0881	-2.0406	65.7165	2.0406
SKDet + FSI/SI 13; E_{reco} (0.80 - 1.25)GeV; Osc. ν_e CC (1R _e)	0.0416636	63.3004	-1.66328	64.0452	-0.55443	64.7594	0.55443
SKDet + FSI/SI 9; E_{reco} (0.00 - 0.35)GeV; $\nu_\mu/\bar{\nu}_\mu$ CC (1R _e)	0.300431	64.3482	-0.0839511	64.3843	-0.027984	64.4293	0.027984
SKDet + FSI/SI 10; E_{reco} (0.35 - 0.80)GeV; $\nu_\mu/\bar{\nu}_\mu$ CC (1R _e)	0.321346	62.4257	-0.243223	64.3501	-0.081074	64.4545	0.081074
SKDet + FSI/SI 11; E_{reco} (0.80 - 1.25)GeV; $\nu_\mu/\bar{\nu}_\mu$ CC (1R _e)	0.392969	64.3731	-0.4052823	64.3926	-0.015094	64.412	0.015094
SKDet + FSI/SI 12; E_{reco} (0.35 - 0.80)GeV; $\nu_e/\bar{\nu}_e$ CC (1R _e)	0.35339	64.0289	-0.579849	64.2778	-0.19328	64.5268	0.579849
SKDet + FSI/SI 13; E_{reco} (0.35 - 0.80)GeV; $\nu_e/\bar{\nu}_e$ CC (1R _e)	0.0698928	63.5422	-1.33558	64.1156	-0.44519	64.689	0.44519
SKDet + FSI/SI 14; E_{reco} (0.80 - 1.25)GeV; $\nu_e/\bar{\nu}_e$ CC (1R _e)	0.0771361	63.7745	-0.974818	64.193	-0.32494	64.6116	0.32494
SKDet + FSI/SI 15; E_{reco} (0.00 - 0.35)GeV; all NC (1R _e)	0.194453	63.1388	-1.96183	63.9812	-0.65394	64.8235	0.65394
SKDet + FSI/SI 16; E_{reco} (0.35 - 0.80)GeV; all NC (1R _e)	0.181015	63.8486	-2.41251	63.8844	-0.804117	64.9202	0.804117
SKDet + FSI/SI 17; E_{reco} (0.80 - 1.25)GeV; all NC (1R _e)	0.472078	63.3933	-1.4115	64.0993	-0.4705	64.7053	0.4705
SK energy scale	0.024	64.4023	0	64.4023	-2.2066×10^{-14}	64.4023	0

Table 31: $\pm 1\sigma$ and $\pm 3\sigma$ effect of the systematic parameters on the total number of e-like Super-K events with Run 1-8 POT for neutrino mode pre-BANFF Asimov data set A. Only the systematic parameters which affect this sample are shown.

Parameter	1σ value	BANFF tuned -3 σ	4.19157	-43.144 (%)	BANFF tuned -1 σ	12.51	69.576(%)	BANFF tuned +1 σ	32.2025	BANFF tuned +3 σ	336.497(%)
All syst		1.97992	-73.1627(%)								
BANFF 0, SK number flux, 0.0 - 0.7 GeV; RHC	0.0936822	7.21918	-2.14575	7.32471	-0.71525	7.43025	0.71525	7.53578	2.14575		
BANFF 1, SK number flux, 0.7 - 1.0 GeV; RHC	0.0793343	7.25637	-1.64156	7.33711	-0.54719	7.41785	0.54719	7.4859	1.64156		
BANFF 2, SK number flux, 1.0 - 1.5 GeV; RHC	0.0767271	7.30403	-0.395621	7.353	-0.33187	7.40196	0.33187	7.45093	0.905621		
BANFF 3, SK number flux, 1.5 - 2.5 GeV; RHC	0.0805587	7.31156	-0.48692	7.36351	-0.16231	7.38946	0.16231	7.4134	0.48692		
BANFF 4, SK number flux, 2.5 - 30.0 GeV; RHC	0.0802896	7.33762	-0.540283	7.36119	-0.18009	7.38077	0.18009	7.41734	0.540283		
BANFF 5, SK number flux, 0.0 - 0.4 GeV; RHC	0.104476	7.32538	-0.326617	7.36945	-0.10887	7.38551	0.10887	7.40158	0.326617		
BANFF 6, SK number flux, 0.4 - 0.5 GeV; RHC	0.1015533	7.29096	-1.17275	7.34864	-0.39092	7.40632	0.39092	7.464	1.17275		
BANFF 7, SK number flux, 0.5 - 0.6 GeV; RHC	0.0961673	7.15696	-2.98911	7.30397	-0.90637	7.45099	0.90637	7.598	2.98911		
BANFF 8, SK number flux, 0.6 - 0.7 GeV; RHC	0.0846366	7.11041	-0.62006	7.28866	-1.2067	7.4665	1.2067	7.64455	3.62006		
BANFF 9, SK number flux, 0.7 - 1.0 GeV; RHC	0.125091	6.87786	-6.77227	7.21094	-2.2574	7.54402	2.2574	7.8771	6.77227		
BANFF 10, SK number flux, 1.0 - 1.5 GeV; RHC	0.105291	7.28518	-1.25117	7.34671	-0.41706	7.40825	0.41706	7.46979	1.25117		
BANFF 11, SK number flux, 1.5 - 2.5 GeV; RHC	0.0793987	7.33322	-0.880861	7.36339	-0.10962	7.38557	0.10962	7.40174	0.328861		
BANFF 12, SK number flux, 2.5 - 3.5 GeV; RHC	0.0739384	7.36361	-0.154206	7.37369	-0.051402	7.38127	0.051402	7.38886	0.154206		
BANFF 13, SK number flux, 3.5 - 5.0 GeV; RHC	0.0939023	7.36421	-0.179933	7.37306	-0.059977	7.38191	0.059977	7.39076	0.179933		
BANFF 14, SK number flux, 5.0 - 7.0 GeV; RHC	0.0925126	7.37316	-0.05857575	7.37604	-0.019525	7.37892	0.019525	7.3818	0.05857575		
BANFF 15, SK number flux, 7.0 - 10.0 GeV; RHC	0.130312	7.37411	-0.036339	7.37659	-0.012046	7.37837	0.012046	7.38015	0.036139		
BANFF 16, SK number flux, 0.0 - 2.5 GeV; RHC	0.0688813	7.24397	-1.80973	7.32938	-0.60324	7.42199	0.60324	7.51039	1.80973		
BANFF 17, SK number flux, 2.5 - 30.0 GeV; RHC	0.0794446	7.37509	-0.0324275	7.37668	-0.010809	7.37828	0.010809	7.37987	0.0324275		
BANFF 18, SK number flux, 0.0 - 0.5 GeV; RHC	0.0946954	7.32535	-0.706645	7.3601	-0.23555	7.38486	0.23555	7.42961	0.706645		
BANFF 19, SK number flux, 0.5 - 1.7 GeV; RHC	0.0910393	7.31731	-0.816559	7.35742	-0.27186	7.38754	0.27186	7.43765	0.81559		
BANFF 20, SK number flux, 0.7 - 0.8 GeV; RHC	0.0910124	7.34444	-0.447891	7.36647	-0.1493	7.3885	0.1493	7.41052	0.447891		
BANFF 21, SK number flux, 0.8 - 1.5 GeV; RHC	0.0838665	7.26836	-1.4791	7.34111	-0.49303	7.41385	0.49303	7.4866	1.4791		
BANFF 22, SK number flux, 1.5 - 2.5 GeV; RHC	0.0795776	7.37079	-0.06906955	7.37525	-0.030232	7.37971	0.030232	7.38417	0.06906955		
BANFF 23, SK number flux, 2.5 - 30.0 GeV; RHC	0.0890075	7.37611	-0.0185463	7.37702	-0.0061821	7.37794	0.0061821	7.37855	0.0185463		
BANFF 24, SK number flux, 4.0 - 30.0 GeV; RHC	0.155813	7.37635	-0.0253322	7.37771	-0.0051107	7.37786	0.0051107	7.37861	0.0153322		
BANFF, Norm; 2p2h	1.	7.13228	-3.323558	7.31228	-3.3236	7.62268	3.3236	8.11307	9.97075		
BANFF, CA5, RES	0.148515	6.84893	-7.16438	7.1284	-3.3762	7.68946	4.3644	8.56212	16.0575		
BANFF, Norm; BgRES Isospin 1/2	0.307692	7.28615	-2.124296	7.31215	-0.87115	7.47558	1.3297	7.77324	16.0575		
BANFF, MaOE	0.025	7.19864	-2.1242409	7.31805	-0.80561	7.43654	0.80561	7.55311	2.38056		
BANFF, M, RES	0.1577895	6.98682	-5.29535	7.22181	-2.1101	7.54013	2.2047	7.85705	6.50038		
BANFF, Fermi Momentum	0.0577778	7.53015	-0.069353	7.3771	-0.02555	7.29545	0.02555	7.37852	-3.3882		
BANFF; Shape; CC Orth	0.4	7.34409	-0.052601	7.36567	-0.16004	7.38925	0.16004	7.4129	0.480121		
BANFF; Norm; CC Coh	0.3	7.33111	-0.628631	7.36202	-0.20954	7.39294	0.20954	7.42386	0.628631		
BANFF; Norm; NC Coh	0.3	7.13197	-3.322778	7.29565	-1.1093	7.45932	1.1093	7.62299	3.32778		
BANFF; Norm; NC Orth	0.3	7.30247	-1.016177	7.35248	-0.33892	7.40248	0.33892	7.45249	1.01677		
BANFF; Norm; NC 1	1.	7.10133	-7.11713	7.32542	-0.70571	7.42954	0.70571	7.53367	2.11713		
BANFF; Norm; $\bar{\nu}_e$ To $\bar{\nu}_\mu$	0.0282843	7.02855	-4.73033	7.26115	-1.5768	7.43881	1.5768	7.62496	21.3129		
BANFF; Norm; $\bar{\nu}_e$ To $\bar{\nu}_\tau$	1.	7.05487	-4.37286	7.054187	-4.3729	7.70009	4.3729	8.3453	4.73033		
BANFF; Norm; 2p2hBar	0.118	6.48099	-12.1517	7.07865	-4.0506	7.67631	4.0506	8.27597	13.1186		
BANFF; Norm; BpA	0.21	6.6711	-9.57482	7.14202	-3.1916	7.61294	3.1916	8.08386	9.57479		
BANFF; BeRPA D	0.1695	7.05599	-4.35767	7.27032	-1.4526	7.48464	1.4526	7.63897	4.35765		
BANFF; BeRPA E	0.352	7.35957	-0.242812	7.37034	-0.096784	7.38462	0.096784	7.39891	0.290453		
BANFF; Shape; 2p2h	3	7.35746	-0.542431	7.35747	-0.27122	7.40966	0.27122	7.44184	0.872345		
BANFF; Norm; 2p2h C to O	0.2	7.0368	-4.61787	7.26392	-1.5393	7.49104	1.5393	7.71816	4.61787		
SKDeta + FSU/SI 6; E_{reco} (0.00 - 0.35) GeV; Osc. ν_e CC ($1R_e$); RHC	0.108165	7.26351	-1.54486	7.33949	-0.514495	7.41547	0.514495	7.49145	1.54486		
SKDeta + FSU/SI 7; E_{reco} (0.35 - 0.80) GeV; Osc. ν_e CC ($1R_e$); RHC	0.0663039	7.0458	-4.4959	7.26692	-1.4986	7.48804	1.4986	7.70947	4.4959		
SKDeta + FSU/SI 8; E_{reco} (0.80 - 1.25) GeV; Osc. ν_e CC ($1R_e$); RHC	0.0667315	7.21619	-2.18626	7.32372	-1.4526	7.43124	1.4526	7.63897	2.18626		
SKDeta + FSU/SI 9; E_{reco} (0.00 - 0.35) GeV; $\bar{\nu}_e$ CC ($1R_e$); RHC	0.348644	7.36759	-0.134016	7.37419	-0.044672	7.38078	0.044672	7.38737	0.134016		
SKDeta + FSU/SI 10; E_{reco} (0.35 - 0.80) GeV; $\bar{\nu}_e$ CC ($1R_e$); RHC	0.431647	7.34054	-0.500721	7.36517	-0.16691	7.38979	0.16691	7.41442	0.500721		
SKDeta + FSU/SI 11; E_{reco} (0.80 - 1.25) GeV; $\bar{\nu}_e$ CC ($1R_e$); RHC	0.417164	7.36076	-0.226635	7.37191	-0.075545	7.38305	0.075545	7.3942	0.226635		
SKDeta + FSU/SI 12; E_{reco} (0.00 - 0.35) GeV; $\bar{\nu}_e$ CC ($1R_e$); RHC	0.0845563	7.33687	-0.550513	7.36394	-0.1835	7.39102	0.1835	7.41809	0.550513		
SKDeta + FSU/SI 13; E_{reco} (0.35 - 0.80) GeV; $\bar{\nu}_e$ CC ($1R_e$); RHC	0.0660697	7.2336	-1.81467	7.33286	-0.60489	7.44211	0.60489	7.51136	1.81467		
SKDeta + FSU/SI 14; E_{reco} (0.80 - 1.25) GeV; $\bar{\nu}_e$ CC ($1R_e$); RHC	0.0780241	7.2246	-2.07223	7.32652	-0.69074	7.42844	0.69074	7.53036	2.07223		
SKDeta + FSU/SI 15; E_{reco} (0.00 - 0.35) GeV; $\bar{\nu}_e$ CC ($1R_e$); RHC	0.214066	7.06469	-4.23982	7.27322	-1.4133	7.48174	1.4133	7.69027	4.23982		
SKDeta + FSU/SI 16; E_{reco} (0.35 - 0.80) GeV; all NC ($1R_e$); RHC	0.190575	6.97398	-5.46932	7.24298	-1.8231	7.51198	1.8231	7.78098	5.46932		
SKDeta + FSU/SI 17; E_{reco} (0.80 - 1.25) GeV; all NC ($1R_e$); RHC	0.40486	7.13717	-3.2574	7.29738	-1.0658	7.45759	1.0658	7.61779	3.2574		
SK energy scale	0.024	7.37748	0	7.37748	-1.2039 $\times 10^{-14}$	7.37748	-1.2039 $\times 10^{-14}$	7.37748	-2.4078 $\times 10^{-14}$	7.37748	0

Table 32: $\pm 1\sigma$ and $\pm 3\sigma$ effect of the systematic parameters on the total number of e-like Super-K events with Run 1-8 POT for antineutrino mode pre-BANFF Asimov data set A. Only the systematic parameters which affect this sample are shown.

Parameter	1σ value	BANFF tuned -3 σ		BANFF tuned +3 σ		BANFF tuned +1 σ	BANFF tuned -1 σ	BANFF tuned +3 σ	BANFF tuned -3 σ
		0.424293	-94.5073(%)	3.6093	-53.276(%)	14.919	93.127(%)	45.8854	494.009(%)
All system									
BANFF 0, SK numm flux, 0.0 - 0.4 GeV	0.0987223	7.72182	-0.0373558	7.72575	-0.012452	7.72567	0.012452	7.72575	0.0373558
BANFF 1, SK numm flux, 0.4 - 0.5 GeV	0.163488	7.63342	-1.18175	7.69428	-0.393932	7.7554	7.81539	1.18175	1.18175
BANFF 2, SK numm flux, 0.5 - 0.6 GeV	0.096444	7.35943	-4.72745	7.60298	-1.5758	7.84643	1.5758	4.72745	4.72745
BANFF 3, SK numm flux, 0.6 - 0.7 GeV	0.0866958	7.20413	-6.73909	7.55118	-2.264	7.89823	2.264	6.73909	6.73909
BANFF 4, SK numm flux, 0.7 - 1.0 GeV	0.113052	6.90702	-10.5853	7.45215	-3.5284	7.99727	3.5284	10.5853	10.5853
BANFF 5, SK numm flux, 1.0 - 1.5 GeV	0.0917476	7.62335	-1.30951	7.69099	-0.4365	7.75843	0.4365	1.30951	1.30951
BANFF 6, SK numm flux, 1.5 - 2.5 GeV	0.0701742	7.70259	-0.286339	7.71733	-0.095146	7.72008	0.095146	0.286339	0.286339
BANFF 7, SK numm flux, 2.5 - 3.5 GeV	0.0736805	7.71056	-0.183134	7.71999	-0.061045	7.72942	0.061045	0.183134	0.183134
BANFF 8, SK numm flux, 3.5 - 5.0 GeV	0.0873733	7.6978	-0.348282	7.71574	-0.11669	7.73368	0.11669	0.348282	0.348282
BANFF 9, SK numm flux, 5.0 - 7.0 GeV	0.0979369	7.71317	-0.149381	7.72086	-0.049794	7.72855	0.049794	0.149381	0.149381
BANFF 10, SK numm flux, 7.0 - 30.0 GeV	0.11436	7.7233	-0.018241	7.72424	-0.0060803	7.72518	0.0060803	0.72612	0.132411
BANFF 11, SK numm flux, 0.0 - 0.7 GeV	0.102576	7.72385	-0.0110333	7.72442	-0.0037011	7.72499	0.0037011	0.72556	0.0110333
BANFF 12, SK numm flux, 0.7 - 1.0 GeV	0.0785311	7.72378	-0.012024	7.7244	-0.004008	7.72502	0.004008	0.012024	0.012024
BANFF 13, SK numm flux, 1.0 - 1.5 GeV	0.0844536	7.72326	-0.0186907	7.72423	-0.0062302	7.72519	0.0062302	0.72615	0.0186907
BANFF 14, SK numm flux, 1.5 - 2.5 GeV	0.0855683	7.72255	-0.0279626	7.72399	-0.012939	7.72543	0.012939	0.72687	0.0279626
BANFF 15, SK numm flux, 2.5 - 30.0 GeV	0.0864284	7.721	-0.0337547	7.72384	-0.011252	7.72558	0.011252	0.72731	0.0337547
BANFF 16, SK numm flux, 0.0 - 0.5 GeV	0.0896983	7.71448	-0.132379	7.7213	-0.044126	7.72812	0.044126	0.73493	0.132379
BANFF 17, SK numm flux, 0.5 - 0.7 GeV	0.089952	7.66823	-0.731188	7.70588	-0.24373	7.74353	0.24373	0.731188	0.731188
BANFF 18, SK numm flux, 0.7 - 0.8 GeV	0.0859648	7.6858	-0.503612	7.71174	-0.16787	7.73767	0.16787	0.73631	0.503612
BANFF 19, SK numm flux, 0.8 - 1.5 GeV	0.0809182	7.58596	-1.79618	7.67846	-0.59873	7.77096	0.59873	0.786346	1.79618
BANFF 20, SK numm flux, 1.5 - 2.5 GeV	0.0789719	7.71381	-0.141038	7.72108	-0.047013	7.72834	0.047013	0.7356	0.141038
BANFF 21, SK numm flux, 2.5 - 4.0 GeV	0.08385	7.72324	-0.0189655	7.72422	-0.0063218	7.7252	0.0063218	0.73617	0.0189655
BANFF 22, SK numm flux, 4.0 - 30.0 GeV	0.0938943	7.72412	-0.00760552	7.72451	-0.0023352	7.7249	0.0023352	0.72529	0.00760552
BANFF 23, SK numm flux, 0.0 - 2.5 GeV	0.0740279	7.72291	-0.023243	7.72411	-0.0077477	7.72531	0.0077477	0.72615	0.023243
BANFF 24, SK numm flux, 2.5 - 30.0 GeV	0.128416	7.72428	-0.00548076	7.72457	-0.0015289	7.72485	0.0015289	0.72513	0.00548076
BANFF, Norm: 2p2h	1	7.62198	-1.32985	7.621198	-1.32985	7.82743	1.32985	8.03289	3.98954
BANFF, CAS RES	0.148515	7.49189	-35.9839	7.68439	-13.46739	8.88011	14.967	11.36382	49.3109
BANFF, Norm: EgREES Isospin 1/2	0.307692	7.420	-3.93473	7.51082	-2.7689	8.05117	4.2262	9.04181	17.0505
BANFF, Ma QE	0.025	7.70958	-0.195853	7.7198	-0.0633338	7.72948	0.061781	7.73862	0.180117
BANFF, Ma IRES	0.157895	5.35765	-28.0536	7.12125	-7.8121	8.22751	6.509	9.00484	16.5719
BANFF, Fermi Momentum	0.0577778	7.73075	0.0759039	7.72776	0.039489	7.72122	-0.0450997	7.71341	-0.146216
BANFF, Shape: CC Oth	0.4	7.53721	-2.42724	7.64813	-0.9917	7.78029	0.99137	7.95445	2.97411
BANFF, Norm: CC Coh	0.3	7.58906	-1.75598	7.67949	-0.58533	7.7992	0.58533	7.86035	1.75598
BANFF, Norm: NC Oth	0.3	7.52266	-2.61563	7.65736	-0.87188	7.73206	0.87188	7.92676	2.61563
BANFF, Norm: ν_e To $\bar{\nu}_\mu$	0.0282843	7.11846	-7.84814	7.52263	-2.616	7.73279	2.616	8.33095	7.84814
BANFF, Norm: NC 1, γ	1	7.66615	-0.758101	7.66615	-0.758101	7.78327	0.7581	7.90039	2.2743
BANFF, Norm: $\bar{\nu}_e$ To $\bar{\nu}_\mu$	0.0282843	7.7235	-0.0156814	7.7243	-0.0055227	7.72511	0.0052271	7.72592	0.0156814
BANFF, Norm: 2p2h Bar	1	7.72312	-0.0206066	7.72312	-0.0206067	7.7263	0.0206067	7.72948	0.0618198
BANFF, BerPA A	0.118	7.687	-0.485527	7.71221	-0.16184	7.73721	0.16184	7.76221	0.485327
BANFF, BerPA B	0.21	7.663389	-0.787311	7.70443	-0.26234	7.74498	0.26234	7.78552	0.78731
BANFF, BerPA D	0.1695	7.68658	-0.195503	7.712	-0.164562	7.73742	0.164562	7.76283	0.493568
BANFF, BerPA E	0.352	7.72255	-0.0279701	7.72385	-0.011147	7.72557	0.011147	7.72729	0.0334428
BANFF, Norm: 2p2h	3	7.6796	-0.583888	7.70216	-0.290194	7.74243	0.290194	7.76014	0.458739
BANFF, Norm: C to O	0.2	7.660212	-0.810272	7.70384	-0.27009	7.74557	0.27009	7.7873	0.810272
BANFF, Norm: CC ($MultiRing$)	0.248951	4.60312	-0.404104	6.68418	-13.47	8.76524	13.47	10.8463	40.4104
BANFF, Norm: E_{reco} (0.30 - 0.80) GeV; Osc. ν_e CC ($MultiRing$)	0.214994	6.46097	-5.16397	7.30346	-5.4532	8.14595	5.4532	8.98845	16.3597
BANFF, Norm: E_{reco} (0.30 - 0.80) GeV; Osc. $\nu_\mu/\bar{\nu}_\mu$ CC ($MultiRing$)	0.236118	5.057403	-2.00453	7.67399	-0.66818	7.77632	0.66818	7.87955	2.00453
BANFF, Norm: E_{reco} (0.30 - 0.80) GeV; Osc. $\nu_\mu/\bar{\nu}_\mu$ CC ($MultiRing$)	0.2441289	7.68785	-0.477076	7.71242	-0.15903	7.73699	0.15903	7.76156	0.477076
BANFF, Norm: E_{reco} (0.30 - 0.80) GeV; Osc. $\nu_\mu/\bar{\nu}_\mu$ CC ($MultiRing$)	0.23455	7.42686	-3.85577	7.62542	-1.2853	7.82399	1.2853	3.85577	3.85577
BANFF, Norm: E_{reco} (0.30 - 0.80) GeV; all NC ($MultiRing$)	0.983178	6.846411	-11.37	7.43194	-3.79	7.86861	1.8629	8.15642	5.58877
BANFF, Norm: E_{reco} (0.30 - 0.80) GeV; all NC ($MultiRing$)	0.523609	7.54527	-2.3229	7.66489	-0.7743	8.01747	3.79	8.66301	11.37
BANFF, Norm: E_{reco} (0.80 - 1.25) GeV; all NC ($MultiRing$)	0.024	7.72471	0	7.72471	0	2.29968 $\times 10^{-14}$	7.72471	7.72471	1.14979 $\times 10^{-14}$
SCK energy scale									

Table 33: $\pm 1\sigma$ and $\pm 3\sigma$ effect of the systematic parameters on the total number of e-like Super-K events with one decay electron with Run 1-8 POT for neutrino mode pre-BANFF Astrov data set A. Only the systematic parameters which affect this sample are shown.

Parameter	$1\ \sigma$ value	BANFF tuned -3 σ	BANFF tuned -1 σ	BANFF tuned +1 σ	BANFF tuned +3 σ
All syst		107.89	-58.8929 (%)	200.066	-23.773 (%)
BANFF 0, SK neutrino flux, 0.0 - 0.4 GeV	0.0574967	-1.83631	-0.6121	264.066	550.51
BANFF 1, SK neutrino flux, 0.4 - 0.5 GeV	0.0519363	-1.54403	-0.51468	263.811	266.512
BANFF 2, SK neutrino flux, 0.5 - 0.6 GeV	0.0443682	-0.337759	-0.11259	262.755	263.346
BANFF 3, SK neutrino flux, 0.6 - 0.7 GeV	0.0413886	-0.273275	-0.091092	262.699	0.091092
BANFF 4, SK neutrino flux, 0.7 - 1.0 GeV	0.05416	-3.30958	-1.1032	265.355	1.1032
BANFF 5, SK neutrino flux, 1.0 - 1.5 GeV	0.0490261	-2.68471	-0.8949	264.809	0.8949
BANFF 6, SK neutrino flux, 1.5 - 2.5 GeV	0.0475572	-1.86232	-0.620777	264.089	0.620777
BANFF 7, SK neutrino flux, 2.5 - 3.5 GeV	0.0436069	-0.959321	-0.31977	263.299	0.31977
BANFF 8, SK neutrino flux, 3.5 - 5.0 GeV	0.040772	-0.769586	-0.25653	263.133	264.48
BANFF 9, SK neutrino flux, 5.0 - 7.0 GeV	0.0410958	-0.2401334	-0.066751	262.635	0.066751
BANFF 10, SK neutrino flux, 7.0 - 30.0 GeV	0.048214	-0.0171738	-0.0057246	262.445	0.0057246
BANFF 11, SK neutrino flux, 0.0 - 0.7 GeV	0.073717	-262.238	-0.028189	262.354	0.028189
BANFF 12, SK neutrino flux, 0.7 - 1.0 GeV	0.04777	-262.299	-0.0614241	262.406	0.020475
BANFF 13, SK neutrino flux, 1.0 - 1.5 GeV	0.0574721	-261.806	-0.249264	262.242	-0.083088
BANFF 14, SK neutrino flux, 1.5 - 2.5 GeV	0.0618807	-261.514	-0.360463	262.145	-0.12015
BANFF 15, SK neutrino flux, 2.5 - 30.0 GeV	0.0674673	-261.784	-0.25758	262.235	-0.08586
BANFF 16, SK neutrino flux, 0.0 - 0.5 GeV	0.0464719	-262.459	-0.000248152	262.46	-8.2717 $\times 10^{-5}$
BANFF 17, SK neutrino flux, 0.5 - 0.7 GeV	0.0422400	-262.459	-0.000125298	262.46	-0.00014177
BANFF 18, SK neutrino flux, 0.7 - 0.8 GeV	0.0411175	-262.459	-0.000313178	262.46	-0.00010439
BANFF 19, SK neutrino flux, 0.8 - 1.5 GeV	0.0390566	-262.454	-0.00220589	262.458	-0.0007753
BANFF 20, SK neutrino flux, 1.5 - 2.5 GeV	0.0400552	-262.453	-0.00277052	262.458	-0.00092351
BANFF 21, SK neutrino flux, 2.5 - 4.0 GeV	0.0414685	-262.455	-0.00194169	262.458	-0.000646723
BANFF 22, SK neutrino flux, 4.0 - 30.0 GeV	0.0586814	-262.457	-0.00127222	262.459	-0.00042374
BANFF 23, SK neutrino flux, 0.0 - 2.5 GeV	0.0535293	-262.459	-0.000493365	262.46	-0.00016462
BANFF 24, SK neutrino flux, 2.5 - 30.0 GeV	0.1144234	-262.456	-0.00143486	262.459	-0.00047829
BANFF; Norm; 2p2h	0.182443	-249.661	-0.878737	258.194	-1.6255
BANFF; CA5 RES	0.0591704	-255.895	-2.50122	260.15	-0.88007
BANFF; Norm; BgRES Isospin 1/2	0.18977	-258.529	-1.49755	260.792	-0.63564
BANFF; Norm; Ma QE	0.0566483	-234.686	-1.58233	263.493	-3.4164
BANFF; Norm; RES	0.0452921	-256.99	-2.08416	260.608	-0.70568
BANFF; Norm; RES	0.0711661	-260.153	-0.878886	263.803	0.51159
BANFF; Shape; CC Orth	0.18663	-261.304	-0.440596	262.074	-0.14684
BANFF; Norm; CC Coh	0.274896	-262.097	-0.138277	262.339	-0.016092
BANFF; Norm; NC Coh	0.297126	-262.46	-0.000172198	262.46	-5.7399 $\times 10^{-5}$
BANFF; Norm; NC Orth	0.260395	-241.706	-7.90732	255.542	-0.26223
BANFF; Norm; ν_e To ν_μ	0.0298284	-262.453	-0.00245452	262.458	-0.00084851
BANFF; Norm; ν_e To $\bar{\nu}_\mu$	0.0298284	-262.46	-2.093 $\times 10^{-5}$	262.46	-6.9767 $\times 10^{-6}$
BANFF; Norm; 2p2h Bar	0.201069	-261.848	-0.233015	262.237	-0.084844
BANFF; Norm; BerPA A	0.0558267	-244.308	-6.91612	266.409	-0.23054
BANFF; BerPA B	0.117134	-244.85	-6.70968	256.549	-2.2366
BANFF; BerPA D	0.127806	-241.706	-7.90732	255.542	-2.6358
BANFF; BerPA E	0.354515	-261.309	-0.438693	261.985	-0.18078
BANFF; Shape; 2p2h	0.338124	-264.448	-0.769209	263.47	0.38476
BANFF; Norm; 2p2h C to O	0.161427	-244.058	-6.66847	256.626	-2.2228
SKD ν + FSU/SI 0; E_{reco} (0.00 - 0.40) GeV; $\nu_\mu/\bar{\nu}_\mu$ CCQE (1/R _p)	0.0087853	-261.826	-6.91612	262.227	0.088897
SKD ν + FSU/SI 1; E_{reco} (0.40 - 1.10) GeV; $\nu_\mu/\bar{\nu}_\mu$ CCQE (1/R _p)	0.0074038	-260.255	-0.840095	261.725	-0.28003
SKD ν + FSU/SI 2; E_{reco} (1.10 - 30.00) GeV; $\nu_\mu/\bar{\nu}_\mu$ CCQE (1/R _p)	0.0072044	-260.417	-0.758196	263.123	0.25273
SKD ν + FSU/SI 3; E_{reco} (0.00 - 30.00) GeV; $\nu_\mu/\bar{\nu}_\mu$ sig _{CC} (1/R _p)	0.169035	-243.977	-7.04231	256.299	-2.3474
SKD ν + FSU/SI 4; E_{reco} (0.00 - 30.00) GeV; $\nu_e/\bar{\nu}_e$ sig _{CC} (1/R _p)	1.00548	-262.22	-0.0912351	262.38	-0.030412
SKD ν + FSU/SI 5; E_{reco} (0.00 - 30.00) GeV; all NC (1/R _p)	0.658101	-246.611	-6.03901	257.177	2.013
SK energy scale	0.024	-4.33159 $\times 10^{-14}$	262.46	-2.1658 $\times 10^{-14}$	262.46

Table 34: $\pm 1\sigma$ and $\pm 3\sigma$ effect of the systematic parameters on the total number of μ -like Super-K events with Run 1-8 POT for neutrino mode post-BANFF Asimov data set A. Only the systematic parameters which affect this sample are shown.

Parameter	1σ value	BANFF tuned -3 σ	BANFF tuned +3 σ	BANFF tuned -1 σ	BANFF tuned +1 σ	BANFF tuned
All syst.		30.5141	-50.7005 (%)	49.2477	-20.434 (%)	77.269
BANFF 0, SK muon flux, 0.0 - 0.7 GeV; RHC	0.0656432	61.5824	-0.503456	61.791	-0.16849	61.9935
BANFF 1, SK muon flux, 0.7 - 1.0 GeV; RHC	0.0486119	61.5733	-0.520155	61.7879	-0.17338	62.0026
BANFF 2, SK muon flux, 1.0 - 1.5 GeV; RHC	0.0454048	61.0082	-1.4352	61.5966	-0.47773	62.1909
BANFF 3, SK muon flux, 1.5 - 2.5 GeV; RHC	0.0486206	61.7269	-1.88759	61.5058	-0.6292	62.2847
BANFF 4, SK muon flux, 2.5 - 30.0 GeV; RHC	0.0430627	61.1628	-1.18334	61.6511	-0.39445	62.1394
BANFF 5, SK muonflux, 0.0 - 0.4 GeV; RHC	0.0647795	60.8622	-1.66906	61.5539	-0.53635	62.2396
BANFF 6, SK muonflux, 0.4 - 0.5 GeV; RHC	0.0524864	61.34	-0.897129	61.7102	-0.29904	62.0803
BANFF 7, SK muonflux, 0.5 - 0.6 GeV; RHC	0.0448288	61.7886	-0.172346	61.8597	-0.057449	61.9308
BANFF 8, SK muonflux, 0.6 - 0.7 GeV; RHC	0.0409543	61.8144	-0.130581	61.8683	-0.043527	61.9222
BANFF 9, SK muonflux, 0.7 - 1.0 GeV; RHC	0.0521651	61.8576	-1.67654	61.5194	-0.55885	62.2411
BANFF 10, SK muonflux, 1.0 - 1.5 GeV; RHC	0.0470323	61.8991	-1.60936	61.6562	-0.53645	62.2273
BANFF 11, SK muonflux, 1.5 - 2.5 GeV; RHC	0.0421043	61.0123	-1.37799	61.6109	-0.45933	62.1796
BANFF 12, SK muonflux, 2.5 - 3.5 GeV; RHC	0.0462426	61.4714	-0.084739	61.754	-0.22825	62.0365
BANFF 13, SK muonflux, 3.5 - 5.0 GeV; RHC	0.0628807	61.4938	-0.648517	61.7614	-0.21619	62.0291
BANFF 14, SK muonflux, 5.0 - 7.0 GeV; RHC	0.0655197	61.8265	-0.111012	61.8723	-0.037004	61.9182
BANFF 15, SK muonflux, 7.0 - 30.0 GeV; RHC	0.0926475	61.8878	-0.0119875	61.8928	-0.0039958	61.8945
BANFF 16, SK muonflux, 0.0 - 2.5 GeV; RHC	0.0645452	61.893	-0.00366041	61.8941	-0.0012201	61.8945
BANFF 17, SK muonflux, 2.5 - 30.0 GeV; RHC	0.064639	61.8919	-0.0053391	61.8941	-0.001778	61.8963
BANFF 18, SK muonflux, 0.0 - 0.5 GeV; RHC	0.0513755	61.8952	-9.4396 $\times 10^{-6}$	61.8952	-3.1465 $\times 10^{-5}$	61.8953
BANFF 19, SK muonflux, 0.5 - 0.7 GeV; RHC	0.0655197	61.8952	-0.00123246	61.8952	-8.0013 $\times 10^{-5}$	61.8953
BANFF 20, SK muonflux, 0.7 - 1.0 GeV; RHC	0.0438365	61.8952	-0.000933981	61.8952	-4.1082 $\times 10^{-5}$	61.8953
BANFF 21, SK muonflux, 0.8 - 1.5 GeV; RHC	0.0398806	61.8946	-0.0016193	61.895	-0.00033133	61.8955
BANFF 22, SK muonflux, 1.5 - 2.5 GeV; RHC	0.0454445	61.8944	-0.00132837	61.8945	-0.00044279	61.8955
BANFF 23, SK muonflux, 2.5 - 4.0 GeV; RHC	0.0644807	61.894	-0.00202042	61.8948	-0.00067347	61.8957
BANFF 24, SK muonflux, 4.0 - 30.0 GeV; RHC	0.132852	61.894	-0.00194578	61.8948	-0.00068559	61.8957
BANFF, Norm, 2p2h						
BANFF, CA5 RBS	0.0594704	60.2874	-2.39771	61.3533	-8.0659	62.4312
BANFF, Norm, 3gRES Isospin 1/2	0.18977	60.7952	-2.82881	61.2586	-1.0287	62.5855
BANFF, Norm, NC Oth	0.0566483	57.55602	-1.77735	61.1283	-0.75441	62.4624
BANFF, Ma RES	0.0452921	60.8824	-7.01936	60.4125	-2.3956	63.3914
BANFF, Fermi Momentum	0.0716681	61.3847	-1.73071	61.5157	-0.61317	62.2944
BANFF, Shape, CC Oth	0.18663	61.5816	-0.824911	62.1854	-0.46883	61.0781
BANFF, Shape, CC Coh	0.0274896	61.6883	-0.506818	61.7907	-0.16894	61.9398
BANFF, Shape, CC Coh	0.0558267	58.3023	-0.342957	61.8245	-0.11432	62.1075
BANFF, Norm, NC Coh	0.117434	58.4846	-0.0314137	61.8946	-0.0010471	61.8959
BANFF, Norm, NC Oth	0.3	61.4044	-0.792965	61.7316	-0.26432	62.0589
BANFF, Norm, ν_e To $\bar{\nu}_e$	0.0282843	61.895	-0.00474143	61.8952	-0.00015805	61.8953
BANFF, Norm, $\bar{\nu}_e$ To ν_e	0.0282843	61.895	-0.00475571	61.8952	-0.0004883	61.8953
BANFF, Norm, 2p2hBar	0.201069	60.6651	-1.98746	61.4473	-0.72367	62.0483
BANFF, Norm, 2p2hBar	0.00851249	61.7509	-0.80184	60.6979	-1.985	61.9932
BANFF, BeRPA A	0.117434	58.15329	-4.92225	60.8797	-1.6407	62.1016
BANFF, BeRPA B	0.127806	58.4384	-5.59162	60.7416	-1.8639	63.0489
BANFF, BeRPA D	0.354515	61.7148	-0.291494	61.8205	-0.1208	61.9711
BANFF, BeRPA E	0.338124	61.957	0.09916883	61.9261	0.049839	62.0044
BANFF, Norm, 2p2h C to O	0.161427	56.1121	-1.5042	60.962	-1.5042	62.8263
SKDdet + FS1/SU(0; E_{Reco} (0.00 - 0.40) GeV; $\nu_\mu/\bar{\nu}_\mu$ CCQE (IR_μ); RHC)	0.00851249	61.7509	-0.233153	61.8471	-0.077718	61.9434
SKDdet + FS1/SU(1; E_{Reco} (0.40 - 1.00) GeV; $\nu_\mu/\bar{\nu}_\mu$ CCQE (IR_μ); RHC)	0.00705099	61.5329	-4.92225	61.7745	0.19515	62.1016
SKDdet + FS1/SU(2; E_{Reco} (1.10 - 3.00) GeV; $\nu_\mu/\bar{\nu}_\mu$ CCQE (IR_μ); RHC)	0.006754	61.3387	-0.89918	61.7097	-0.29973	62.0808
SKDdet + FS1/SU(3; E_{Reco} (0.00 - 30.00) GeV; $\nu_\mu/\bar{\nu}_\mu$ CCQE (IR_μ); RHC)	0.129646	57.9032	-6.44968	60.5646	-2.1499	63.2259
SKDdet + FS1/SU(4; E_{Reco} (0.00 - 30.00) GeV; $\nu_e/\bar{\nu}_e$ sige CC (IR_μ); RHC)	1.00454	61.8744	-0.0337299	61.8883	-0.011243	61.9022
SKDdet + FS1/SU(5; E_{Reco} (0.00 - 30.00) GeV; all NC (IR_μ); RHC)	0.637251	58.9447	-4.76696	60.9117	-1.589	62.8788
SK energy scale	0.024	61.8952	1.14798 $\times 10^{-14}$	61.8952	-5.739 $\times 10^{-14}$	61.8952
SK energy scale					0	0

Table 35: $\pm 1\sigma$ and $\pm 3\sigma$ effect of the systematic parameters on the total number of μ -like Super-K events with Run 1-8 POT for antineutrino mode post-BANFF Asimov data set A. Only the systematic parameters which affect this sample are shown.

Parameter	1 σ value	BANFF tuned -3 σ	BANFF tuned +3 σ	BANFF tuned -1 σ	BANFF tuned +1 σ	BANFF tuned +3 σ
All syst	24.922	-65.9618(%)	51.4515	-29.728 (%)	102.19	39.569(%)
BANFF 0, SK numm flux, 0.0 - 0.4 GeV	0.0574967	-0.403375	73.1192	-0.13446	73.3466	0.403375
BANFF 1, SK numm flux, 0.4 - 0.5 GeV	0.0513633	72.1503	-1.45778	72.8619	-0.48593	74.285
BANFF 2, SK numm flux, 0.5 - 0.6 GeV	0.0445682	71.1561	-2.81569	72.5305	-0.93856	2.81569
BANFF 3, SK numm flux, 0.6 - 0.7 GeV	0.0418861	70.9918	-3.04009	72.4757	-1.0134	3.04009
BANFF 4, SK numm flux, 0.7 - 1.0 GeV	0.05416	70.287	-4.00265	72.2408	-1.3342	4.00265
BANFF 5, SK numm flux, 1.0 - 1.5 GeV	0.0490261	72.8314	-0.527495	73.0889	-0.17583	73.6039
BANFF 6, SK numm flux, 1.5 - 2.5 GeV	0.0417789	73.1531	-0.0881396	73.1962	-0.02938	73.2822
BANFF 7, SK numm flux, 2.5 - 3.5 GeV	0.0436069	73.1782	-0.0358422	73.2045	-0.017947	73.2571
BANFF 8, SK numm flux, 3.5 - 5.0 GeV	0.040772	73.1759	-0.0569879	73.2038	-0.018986	73.2594
BANFF 9, SK numm flux, 5.0 - 7.0 GeV	0.0400958	73.2002	-0.0238941	73.2118	-0.0079047	73.2235
BANFF 10, SK numm flux, 7.0 - 30.0 GeV	0.048214	73.2008	-0.0177924	73.2144	-0.0044192	73.2294
BANFF 11, SK numm flux, 0.0 - 0.7 GeV	0.073717	73.1847	-0.0449832	73.2067	-0.014994	73.2286
BANFF 12, SK numm flux, 0.7 - 1.0 GeV	0.0477	73.1928	-0.0338926	73.2094	-0.011298	73.2259
BANFF 13, SK numm flux, 1.0 - 1.5 GeV	0.0574721	73.1952	-0.0366208	73.2102	-0.010207	73.2251
BANFF 14, SK numm flux, 1.5 - 2.5 GeV	0.0618907	73.2042	-0.0184181	73.2132	-0.0061394	73.2222
BANFF 15, SK numm flux, 2.5 - 30.0 GeV	0.0646763	73.2046	-0.0177924	73.2133	-0.0059308	73.222
BANFF 16, SK me flux, 0.0 - 0.5 GeV	0.0464719	72.9814	-0.322666	73.1389	-0.10756	73.2209
BANFF 17, SK me flux, 0.5 - 0.7 GeV	0.0424043	72.9412	-0.0424043	73.1255	-0.12587	73.2286
BANFF 18, SK me flux, 0.7 - 0.8 GeV	0.0411755	73.0844	-0.182013	73.1732	-0.060671	73.2251
BANFF 19, SK me flux, 0.8 - 1.5 GeV	0.0390566	72.8167	-0.54763	73.084	-0.18254	73.2151
BANFF 20, SK me flux, 1.5 - 2.5 GeV	0.0400552	73.1876	-0.0410833	73.2076	-0.013694	73.2222
BANFF 21, SK me flux, 2.5 - 40 GeV	0.0414685	73.2139	-0.00512328	73.2164	-0.0017078	73.222
BANFF 22, SK me flux, 4.0 - 30.0 GeV	0.0586881	73.216	-0.00231432	73.2171	-0.00077144	73.2194
BANFF 23, SK mebar flux, 0.0 - 2.5 GeV	0.0538293	73.1626	-0.0538293	73.1993	-0.025089	73.2182
BANFF 24, SK mebar flux, 2.5 - 30.0 GeV	0.114234	73.2155	-0.00300859	73.2169	-0.001029	73.2199
BANFF; Norm; 2p2h	0.182443	69.50056	-0.507671	71.9786	-1.6922	74.4567
BANFF; CA5 RES	0.0594704	71.8118	-1.92013	72.7247	-0.67329	73.735
BANFF; Norm; BgRES Isospin 1/2	0.18977	72.627	-0.806784	72.9869	-0.34244	73.5222
BANFF; Na OFe	0.0566483	64.696	-11.6388	70.5376	-3.6604	75.731
BANFF; Ma RRS	0.0452921	72.1583	-1.4469	72.8705	-0.47412	73.5578
BANFF; Fermi Momentum	0.0716681	72.6124	-0.826631	73.5743	-0.45705	73.1632
BANFF; Shape: CC Oth	0.18663	73.137	-0.110225	73.1908	-0.036741	73.2446
BANFF; Norm; CC Coh	0.274896	73.1696	-0.065688	73.2016	-0.021896	73.2337
BANFF; Norm; NC Coh	0.297426	72.6524	-0.772032	73.0292	-0.25734	73.4061
BANFF; Norm; NC Oth	0.3	72.8927	-0.443771	73.1094	-0.14792	73.326
BANFF; Norm; ν_e To ν_μ	0.0282843	67.5071	-7.79941	71.3141	-2.5998	75.1212
BANFF; Norm; NC 1/2	1	71.1672	-2.80047	71.1672	-2.8005	75.2681
BANFF; Norm; ν_e To $\bar{\nu}_\mu$	0.0282843	73.1582	-0.0811966	73.1978	-0.027066	73.2046
BANFF; Norm; 2p2hBar	0.201069	73.1818	-0.0498964	73.2046	-0.01784	73.2307
BANFF; BarPA A	0.0558267	68.1306	-6.9479	71.522	-2.316	74.9134
BANFF; BarPA B	0.117434	67.4635	-6.7898	71.2996	-2.6197	75.1357
BANFF; BarPA D	0.127806	67.8054	-7.39204	71.4136	-2.464	75.0218
BANFF; BarPA E	0.354515	72.8409	-0.514573	73.0684	-0.20988	73.3713
BANFF; Shape: 2p2h	0.338124	72.6822	-0.731326	72.9499	-0.36566	73.9761
BANFF; Norm; 2p2h C to O	0.161427	68.2076	-6.84265	71.5477	-2.2809	74.8877
SKD δ t + FSU/SI 6; E_{reco} (0.00 - 0.35 GeV); Osc. ν_e CC (1 R_e)	0.181271	68.74793	-6.1029	71.7282	-2.0343	73.2086
SKD δ t + FSU/SI 7; E_{reco} (0.35 - 0.80 GeV); Osc. ν_e CC (1 R_e)	0.036083	68.6468	-6.23286	71.694	-2.081	74.7413
SKD δ t + FSU/SI 8; E_{reco} (0.80 - 1.25 GeV); Osc. ν_e CC (1 R_e)	0.0416633	72.1642	-1.43886	72.8865	-0.47962	73.5688
SKD δ t + FSU/SI 9; E_{reco} (0.00 - 0.35 GeV); $\nu_\mu/\bar{\nu}_\mu$ CC (1 R_e)	0.300431	73.1543	-0.0865317	73.2086	-0.028844	73.3388
SKD δ t + FSU/SI 10; E_{reco} (0.35 - 0.80 GeV); $\nu_\mu/\bar{\nu}_\mu$ CC (1 R_e)	0.321346	73.0587	-0.217089	73.1647	-0.072363	73.2706
SKD δ t + FSU/SI 11; E_{reco} (0.80 - 1.25 GeV); $\nu_\mu/\bar{\nu}_\mu$ CC (1 R_e)	0.392969	73.1904	-0.0372322	73.2086	-0.012411	73.2967
SKD δ t + FSU/SI 12; E_{reco} (0.90 - 0.35 GeV); $\nu_e/\bar{\nu}_e$ CC (1 R_e)	0.135399	72.7003	-0.706539	73.0452	-0.23553	73.3901
SKD δ t + FSU/SI 13; E_{reco} (0.35 - 0.80 GeV); $\nu_e/\bar{\nu}_e$ CC (1 R_e)	0.0698928	72.1921	-1.40077	72.8758	-0.46692	73.5505
SKD δ t + FSU/SI 14; E_{reco} (0.80 - 1.25 GeV); $\nu_e/\bar{\nu}_e$ CC (1 R_e)	0.0771361	72.5317	-0.936824	72.989	-0.31227	73.4463
SKD δ t + FSU/SI 15; E_{reco} (0.00 - 0.35 GeV); all NC (1 R_e)	0.194453	72.0874	-1.54371	72.8409	-0.51457	73.5944
SKD δ t + FSU/SI 16; E_{reco} (0.35 - 0.80 GeV); all NC (1 R_e)	0.181015	71.849	-1.86926	72.7615	-0.62309	73.6739
SKD δ t + FSU/SI 17; E_{reco} (0.80 - 1.25 GeV); all NC (1 R_e)	0.472078	72.5075	-0.969968	72.9809	-0.32332	73.4544
SK energy scale	0.024	73.2177	$1.940 \cdot 91 \times 10^{-14}$	73.2177	1.9409×10^{-14}	73.2177
						0

Table 36: $\pm 1\sigma$ and $\pm 3\sigma$ effect of the systematic parameters on the total number of e -like Super-K events with Run 1-8 POT for neutrino mode post-BANFF Asimov data set A. Only the systematic parameters which affect this sample are shown.

Parameter	BANFF tuned -3 σ		BANFF tuned -1 σ		BANFF tuned +1 σ		BANFF tuned +3 σ	
	1 σ value	BANFF tuned	5.46214	-30.475 (%)	11.115	41.472(%)	21.274	170.785(%)
All systematics								
BANFF 0, SK muon flux, 0.0 - 0.7 GeV; RHC	0.0656432	7.72362	-1.69035	7.81216	-0.563482	7.90069	0.56345	7.98922
BANFF 1, SK muon flux, 0.7 - 1.0 GeV; RHC	0.0486119	7.77633	-1.01945	7.82973	-0.339482	7.88312	0.33982	7.93652
BANFF 2, SK muon flux, 1.0 - 1.5 GeV; RHC	0.0454048	7.81229	-0.561803	7.84171	-0.18727	7.87114	0.18727	7.90056
BANFF 3, SK muon flux, 1.5 - 2.5 GeV; RHC	0.0489206	7.83735	-0.242765	7.85007	-0.049022	7.86246	0.049022	7.87755
BANFF 4, SK muon flux, 2.5 - 30.0 GeV; RHC	0.0436272	7.83832	-0.230369	7.85039	-0.076759	7.86246	0.076759	7.87452
BANFF 5, SK muon flux, 0.0 - 0.4 GeV; RHC	0.0647793	7.84	-0.209058	7.85095	-0.069686	7.86119	0.069686	7.87285
BANFF 6, SK muon flux, 0.4 - 0.5 GeV; RHC	0.0521864	7.80795	-0.616928	7.816927	-0.20564	7.82758	0.20564	7.90489
BANFF 7, SK muon flux, 0.5 - 0.6 GeV; RHC	0.0442828	7.74607	-1.404526	7.81964	-0.46819	7.89321	0.46819	7.96677
BANFF 8, SK muon flux, 0.6 - 0.7 GeV; RHC	0.04040543	7.72003	-1.73607	7.81096	-0.57869	7.90189	0.57869	7.99282
BANFF 9, SK muon flux, 0.7 - 1.0 GeV; RHC	0.0521651	7.64076	-2.745	7.78454	0.915	7.92831	0.915	2.745
BANFF 10, SK muon flux, 1.0 - 1.5 GeV; RHC	0.0473232	7.81642	-0.509156	7.84309	-0.16972	7.86976	0.16972	7.89642
BANFF 11, SK muon flux, 1.5 - 2.5 GeV; RHC	0.0424043	7.84495	-0.146092	7.85206	-0.048697	7.86025	0.048697	7.86779
BANFF 12, SK muon flux, 2.5 - 3.5 GeV; RHC	0.0462426	7.85033	-0.076759	7.85439	-0.02586	7.86254	0.02586	7.86254
BANFF 13, SK muon flux, 3.5 - 5.0 GeV; RHC	0.0622890	7.84905	-0.093860	7.85396	-0.031287	7.85888	0.031287	7.86338
BANFF 14, SK muon flux, 5.0 - 7.0 GeV; RHC	0.0555197	7.85431	-0.0269095	7.85572	-0.0089698	7.85713	0.0089698	0.0269095
BANFF 15, SK muon flux, 7.0 - 30.0 GeV; RHC	0.04996475	7.81547	-0.0281857	7.85385	-0.027986	7.85814	0.027986	0.0218857
BANFF 16, SK muon flux, 0.0 - 2.5 GeV; RHC	0.0461452	7.75435	-1.29928	7.8224	-0.43309	7.89045	0.43309	7.9385
BANFF 17, SK muon flux, 2.5 - 30.0 GeV; RHC	0.0644339	7.85484	-0.201328	7.85539	-0.0067109	7.85695	0.0067109	7.86779
BANFF 18, SK nuclear flux, 0.0 - 0.5 GeV; RHC	0.0513755	7.82484	-0.401976	7.84539	-0.13399	7.86955	0.13399	7.88834
BANFF 19, SK nuclear flux, 0.5 - 0.7 GeV; RHC	0.043268	7.8255	-0.393588	7.84612	-0.1312	7.86773	0.1312	0.393588
BANFF 20, SK nuclear flux, 0.7 - 0.8 GeV; RHC	0.0433635	7.83941	-0.216534	7.85075	-0.072178	7.86209	0.072178	7.87343
BANFF 21, SK nuclear flux, 0.8 - 1.5 GeV; RHC	0.0439880	7.80253	-0.685932	7.83846	-0.22864	7.87439	0.22864	7.91031
BANFF 22, SK nuclear flux, 1.5 - 2.5 GeV; RHC	0.0514445	7.85238	-0.0514339	7.85508	-0.01745	7.87777	0.01745	7.86846
BANFF 23, SK nuclear flux, 2.5 - 30.0 GeV; RHC	0.0644807	7.85554	-0.0112521	7.85613	-0.0037507	7.85672	0.0037507	7.86731
BANFF 24, SK nuclear flux, 4.0 - 30.0 GeV; RHC	0.132062	7.85562	-0.0101603	7.85616	-0.0038686	7.85669	0.0038686	7.85722
BANFF, Norm: 2p2h	0.18243	7.72015	-1.7346	7.811	-0.5782	7.90185	0.5782	7.90227
BANFF, Norm: CA5 RES	0.0594704	7.63337	-2.8391	7.77072	-1.0909	7.95348	1.2354	1.7346
BANFF, Norm: BgRHS Isospin 1/2	0.18977	7.74077	-1.74077	7.80718	-0.60007	7.91624	0.76132	0.13976
BANFF, MaQE 55	0.0569483	7.38072	-6.05495	7.69353	-0.20734	8.01955	0.20764	8.33805
BANFF, MaRES	0.0452921	7.74805	-1.37941	7.8167	-0.50559	7.85955	0.504313	7.90145
BANFF, Fermi Momentum	0.0716681	7.78577	-0.900157	7.80937	-0.50753	7.74312	0.50753	7.750625
BANFF, Shape: CC Oth	0.18663	7.83938	-0.216893	7.85074	-0.07298	7.8621	0.07298	7.87346
BANFF, Norm: CC Coh	0.2741869	7.81383	-0.542185	7.84222	-0.18073	7.87062	0.18073	7.89092
BANFF, Norm: NC Coh	0.2972426	7.61022	-1.31035	7.74735	-1.0447	7.9385	1.0447	1.31035
BANFF, Norm: NC Oth	0.3	7.77788	-0.999766	7.83024	-0.33226	7.88226	0.33226	7.934497
BANFF, Norm: ν_e To ν_μ	7.67748	7.74805	-2.31178	7.79588	-0.77059	7.91696	0.77059	8.03805
BANFF, Norm: NC 1/2	1	7.32503	-6.76374	7.73253	-6.76377	7.74312	-6.76377	7.94959
BANFF, Norm: ν_e To $\bar{\nu}_\mu$	7.48199	7.48199	-4.765917	7.73161	-1.5887	7.98124	1.5887	8.23086
BANFF, Norm: 2p2hBar	0.201069	7.66282	-2.46432	7.78593	-0.8973	7.92692	0.8973	2.6919
BANFF, BelPA A	0.0578267	7.37628	-6.11145	7.69638	-2.0371	8.01765	2.0371	8.33656
BANFF, BelPA B	0.1171334	7.47156	-4.89873	7.72813	-1.6329	7.98471	1.6329	8.24129
BANFF, BelPA D	0.127806	7.58443	-3.46199	7.76576	-1.154	7.94709	1.154	8.12841
BANFF, BelPA E	0.354515	7.83736	-2.42258	7.84865	-0.998949	7.8642	0.998949	7.87975
BANFF, Shape: 2p2h	0.338124	7.81059	-0.583371	7.83352	-0.29169	7.91607	0.29169	8.04675
BANFF, Norm: 2p2h C to O	0.1611227	7.57364	-3.59942	7.76216	-1.1998	7.95068	1.1998	8.13921
BKDet + FSU/SU(6; E_{reco}) (0.00 - 0.35) GeV; Osc. ν_e CC (1 R_e); RHC	0.108165	7.71943	-1.74375	7.81076	-0.58126	7.89357	0.58126	7.93842
BKDet + FSU/SU(12; E_{reco}) (0.00 - 0.35) GeV; Osc. ν_e CC (1 R_e); RHC	0.0363039	7.49443	-4.60764	7.73576	-1.5359	7.97909	1.5359	8.21842
BKDet + FSU/SU(8; E_{reco}) (0.80 - 1.25) GeV; Osc. ν_e CC (1 R_e); RHC	0.0567315	7.68741	-2.15125	7.80009	-0.71708	7.91276	0.71708	8.02513
BKDet + FSU/SU(9; E_{reco}) (0.00 - 0.35) GeV; Osc. ν_e CC (1 R_e); RHC	0.0348644	7.8459	-1.033966	7.85291	-0.044655	7.869393	0.044655	7.86635
BKDet + FSU/SU(10; E_{reco}) (0.35 - 0.80) GeV; ν_μ CC (1 R_e); RHC	0.341647	7.81676	-0.494211	7.84348	-0.16174	7.86937	0.16174	8.04624
BKDet + FSU/SU(11; E_{reco}) (0.80 - 1.25) GeV; ν_μ CC (1 R_e); RHC	0.417164	7.84041	-0.203851	7.85108	-0.06795	7.86176	0.06795	7.87244
BKDet + FSU/SU(12; E_{reco}) (0.00 - 0.35) GeV; ν_e CC (1 R_e); RHC	0.0845563	7.80585	-0.643709	7.83957	-0.21457	7.87328	0.21457	7.907
BKDet + FSU/SU(13; E_{reco}) (0.35 - 0.80) GeV; ν_e CC (1 R_e); RHC	0.0560697	7.70477	-1.93028	7.80587	-0.64343	7.90697	0.64343	8.00807
BKDet + FSU/SU(14; E_{reco}) (0.80 - 1.25) GeV; ν_e CC (1 R_e); RHC	0.0782411	7.68946	-2.12519	7.80077	-0.7084	7.91208	0.7084	8.02339
BKDet + FSU/SU(15; E_{reco}) (0.00 - 0.35) GeV; all NC (1 R_e); RHC	0.214066	7.57167	-3.63077	7.76134	-1.2103	7.95151	1.2103	8.14167
BKDet + FSU/SU(16; E_{reco}) (0.35 - 0.80) GeV; all NC (1 R_e); RHC	0.190575	7.48766	-4.63875	7.73535	-1.56436	7.97934	1.56436	8.22518
BKDet + FSU/SU(17; E_{reco}) (0.80 - 1.25) GeV; all NC (1 R_e); RHC	0.46436	7.64265	-2.721	7.78517	-0.907	7.92768	0.907	8.0702
SK energy scale	0.024	7.85642	2.26102 $\times 10^{-14}$	7.85642	2.261 $\times 10^{-14}$	7.85642	3.395 $\times 10^{-14}$	7.85642

Table 37: $\pm 1\sigma$ and $\pm 3\sigma$ effect of the systematic parameters on the total number of e-like Super-K events with Run 1-8 POT for antineutrino mode post-BANFF Asimov data set A. Only the systematic parameters which affect this sample are shown.

Parameter	1 σ value	BANFF tuned -3 σ	BANFF tuned +3 σ	BANFF tuned -1 σ	BANFF tuned +1 σ	BANFF tuned +3 σ
All syst		0.804711	-88.4314(%)	4.00833	-12.376 (%)	25.0389
BANFF 0, SK numm flux, 0.0 - 0.4 GeV	0.0574967	6.95424	-0.0252963	6.95544	-0.0084021	6.95775
BANFF 1, SK numm flux, 0.4 - 0.5 GeV	0.0513933	6.91004	-0.000601	6.94068	0.020922	7.00135
BANFF 2, SK numm flux, 0.5 - 0.6 GeV	0.0443682	6.70899	-2.25711	6.90566	0.75237	7.113
BANFF 3, SK numm flux, 0.6 - 0.7 GeV	0.0418861	6.72793	-3.27866	6.87979	-1.02929	7.03201
BANFF 4, SK numm flux, 0.7 - 1.0 GeV	0.040516	6.61026	-4.97027	6.84075	-1.63688	7.30173
BANFF 5, SK numm flux, 1.0 - 1.5 GeV	0.0409261	6.90632	-0.009124	6.93944	-0.28304	7.00567
BANFF 6, SK numm flux, 1.5 - 2.5 GeV	0.0417789	6.9436	-0.178111	6.95186	-0.05937	7.014124
BANFF 7, SK numm flux, 2.5 - 3.5 GeV	0.048664	6.94479	-0.105658	6.95254	-0.035219	7.018111
BANFF 8, SK numm flux, 3.5 - 5.0 GeV	0.040772	6.95121	-0.16107	6.95296	-0.008563	6.96334
BANFF 9, SK numm flux, 5.0 - 7.0 GeV	0.0409058	6.94824	-0.0687454	6.9544	-0.022915	6.9672
BANFF 10, SK numm flux, 7.0 - 30.0 GeV	0.048654	6.95531	-0.0085426	6.9558	-0.0028468	6.96078
BANFF 11, SK numm flux, 0.0 - 0.7 GeV	0.073717	6.95531	-0.00981525	6.95577	-0.0032718	6.95659
BANFF 12, SK numm flux, 0.7 - 1.0 GeV	0.0477	6.95539	-0.0087339	6.95579	-0.0029144	6.95666
BANFF 13, SK numm flux, 1.0 - 1.5 GeV	0.0547721	6.95497	-0.0146837	6.95655	-0.0045916	6.95792
BANFF 14, SK numm flux, 1.5 - 2.5 GeV	0.0618907	6.95456	-0.0206588	6.95551	-0.0068863	6.95743
BANFF 15, SK numm flux, 2.5 - 30.0 GeV	0.0646763	6.9542	-0.0257846	6.9554	-0.0085949	6.95779
BANFF 16, SK numm flux, 0.0 - 0.5 GeV	0.0464719	6.95048	-0.0792773	6.95116	-0.026426	6.95783
BANFF 17, SK numm flux, 0.5 - 0.7 GeV	0.0424703	6.93168	-0.349548	6.94789	-0.116152	6.9641
BANFF 18, SK numm flux, 0.7 - 0.8 GeV	0.0411175	6.93998	-0.203278	6.95065	-0.0506759	6.9641
BANFF 19, SK numm flux, 0.8 - 1.5 GeV	0.0395666	6.93641	-0.856582	6.93813	-0.28553	6.97586
BANFF 20, SK numm flux, 1.5 - 2.5 GeV	0.049968	6.95529	-0.0907415	6.95589	-0.030247	6.96231
BANFF 21, SK numm flux, 2.5 - 4.0 GeV	0.0414685	6.95529	-0.0101187	6.95576	-0.0033729	6.9567
BANFF 22, SK numm flux, 4.0 - 30.0 GeV	0.0588054	6.95563	-0.00530211	6.95587	-0.0017674	6.95612
BANFF 23, SK numm flux, 0.0 - 2.5 GeV	0.0545623	6.95456	-0.0206601	6.9551	-0.0068867	6.95647
BANFF 24, SK numm flux, 2.5 - 30.0 GeV	0.1114234	6.95564	-0.00504217	6.95588	-0.0016807	6.95611
BANFF, Norm: 2p2h		0.88667	-0.906676	6.93288	-0.33223	6.9791
BANFF, C4S RES		3.89754	-15.2164	6.8587	-5.2994	6.971343
BANFF, Norm: BerPA Isospin 1/2	0.18977	6.57078	-5.53726	6.77937	-2.3503	7.15458
BANFF, Ma QE		6.9079	-0.691353	6.94074	-0.21933	6.97039
BANFF, Ma RES		0.0452921	6.20812	-10.7516	-3.4339	6.71713
BANFF, Fermi Momentum		0.0716681	6.95402	-0.0284045	6.95754	0.020253
BANFF, Shape: CC Orth		0.18663	6.85023	-1.52053	6.92074	-0.50684
BANFF, Norm: CC Coh		0.274896	6.83207	-1.78154	6.91949	-0.59385
BANFF, Norm: NC Orth	0.3	6.7186	-2.9815	6.88686	-0.98383	7.02512
BANFF, Norm: ν_e To ν_μ		6.41277	-7.80949	6.77192	-2.6032	7.49922
BANFF, Norm: NC 1 γ	1.0	0.89695	-0.848755	6.89695	-0.84876	7.10153
BANFF, Shape: 2p2h		0.0282843	6.954642	-0.0157217	6.95554	-0.0065739
BANFF, Norm: ν_e To $\bar{\nu}_e$		0.201069	6.95491	-0.015515	6.9556	-0.0066492
BANFF, Norm: 2p2hBar		0.0552967	6.93541	-0.29595	6.94013	-0.09865
BANFF, BerPA A		0.0282843	6.92323	-0.44374	6.9456	-0.14946
BANFF, BerPA B		0.127806	-0.47098	6.94507	-0.16699	6.96691
BANFF, BerPA D		0.354515	6.95369	-0.033736	6.95056	-0.013489
BANFF, BarPA E		0.3383124	6.90988	-0.662967	6.93294	-0.33147
BANFF, Norm: 2p2h		0.161427	6.862234	-1.34641	6.92978	-0.4488
BANFF, Norm: 2p2hBar		0.248051	4.116161	-40.8193	6.00953	-13.606
BANFF, Norm: NC		5.8806	-15.46	6.59753	-5.153	6.90246
BANFF, Norm: CC		6.117334	-6.9248	6.43874	-2.38812	6.90662
BANFF, Norm: MultiRing		0.41277	-0.47098	6.94507	-0.16699	6.96691
BANFF, Norm: MultiRing		0.354515	6.95369	-0.033736	6.95056	-0.013489
BANFF, Norm: MultiRing		0.244289	6.6652	-4.18041	6.85006	-1.3935
BANFF, Norm: MultiRing		0.234289	6.5674	-5.58639	6.8261	-1.8621
BANFF, Norm: MultiRing		0.16529	6.16529	-11.3673	6.69242	-3.7891
BANFF, Norm: MultiRing		0.523609	6.78329	-2.48274	6.89843	-0.82758
BANFF, Norm: MultiRing		0.024	6.95599	-1.27685 $\times 10^{-14}$	6.95599	0
SK energy scale						1.27685 $\times 10^{-14}$
						6.35599
						0
						1.27685 $\times 10^{-14}$
						6.35599
						0

Table 38: $\pm 1\sigma$ and $\pm 3\sigma$ effect of the systematic parameters on the total number of e-like Super-K events with one decay electron with Run 1-8 POT for neutrino mode post-BANFF Asimov data set A. Only the systematic parameters which affect this sample are shown.

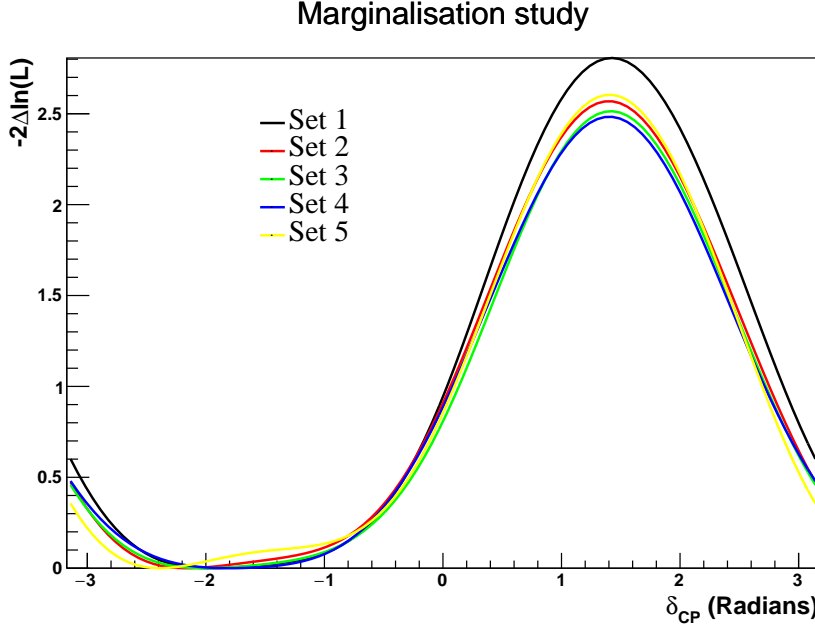


Figure 43: Asimov A δ_{CP} normal hierarchy contours without reactor constraint for independent sets of 10K marginalisation toys

D. Marginalisation studies

The increase in sensitivity to δ_{CP} provided by a doubling of FHC statistics in Run 1-8 relative to Run 1-7c has made sampling of the tails of oscillation parameters (particularly $\sin^2 \theta_{13}$) more significant for 1D fits. In previous analyses all fits were performed with 10K marginalisation toys, but in the present analysis this is no longer sufficient to ensure that fits return consistent results for independent sets of marginalisation toys. One can see the nature of the problem in fig. 43, in which five independent sets of 10K marginalisation toys were fitted under the Asimov A oscillation parameter hypothesis without the reactor constraint; a large spread in $\Delta\chi^2$ contours is evident.

To determine a sufficient number of marginalisation toys to use checks of fit stability were carried out for different numbers of marginalisation toys. Figures 44 to 45 show the $\Delta\chi^2$ contours for the case of 40K and 80K marginalisation toys respectively. These studies indicate that good agreement among fits is achieved for 80K marginalisation toys (40k toys was found to be sufficient in the with reactor case due to the smaller marginalisation range for $\sin^2 \theta_{13}$).

Further to the Asimov-based marginalisation studies, the stronger constraint seen in the data fits prompted a check of the data fit stability. Figures 46 to 46 show the result of fitting δ_{CP} with the reactor constraint for both normal and inverted hierarchy. Variations of $\Delta\chi^2 \sim 1$ are evident around the maximum in the region of $\delta_{CP} \sim \pi/2$, but that good stability is maintained in the preferred region and at the values of $\delta_{CP} = 0$ and π .

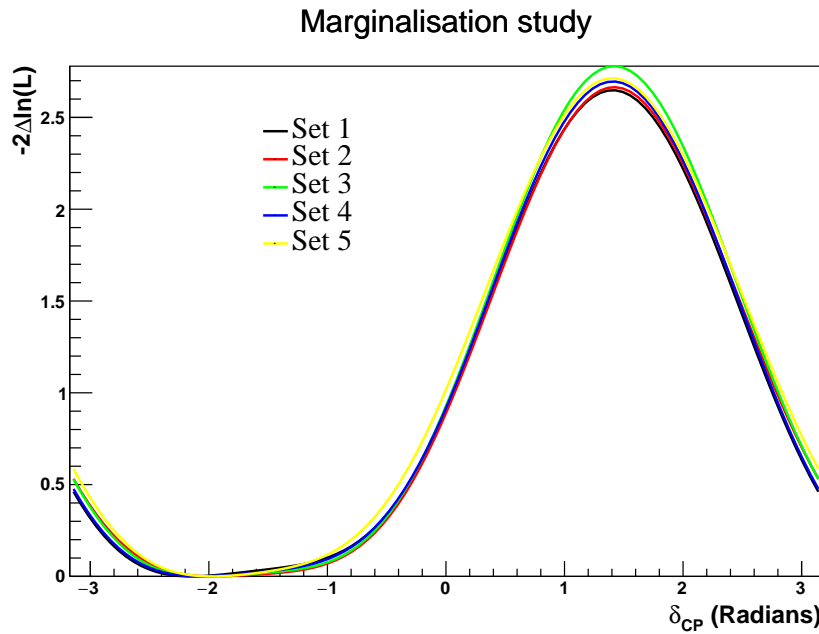


Figure 44: Asimov A δ_{CP} normal hierarchy contours without reactor constraint for independent sets of 40K marginalisation toys

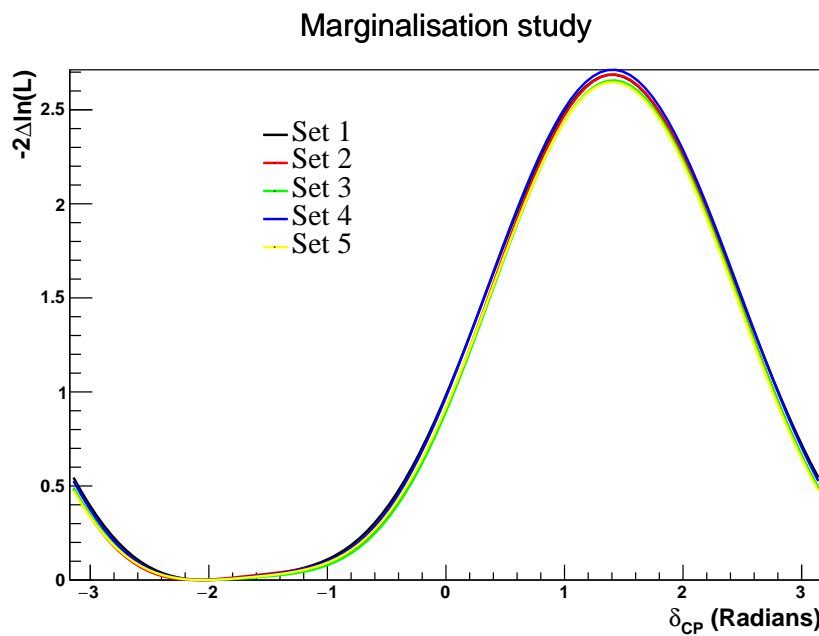


Figure 45: Asimov A δ_{CP} normal hierarchy contours without reactor constraint for independent sets of 80K marginalisation toys

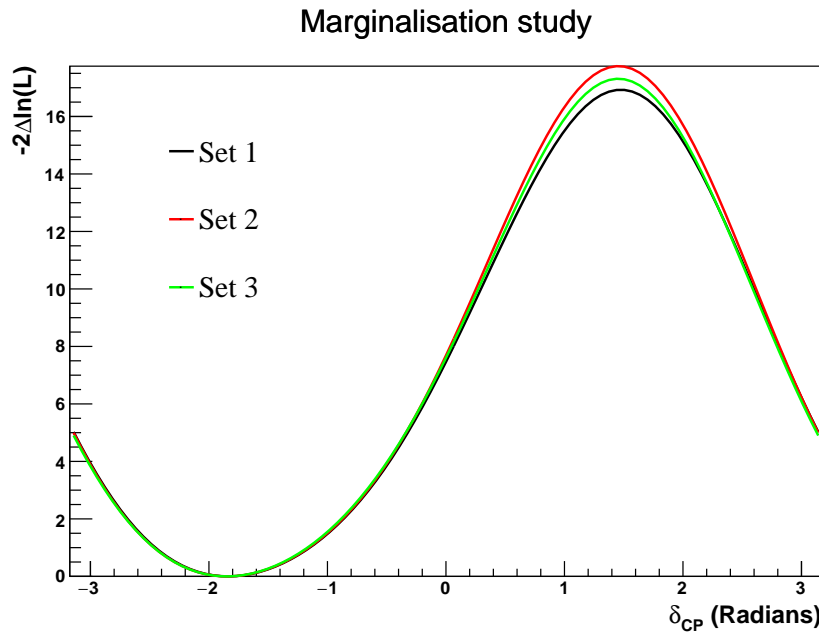


Figure 46: Data fit of δ_{CP} normal hierarchy contours with reactor constraint for independent sets of 40K marginalisation toys

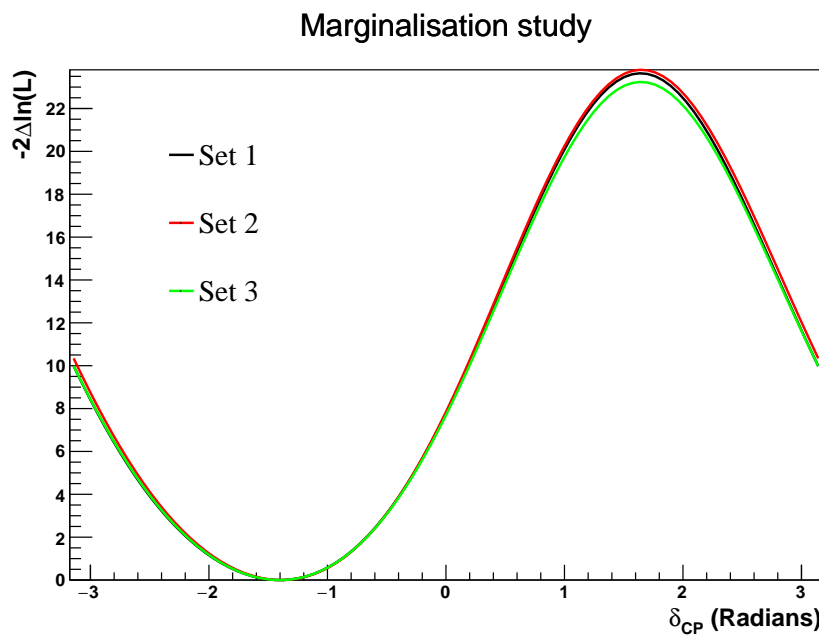


Figure 47: Data fit of δ_{CP} inverted hierarchy contours with reactor constraint for independent sets of 40K marginalisation toys

914 E. Effect of systematic errors on Super-K predictions

Group	Pre-BANFF			Post-BANFF		
	Mean	1σ	%	Mean	1σ	%
SK Detector	-	-	-	269.11	5.01	1.86
SK FSI+SI+PN	-	-	-	268.38	5.91	2.20
Flux+Xsec constrained	250.34	35.35	14.12	266.68	8.60	3.22
$\sigma(\nu_e)/\sigma(\bar{\nu}_e)$	-	-	-	268.42	0.00	0.00
NC1 γ	-	-	-	268.42	0.00	0.00
NC Other	-	-	-	268.42	0.67	0.25
Osc	-	-	-	268.42	0.09	0.04
All	250.95	35.71	14.23	267.78	11.79	4.40
All with osc	250.95	35.71	14.23	267.78	11.79	4.40

Table 39: Average event rate and RMS error broken down by systematic parameter group for μ -like Super-K events with Run 1-8 POT for neutrino mode.

Group	Pre-BANFF			Post-BANFF		
	Mean	1σ	%	Mean	1σ	%
SK Detector	-	-	-	64.41	0.97	1.51
SK FSI+SI+PN	-	-	-	64.27	1.27	1.98
Flux+Xsec constrained	62.09	7.18	11.56	63.97	1.74	2.72
$\sigma(\nu_e)/\sigma(\bar{\nu}_e)$	-	-	-	64.28	0.00	0.00
NC1 γ	-	-	-	64.28	0.00	0.00
NC Other	-	-	-	64.28	0.16	0.25
Osc	-	-	-	64.28	0.02	0.03
All	62.18	7.31	11.76	64.17	2.41	3.76
All with osc	62.18	7.31	11.76	64.17	2.41	3.76

Table 40: Average event rate and RMS error broken down by systematic parameter group for μ -like Super-K events with Run 1-8 POT for antineutrino mode.

Group	Pre-BANFF			Post-BANFF		
	Mean	1σ	%	Mean	1σ	%
SK Detector	-	-	-	73.64	2.23	3.03
SK FSI+SI+PN	-	-	-	73.46	2.21	3.01
Flux+Xsec constrained	65.47	9.80	14.97	72.57	2.34	3.22
$\sigma(\nu_e)/\sigma(\bar{\nu}_e)$	-	-	-	73.46	1.93	2.63
NC1 γ	-	-	-	73.76	0.80	1.08
NC Other	-	-	-	73.48	0.11	0.14
Osc	-	-	-	73.49	2.84	3.86
All	65.91	10.26	15.56	73.12	4.46	6.10
All with osc	65.92	10.57	16.03	73.14	5.32	7.27

Table 41: Average event rate and RMS error broken down by systematic parameter group for e -like Super-K events with Run 1-8 POT for neutrino mode.

Group	Pre-BANFF			Post-BANFF		
	Mean	1σ	%	Mean	1σ	%
SK Detector	-	-	-	7.94	0.33	4.22
SK FSI+SI+PN	-	-	-	7.91	0.18	2.31
Flux+Xsec constrained	7.63	0.91	11.94	7.84	0.23	2.88
$\sigma(\nu_e)/\sigma(\bar{\nu}_e)$	-	-	-	7.91	0.12	1.46
NC1 γ	-	-	-	7.98	0.21	2.59
NC Other	-	-	-	7.91	0.03	0.33
Osc	-	-	-	7.91	0.29	3.60
All	7.74	1.03	13.32	7.95	0.52	6.51
All with osc	7.74	1.07	13.79	7.96	0.59	7.44

Table 42: Average event rate and RMS error broken down by systematic parameter group for e -like Super-K events with Run 1-8 POT for antineutrino mode.

Group	Pre-BANFF			Post-BANFF		
	Mean	1σ	%	Mean	1σ	%
SK Detector	-	-	-	7.02	1.17	16.69
SK FSI+SI+PN	-	-	-	6.92	0.79	11.43
Flux+Xsec constrained	7.71	0.91	11.79	6.91	0.28	4.05
$\sigma(\nu_e)/\sigma(\bar{\nu}_e)$	-	-	-	6.92	0.18	2.62
NC1 γ	-	-	-	6.93	0.02	0.33
NC Other	-	-	-	6.92	0.07	0.98
Osc	-	-	-	6.92	0.26	3.78
All	7.79	1.85	23.71	7.00	1.47	20.94
All with osc	7.79	1.87	24.05	7.00	1.49	21.24

Table 43: Average event rate and RMS error broken down by systematic parameter group for ν_e CC1 π^+ -like Super-K events with Run 1-8 POT for neutrino mode.

915 **F. Effect of ν_e CC1 π^+ sample on constraint strength**

916 Section 5 showed stronger than expected constraints from data for δ_{CP} , appearance and disap-
917 pearance fits. To determine a potential explanation for this we chose to run an additional fit without
918 the ν_e CC1 π^+ sample, hereafter referred to as the 4-sample fit, with the fit using all samples being
919 referred to as the 5-sample fit. It should be noted that the full 5-sample marginalisation toys were
920 used for all fits, rather than using 4-sample marginalisation toys for the 4-sample fit. This means
921 that the correlations among samples for the 4-sample fit are not handled correctly, but the effect
922 from this is expected to be small.

923 Figure 48 shows comparisons of the aforementioned fits for normal hierarchy. It can be seen that
924 the constraint on the δ_{CP} and appearance fits is weakened in the absence of the ν_e CC1 π^+ sample,
925 while the disappearance contour is unaffected.

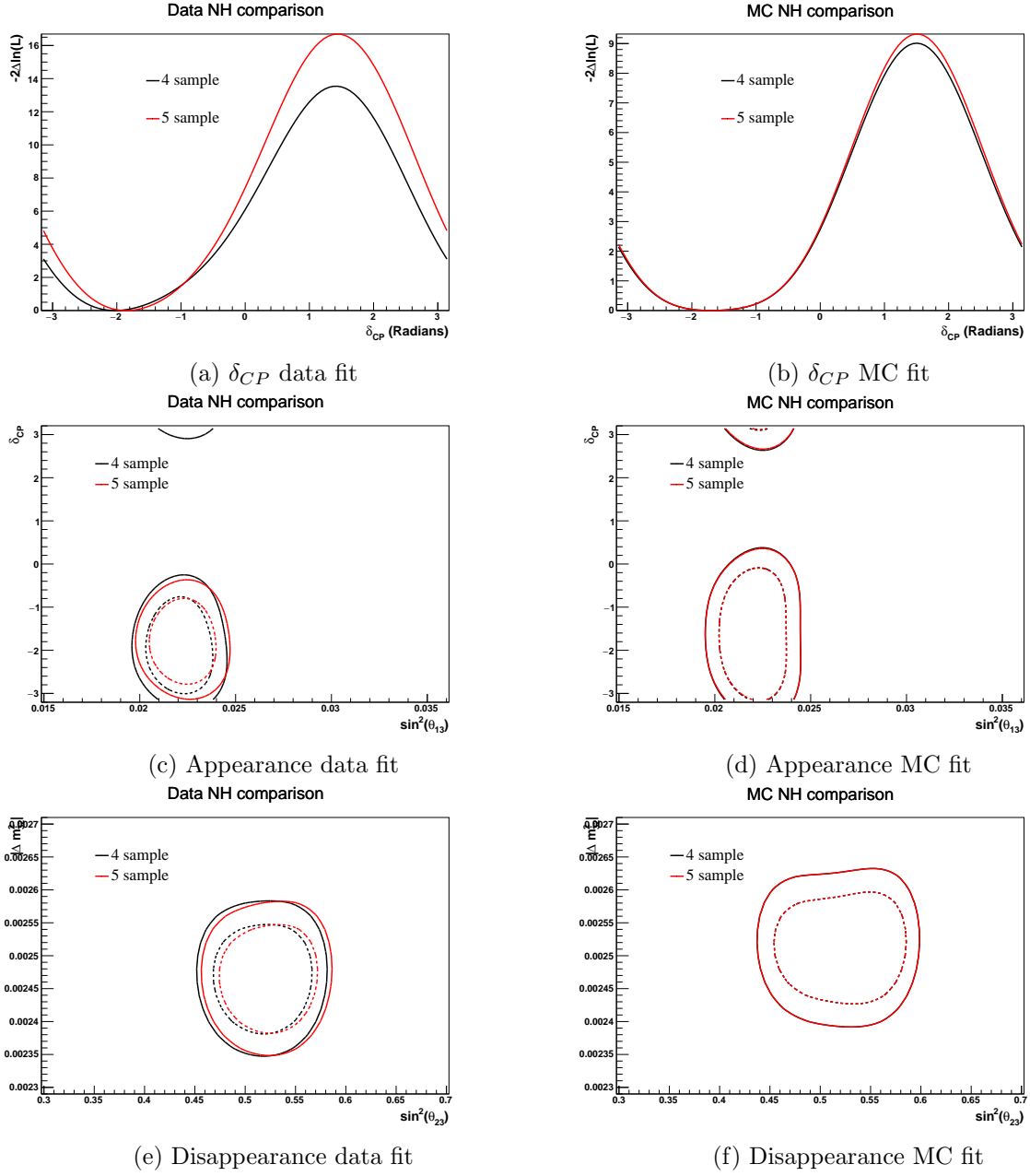


Figure 48: Fits of data and the Asimov A data set with four and five samples respectively.

926 **G. Matter effects and crust density**

927 To check the effect of the error on the average crust density [90] a number of fits of δ_{CP} were
 928 performed varying this value. Figures 49 to 50 show the effect of varying the average crust density
 929 between 2.5, 2.6 and 2.7 g cm⁻³ in normal and inverted hierarchy respectively. 1×10^4 marginali-
 930 sation toys were generated with the average crust density fixed at the value of 2.6 g cm⁻³, whilst
 931 fits were performed using the Asimov A data set where the crust density was varied using the
 932 aforementioned values. The effect on the fit of δ_{CP} can be seen to be small, supporting the use of
 933 a fixed value for the average crust density.

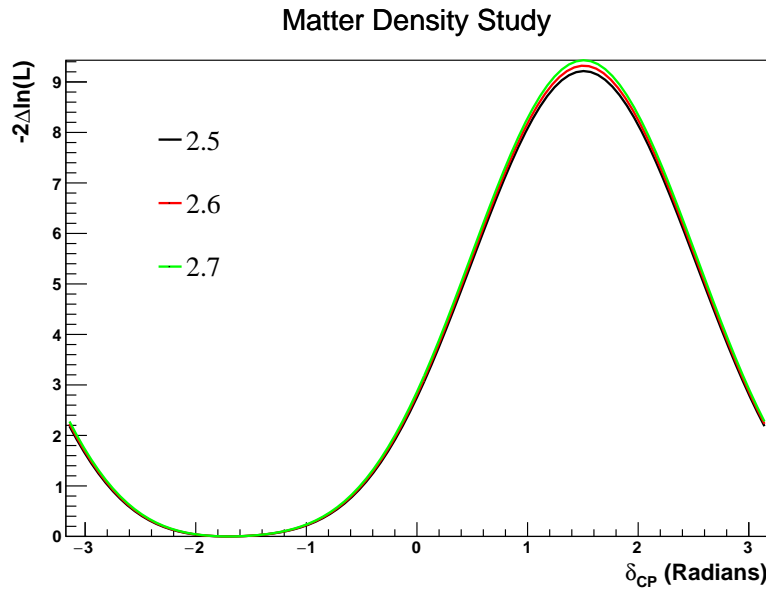


Figure 49: Fits of δ_{CP} using the Asimov A data set whilst varying the average crust density in normal hierarchy for 10K marginalisation toys.

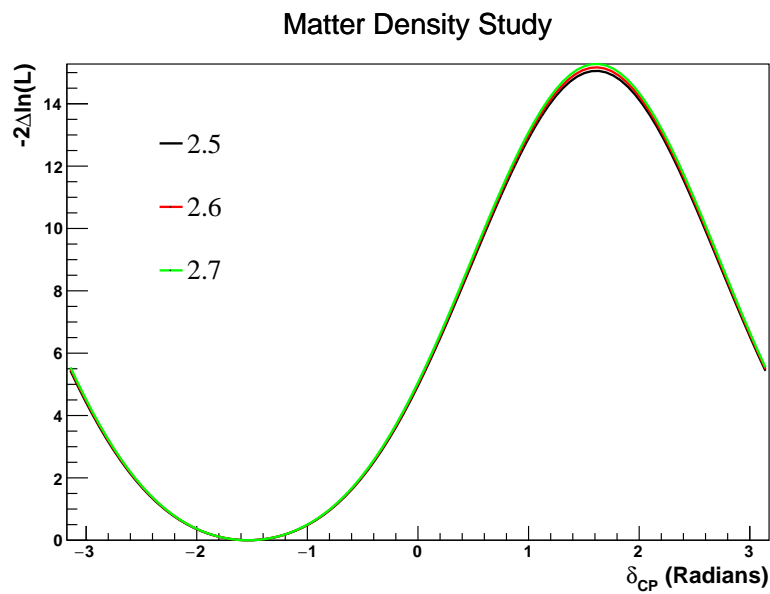


Figure 50: Fits of δ_{CP} using the Asimov A data set whilst varying the average crust density in inverted hierarchy for 10K marginalisation toys.

934 **H. Asimov B δ_{CP} /mass-hierarchy degeneracy**

935 In section 4.2 it was noted that Asimov B fits are affected by a lack of sensitivity to distinguish
 936 $\delta_{CP} = 0$ and $\delta_{CP} = \pi$, for example, the fit of δ_{CP} shown in fig. 22 shows a best-fit point shifted
 937 away from the true value. fig. 51 shows normalised one-ring e -like spectra for Asimov data set B
 938 with mass hierarchy and δ_{CP} varied to demonstrate the problem. It is clear from the plots that
 939 the spectrum for $\delta_{CP} = 0$ in normal hierarchy is similar in shape to the spectrum for $\delta_{CP} = \pi$ in
 940 inverted hierarchy and vice versa.

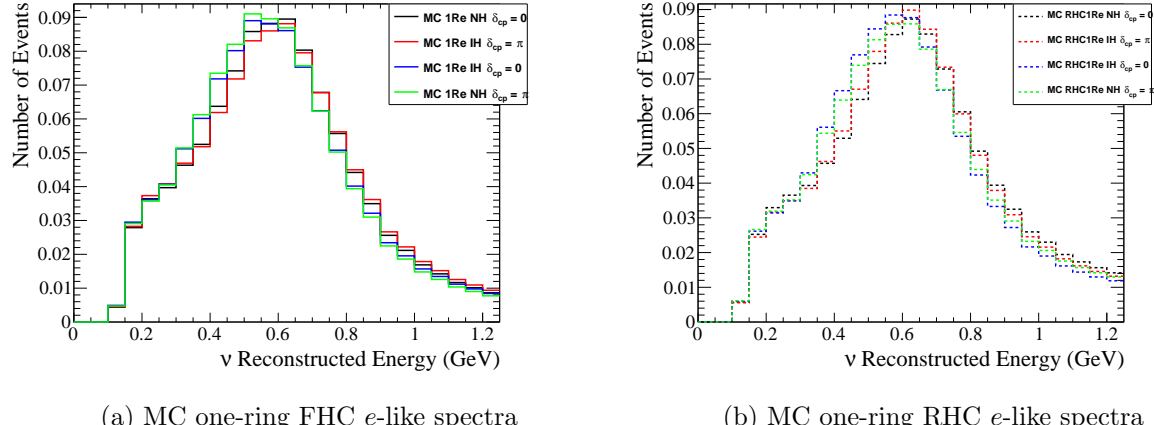


Figure 51: Normalised spectra for one-ring e -like samples showing the effect of changing the mass hierarchy and true value of δ_{CP} for the Asimov B data set.